A Sensor Fusion Concept for Object Detection in Automotive Applications

Master Thesis

Thomas Schlegl

Supervisor:
Dr. Thomas Bretterklieber
Assessor:
Univ.–Doz. Dr. Hubert Zangl

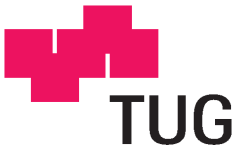

Institute of Electrical Measurement
and Measurement Signal Processing
Graz University of Technology

Graz
February 2010

Deutsche Fassung:
Beschluss der Curricula-Kommission für Bachelor-, Master- und Diplomstudien vom 10.11.2008
Genehmigung des Senates am 1.12.2008

EIDESSTATTLICHE ERKLÄRUNG

Ich erkläre an Eides statt, dass ich die vorliegende Arbeit selbstständig verfasst, andere als die angegebenen Quellen/Hilfsmittel nicht benutzt, und die den benutzten Quellen wörtlich und inhaltlich entnommene Stellen als solche kenntlich gemacht habe.

Graz, am ……. ……..
(Unterschrift)

Englische Fassung:

STATUTORY DECLARATION

I declare that I have authored this thesis independently, that I have not used other than the declared sources / resources, and that I have explicitly marked all material which has been quoted either literally or by content from the used sources.

……. ……..
date (signature)

Danksagung

An dieser Stelle möchte ich mich sehr herzlich bei allen Personen bedanken, die mich während meiner Ausbildung begleitet und unterstützt haben. Ihnen ist meine glückliche Schul- und Studienzeit zu verdanken.

Besonders bedanken möchte ich mich bei meinem Betreuer Dr. Thomas Bretterklieber und dem Begutachter der Diplomarbeit Univ. Doz. Dr. Hubert Zangl für die großartige Unterstützung während der gesamten Diplomarbeit. Ihre Hilfsbereitschaft war außerordentlich und über allen Erwartungen.

Ganz herzlich bedanke ich mich auch bei meinen Eltern, die mir das Studium ermöglicht haben und einen starken Rückhalt in meinem Leben darstellen.

Ich möchte mich auch ganz besonders bei meiner Freundin Eva für die liebevolle Unterstützung während meiner Studienzeit und für die wundervolle Zeit abseits des Studienalltags bedanken.

Ein besonderer Dank geht auch an meine Freunde und Studienkollegen, die unsere gemeinsame Zeit aufregend und unvergesslich gemacht haben.

Abstract

Distance sensing based on ultrasonic sensors is a widely used and cheap technique for automotive parking aids. However, several limiting factors (e.g. limited detection range, angular resolution, no object classification possibility) occur with these sensors. For prospective systems, such as full automated vehicle operation and active pedestrian safety applications, this technique can not be used. The main problem is the limited capability to measure distances below 0.2 m.

In contrast, capacitive sensors are well suited for distance measurements up to 0.5 m. Due to the volumetric measurement principle, capacitive sensors may also provide information about the approaching object itself.

In this master thesis a distance measuring system for future automotive applications is developed. To overcome the different drawbacks of state of the art techniques, a sensor fusion system based on capacitive and ultrasonic distance measurement techniques is applied. This new approach allows for both a gapless detection in a suitable measurement range and a coarse classification of approaching objects.

The properties of the two individual measurement systems and the usefulness of the sensor fusion system is demonstrated by means of experimental investigations.

Kurzfassung

Die Entfernungsmessung mit Hilfe von Ultraschallsensoren ist eine weit verbreitete und preiswerte Technik für Einparkhilfen im Automobilbereich. Für zukünftige Systeme wie voll automatisierte Fahrzeugkontrolle oder aktiven Fußgängerschutz ist diese Technik aber aus verschiedenen Gründen wie zum Beispiel begrenzte Erkennungsreichweite (nur über einer Entfernung von 0.2 m), geringe Winkelauflösung, oder keiner Möglichkeit zur Objektklassifizierung nicht geeignet.

Kapazitive Messtechnik auf der anderen Seite, beruht auf einem volumetrischen Messprinzip und ist für Abstandsmessungen bis zu einer Reichweite von 0.5 m geeignet. Zusätzlich ist mit diesem Messprinzip eine Objektklassifizierung möglich.

In dieser Diplomarbeit wird ein Abstandsmessverfahren entwickelt, welches für die oben genannten zukünftigen Automobilanwendungen geeignet ist. Um die verschiedenen Nachteile der verwendeten Sensorsysteme zu kompensieren, wird eine Sensorfusion von einem kapazitiven und einem ultraschallbasierten Messsystem entworfen. Die Kombination der beiden Messsysteme ermöglicht eine lückenlose Abstandsmessung und eine grobe Objektklassifizierung.

In experimentellen Versuchen werden die Eigenschaften der einzelnen Sensorsysteme untersucht und ihre erfolgreiche Kombination gezeigt. Dies soll einen möglichen Einsatz in zukünftigen Automobilanwendungen argumentieren.

Contents

Chapter 1

Introduction

1.1 Motivation for and Aim of this Work

For prospective parking aids and pedestrian safety applications, the Electronic Control Unit (ECU) requires accurate information about type and position of an approaching object [Dep08]. Based on this information, the ECU may trigger several safety measures in case of an accident.
Efforts have been reported for sensing vehicle surroundings with different visible, non visible (infrared) light and time-of-flight (radar and laser scanner) sensors [GT07]. Imaging sensors provide a perspective view of the scene with high angular resolution but low distance resolution. In addition, complex signal processing methods in order to extract relevant information are required. On the other side, time-of-flight sensors provide accurate information about the distance to an object but do not provide information about material properties of the object [GT07]. According to [LSW09], ultrasonic sensors exhibit a dead zone directly in front of the sensor plane. In this dead zone, no accurate measurement can be taken. This results from oscillations induced in the transducer, which are used to stimulated the generation of a sound wave. An object within the dead zone of the sensor reflects the transmitted wave to the sensor, before the oscillations are subsided to a suitable level. Thus, the echo information can not be reliably detected.
In comparison to ultrasonic sensors, capacitive sensing technology offers the advantage of a volumetric measurement principle which may be used also for short distance sensing [Bax97]. Hence, this technique allows for both detection and classification of objects [GZB08]. Combined with ultrasonic sensors, this could be exploited to design an improved distance measurement system, which provides the possibility to classify the object.

In this work a distance measurement system based on a capacitive and an ultrasonic

sensing principle is proposed. Its usefulness is demonstrated by means of experimental investigations. The measurement range reaches up to two meters whereby blind spots are avoided. With the capacitive measurement, the opportunity for a classification of the object type is also given [BZH+08].

1.2 Review of Automotive Distance Measurement Techniques

In the following section, a brief overview of state of the art techniques for automotive distance measurements is given. The overall aim of automotive distance measurement systems is not only to measure distances more accurately but also to increase the safety for all traffic participants such as vehicle occupants, pedestrians, and bicyclists. Thus, the following sections also describe the capabilities of the sensors with respect to safety applications. [1]

1.2.1 Time of Flight Sensors

Time of flight sensors emit some kind of rays of a defined wavelength. After reflection on the surface of an approaching object, these reflected rays are received by the sensor. The measured time (between transmission and receiving of the rays) provides information about the distance to the approaching object. These sensors provide accurate distance information but have a limited lateral resolution [GT07]. Depending on the frequency of the emitted rays, different sensor types are distinguished.

Ultra Sonic Sensors

Ultra Sonic (US) Sensors are widely used for parking aids. They usually work with a piezoelectric transceiver, which also works as a receiver [LSW09]. Figure 1.1(a) shows the working principle of such a system. Low cost and short range US sensors use frequencies in the region of 50 kHz and have a detection range from 0.2 m up to 2.5 m [Fle08]. Figure 1.1(b) shows a photography of an US sensor, which is used in this work. A more detailed theoretical background to ultra sonic sensors is presented in Chapter 2.1.

[1] More information on state of the art sensors, used for pedestrian safety and distance measurements, can be found in e.g. [Fle08], [Foe06],[GT07], and [SS06].

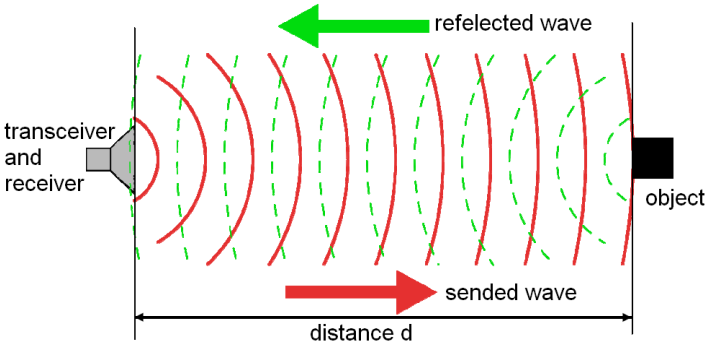

(a) US working principle.

(b) Photography of an US sensor.

Figure 1.1: Principle and photography of an US sensor. (a) The transceiver emits waves, which are reflected by an object. The receiver measures the reflected waves and the time they need. Hence the distance d is calculated. (b) Photography of the US sensor used in this work from Valeo. It works as a transceiver and as a receiver at the same time.

Radar Sensors

Radio Detection And Ranging (Radar) sensors emit electromagnetic waves in the microwave band. In Europe, two frequency bands at 24 GHz and $77 - 81$ GHz with bandwidths of 200 MHz and 4 GHz respectively are used for automotive applications. Two types of radar sensors are used for distance measurements in vehicles:

- Pulsed doppler radar.
- Frequency Modulated Continuous Wave (FMCW) radar.

Both radar types are also able to measure the velocity of approaching of objects. A pulsed doppler radar transmits pulses of a defined duration and measures the time it takes until the reflected pulses are received. The distance d is calculated by the time t the pulse needs and the velocity of light c by:

$$d = \frac{ct}{2} \tag{1.1}$$

To determine the relative velocity of an approaching object, radar can make use of the doppler effect. Due to this effect a frequency shift is introduced to the received echoes by the moving targets. The echo frequency decreases for targets moving away and increases for approaching targets. With a moving car an additional frequency shift occurs. It has to be distinguished between doppler shifts due to approaching objects and doppler shifts due to the movement of the car [LSW09].

With the FMCW radar a wave is emitted permanently. The transmitted frequency is modulated as can be seen in Figure 1.2(a). The frequency shift df of the received signal

consists of two parts:

$$df = df_D + df_\tau \tag{1.2}$$

where df_D is the frequency shift according to the Doppler effect (to determine the relative velocity) and df_τ is the frequency shift due to the flight time τ (proportional to the distance). Both frequency shifts are defined as follows:

$$df_D = -2\frac{v_r}{\lambda} \tag{1.3}$$

$$df_\tau = -2\,\frac{f_{max} - f_{min}}{c\;T_{Chirp}}\;R \tag{1.4}$$

with the relative velocity v_r, the highest and lowest frequencies f_{max} and f_{min} respectively, and the distance R of the approaching object. With the two slope measurement it is possible to determine df_τ and df_D. Thus, the distance R and the velocity v_r can be simultaneously calculated with the received signal. Technical parameters of radar sensors can be found in Table 1.1. For more information on radar sensors please refer to [Fle08] and [Foe06].

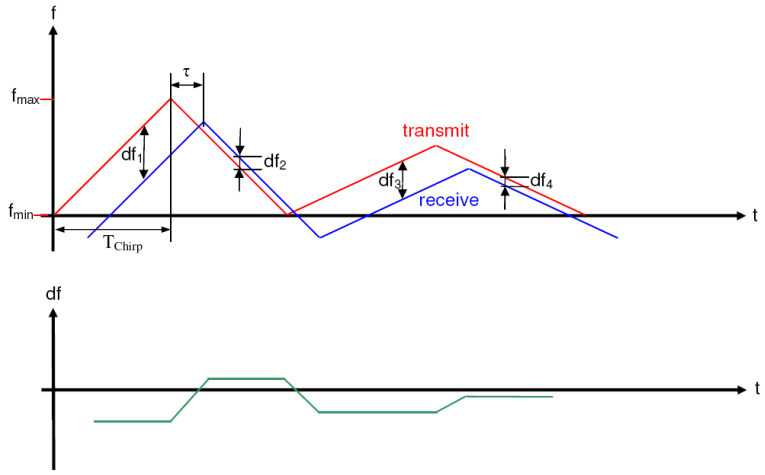

(a) Principle of a FMCW radar.

(b) Photography of a FMCW radar [Fle08].

Figure 1.2: Principle and photography of a FMCW radar. (a) The transmitted wave is received with a frequency shift due to the relative velocity (df_τ) and the distance (df_D) of an approaching object. (b) Photography of a CW radar [Fle08].

Lidar Sensors

Light Detection and Ranging (Lidar) sensors are also used in automotive applications for distance measuring. In most cases, the sender consists of laser diodes and the receiver of

photodiodes. Both are easily implemented in Integrated Circuits (IC).
Two transit time techniques are widely used to determine the distance in automotive applications. The first method uses the phase shift of the modulated received light, as can be seen in Figure 1.3(a). The second technique calculates the distance from the measured time difference between the emitted and received light pulse [SS06].

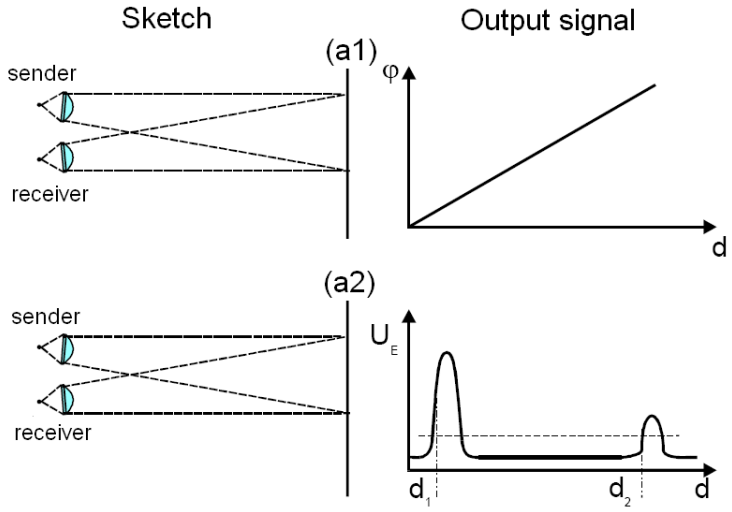

(a) Principle of lidar sensors.

(b) Photography of a lidar sensor [SS06].

Figure 1.3: Principle functionalities and photography of a lidar sensor [SS06]. (a1) The phase of the modulated reflected light is calculated and used to determine the distance. (a2) The time between the emitted and received light pulse is measured. (b) Photography of a lidar sensor.

Table 1.1 gives technical parameters of radar and lidar sensors and compares them with each other.

1.2.2 Imaging Sensors

Imaging sensors deliver a high resolution 2D perspective image out of a 3D scene. Thus, a single picture without additional information usually does not contain depth information. With references (e.g. lines on the streets or traffic signs with known sizes) distance measurement or velocity determination would be possible. Through stereo imaging it is also possible to get a depth information. Substantial amount of complex processing and often ambiguous measurement results are disadvantages of these sensors [GT07]. Ongoing research is done on the two widely used types of imaging sensors, which are presented hereafter.

Radar and Lidar Specifications		
	Lidar	Radar
Relative costs	1	2
Wavelength	$0.8 - 1\,\mu$m	$4 - 12\,$mm
Distance	up to 200 m	up to 200 m with 77 GHz up to 60 m with 24 GHz
Lateral resolution	$< 1\,^\circ$ [SS06]	$2 - 5\,^\circ$ [Sch05]
Velocity	Possible	Depending on technique
Restrictions to environmental influences	Fog	Strong rain

Table 1.1: Comparison of radar and lidar sensors according to [Foe06] and [SS06].

Visible Light Imaging

Video camera technology for so called visible light imaging is a mature and cheap technology. Although this type provides a good lateral resolution, complex calculations have to be applied in order to separate objects from the background of the image. Further more, this technique is less effective when operated in dark conditions, e.g. at night. At present, this type of system is already in use in luxury cars for backing and parking aids [GT07].

Infrared Imaging

Two types of infrared imaging sensors, which are used in automotive applications especially for dark scenes are distinguished:

- Far infrared (FIR) sensors which detect thermal radiation (long wavelength IR).
- Near infrared (NIR) sensors (shorter wavelength IR) accompanied by an illuminator.

Figure 1.4 shows the two types of sensors. Whereas the FIR sensors work without an illumination source, NIR sensors need such an illuminator. An advantage of the NIR infrared sensor is its independence on temperature. NIR sensors are also less expensive and produce images similar to visible light images. This makes it possible to use the same image processing algorithms as for visible light images [Fle08].

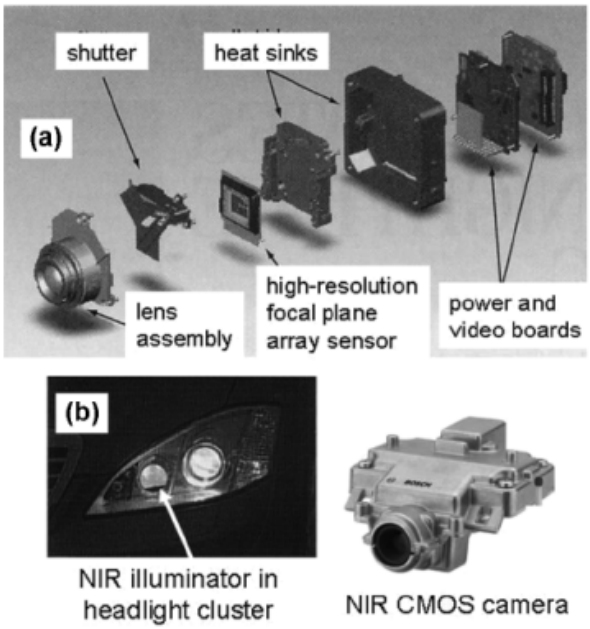

Figure 1.4: Photography of two IR sensors [Fle08]. (a) FIR camera for warm body detection. (b) NIR camera with illuminator.

1.2.3 Multiple Types of Sensors

Since every sensor system has its advantages and limitations, a combination of two or more sensor systems is reasonable. In the following, a list of sensor fusion systems is presented (for further information refer to [GT07]).

- Visible light and FIR.
- Radar and mono vision.
- FIR and laser scanner.
- Lidar and visible light.
- Radar, visible light, and IR.

Novel Sensor Fusion System

All mentioned sensors in this section and their operating range (not in scale) are shown in Figure 1.5. As can be seen, the measurement range up to 30 cm is not covered by any sensor system. Capacitive sensor technology would be able to cover this range. Therefore a sensor fusion system with other sensors, e.g US sensors, may provide a lot of benefits (as described in Section 1.1).

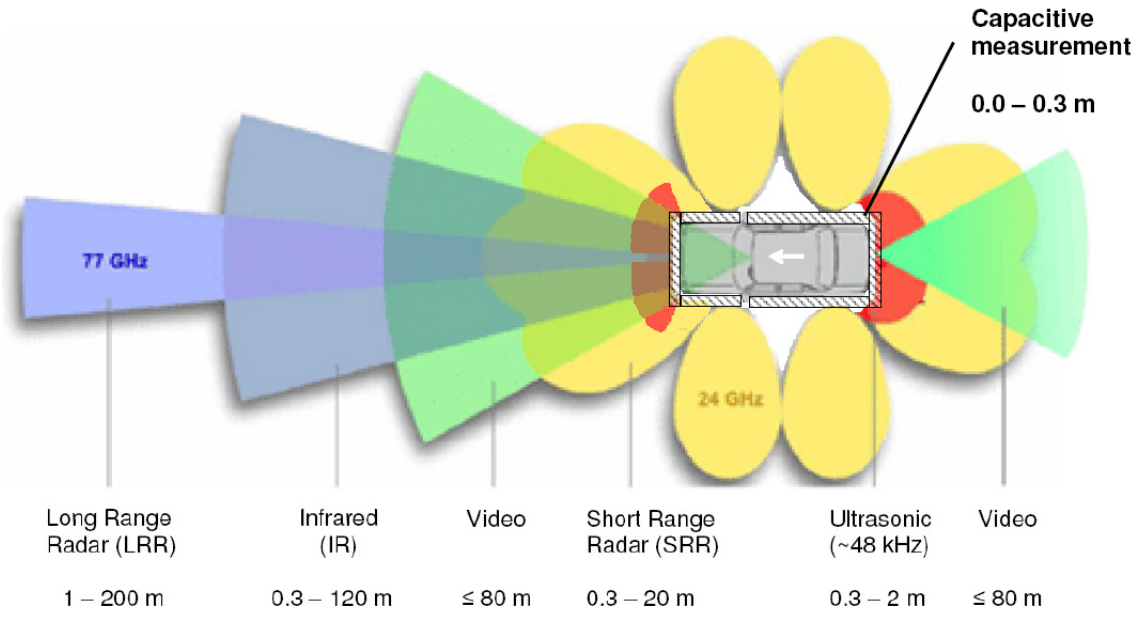

Figure 1.5: Outline of used automotive distance sensors and measurement ranges (not in scale) [TH08]. Capacitive sensors are used to cover the measurement range up to 30 cm. None of the other measurement methods can cover this area.

1.3 Overview of the Work

In Chapter 2, the theoretical backgrounds of ultrasonic and capacitive measurement principles are described.
The development of a prototype is the issue of the next two chapters. Chapter 3 describes the prototype hardware, the developed software is introduced in Chapter 4.
In Chapter 5, experimental investigations on the sensor systems, the sensor fusion system, and influences on the senor systems by means of external disturbances are presented and discussed.
Chapter 6 concludes the work and gives an outlook for further developments.

Chapter 2

Survey of Ultrasonic and Capacitive Distance Measurement Principles

This chapter describes the ultrasonic measurement principle and the capacitive measurement principle. Common US techniques for distance measurement in automotive applications are discussed. Benefits and drawbacks of these techniques are described. An overview of capacitive measurement principles is given. A discussion of benefits and drawbacks of capacitance distance measurement is included. Constraints for both sensor types are provided and the expected benefits of a sensor fusion system are given at the end of this chapter.

2.1 Ultrasonic Measurement Principle

A general overview of the ultrasonic measurement techniques has already been given in Chapter 1.2. The following section discusses ultrasonic sensors used for distance measurement in more detail. [2]

An ultrasonic distance measurement system is generally based on a time-of-flight measurement. For low frequency ranges (from 20 kHz to about 200 kHz), typically piezoelectric dimorph transducers are used [LSW09]. Figure 2.1(a) shows the working principle of such a transducer. By applying a voltage to the transducer, one of the piezoelectric elements gets extended while the other one gets contracted.

For distance measurement, the transducer generates a burst ($\approx 200\,\mu$s) of ultrasonic

[2] Further information can be found in [Bos07], [Hon99], and [LSW09].

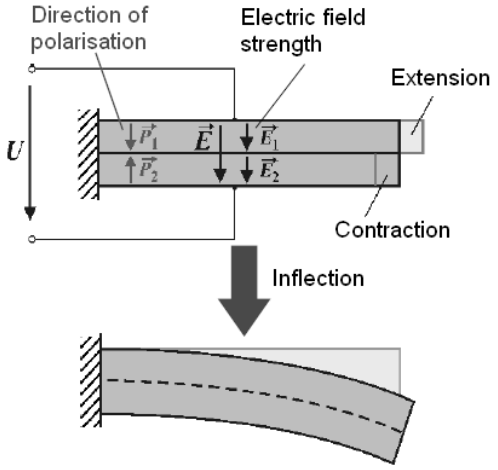

(a) Principle of function of a piezoelectric dimorph transducer.

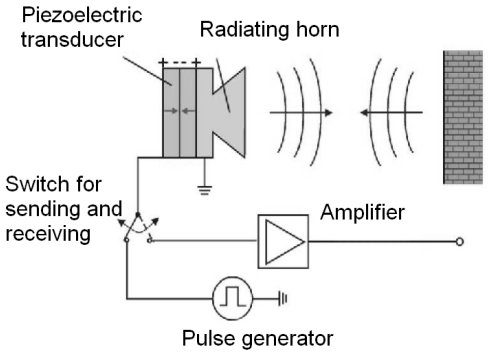

(b) Schematic diagram of a piezoelectric dimorph transducer in pulsed echo operation for distance measuring.

Figure 2.1: Sketch of a piezoelectric dimorph transducer and its application in a distance measurement system [LSW09].

pulses with a defined frequency. For automotive applications, this frequency is typically in the range of 50 kHz [Bos07]. Figure 2.1(b) shows a schematic diagram of an ultrasonic transducer in the so called pulsed echo mode. After sending the ultrasonic pulses, the transducer measures the time T until the echo is received. With this time T and the sonic velocity c in air ($c \approx 340\,\frac{\mathrm{m}}{\mathrm{s}}$), the distance can be calculated through:

$$x = \frac{c\,T}{2} \tag{2.1}$$

Figure 2.2(a) shows a sketch of the sonic field. It can be divided into a dead zone, a near field (also called Fresnel zone), and a far field (also called Fraunhofer zone) with the direction of propagation z.

The distance measurement range is limited. The theoretical lower bound is given by the so called dead zone of the ultrasonic transducer. Ultrasonic sensors exhibit this dead zone directly in front of the sensor plane, where no accurate measurement can be taken. The ring down time t_{down}, which is the time, the ultrasonic transducer needs to switch from sending to receiving mode, is approximately 900 μs for automotive ultrasonic sensors [Bos07]. A transmitted wave must not be reflected on approaching objects and reach the transducer below this time plus the time of the burst ($t_{burst} \approx 200\,\mu\mathrm{s}$). Otherwise the measured travel time between sending and receiving will not be correct. Thus, the dead zone z_d of these sensors can be calculated with the velocity c in air by:

$$z_d = \frac{c\,(t_{down} + t_{burst})}{2} = \frac{340 \times (900 + 200) \times 10^{-6}}{2} = 0.187\,\mathrm{m} \tag{2.2}$$

The boundary between the near field and the far field z_n (also called focal length) is shown in Figure 2.2(b). The focal length z_n is the distance from the transducer to the point where the last maximum of sound pressure (intensity) occurs (in direction of propagation z). It is defined by [LSW09]

$$z_n = \frac{r_{Sensor}^2}{\lambda} \tag{2.3}$$

where r_{Sensor} is the radius of the ultrasonic sensor. For a measurement system as described above with an ultrasonic sensor radius $r_{Sensor} = 0.75\,\text{cm}$ the focal length z_n is:

$$z_n = \frac{0.0075^2}{0.0068} = 0.0083\,\text{m} \tag{2.4}$$

As obtained from Equation 2.2 and Equation 2.4, the focal length is much shorter than the dead zone (for the provided sensor). Thus, the dead zone will be the limiting factor for the lower bound of distance measurements in automotive applications. Therefore distances are measured in the far field of the transducer. According to [SWS04], it is possible to reduce the ringing effect (reduce the length of the dead zone d_z) by choosing a proper control sequence for the transducer.

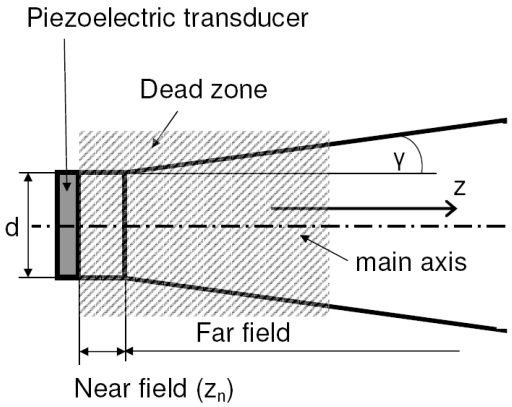

(a) Sketch of the sonic field of an ultrasonic wave. It is divided in a near and a far field. In the dead zone near the surface of the sender no measurements are possible.

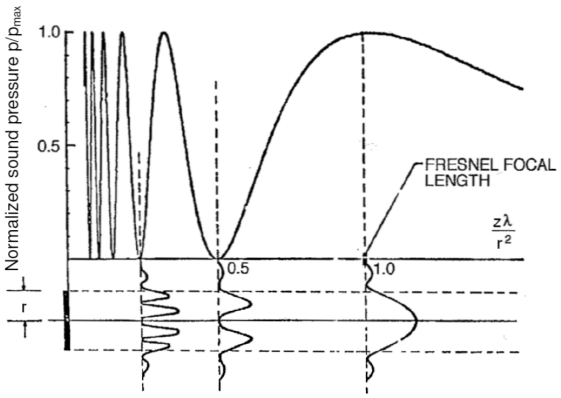

(b) Axial sonic intensity distribution of a piezoelectric transducer with the radius r as a function of z (distance to the transducer) normalized by radius r and wavelength λ.

Figure 2.2: Sonic field and axial intensity of an ultrasonic transducer [LSW09].

In the far field the sonic pressure p varies with:

$$p = \frac{1}{\sqrt{z}} \tag{2.5}$$

where z denotes the distance to the transducer. With higher distances to the approaching object, the sound pressure of the echo reduces. This effect limits the upper bound of the

measurement range (when the sound pressure of the echo is smaller than the detectable pressure of the transducer). State of the art ultrasonic sensors for automotive distance measurements have a measurement range of up to 2.5 m. Future ultrasonic sensors will cover a range of up to 4 m [Bos07]. A limiting factor is the long measurement time, due to the velocity of sound in air (e.g. travel time for four meters $t_{4m} \approx 24\,\text{ms}$). The maximum sensing range z_{max} additionally depends on the object size and the object itself as can be seen in Figure 2.3.

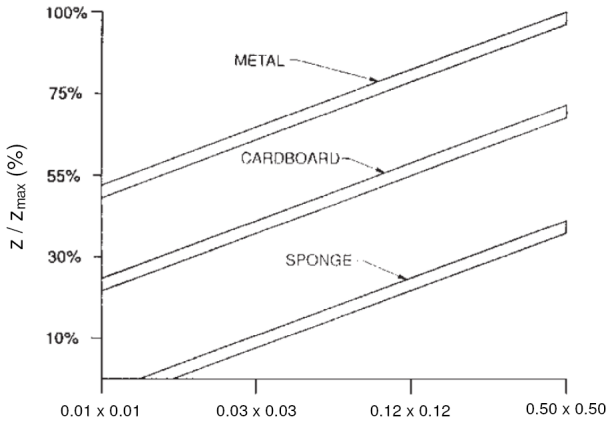

Figure 2.3: Exemplary maximum sensing range of US sensors, depending on the object size and type of the object [Hon99].

Another important property of ultrasonic transducers is the opening angle γ of the sonic field in the far zone. Figure 2.2(a) shows the definition of this angle. It describes the reduction of the sonic pressure for objects which are not on the main axis of the transducer. It is defined by the diameter d of the transducer and the wavelength λ of the sonic pulse. The angle $\gamma_{-6\,\text{dB}Echo}$ in equation 2.6 denotes the angle of the limit where the intensity of the received echo is half the intensity of the main axis (for the described system above) [LSW09].

$$\gamma_{-6\,\text{dB}Echo} = \arcsin \frac{0.51\lambda}{d} = 13.37\,^\circ \tag{2.6}$$

Thus, the maximum sensing range reduces for objects which are not on the main axis of the ultrasonic sensor, because of the reduced sonic pressure of the echo.

2.1.1 Discussion of Benefits and Drawbacks

According to [Bos07], [Fle08], [Hon99] and the theoretical considerations of this section benefits and drawbacks of the US distance measurement for automotive applications are briefly discussed.

Benefits

- Mature and cheap technology.
- Simple structure of the transducer.
- Accurate distance measurements in direction of propagation ($\approx 0.3\,\%$ of the maximum measurable distance).
- Wide measurement range (from 0.2 m to 2.5 m, in the future possibly up to 4 m).
- Detection of nearly all types of approaching object (with different maximum sensing range z_{max}).

Drawbacks

- No information on type or size of object (only the surface influences the measurement signal).
- Limited opening angle λ and limited maximum measurement range outside the radiation axis, due to reduced sonic pressure.
- High speed movements (i.e. wind) affect the measurements, because ultrasonic waves propagate through air.
- Long measurement time because of the comparatively low velocity of sonic in air (e.g. travel time for one meter $t_{1m} \approx 6\,\text{ms}$ and for two meters $t_{2m} \approx 12\,\text{ms}$).
- Possible measurement errors through ultrasonic multi path propagation or sonic waves from ultrasonic sensors from other cars.
- Measurements of the approaching objects are affected by the
  - Surface (through scattering).
  - Temperature (through sound dispersion).
  - Inclination. The echo of the sonic waves can be deflected on smooth objects, which are not in a $90\,^\circ$ angle in relation to the direction of propagation. Thus, the sensor will not receive an echo or receive an echo with reduced pressure (compare Figure 2.4).

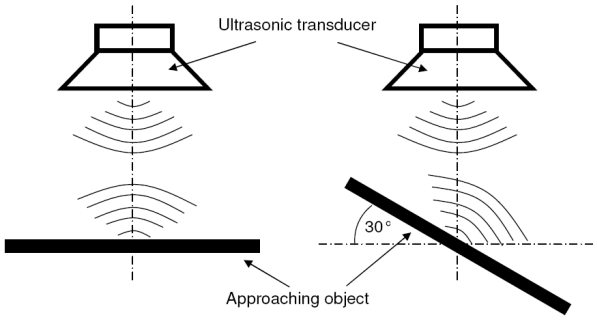

Figure 2.4: Schematic of the effects on US waves through inclination changes.

2.2 Capacitive Measurement Principles

This section discusses the most important aspects of the capacitive distance measurement. Basics of capacitive measurement and influences on the measurement are discussed by means of a simplified model. The physical effects, which are used for the experiments in this work are described. [3]

2.2.1 Capacitive Measurement Basics

The capacitance of two opposite parallel plates, where the spacing d between the plates is much smaller than the square root of the area A of the plates, is given in equation 2.7.

$$C = \epsilon_0 \epsilon_r \frac{A}{d} \tag{2.7}$$

with

C ... Capacitance, in farad (F).
ϵ_0 ... Permittivity of vacuum, $8.854 \times 10^{-12} \frac{F}{m}$.
ϵ_r ... Relative permittivity of material, unit less.

According to the equation 2.7 the capacitance can be influenced through following parameters:

- Area of the plates.
- Distance between the plates.
- Relative permittivity.

In the majority of measurement tasks, the parameter of interest is measured due to the influence of one of these parameters. For distance measurement applications, the plates of

[3] A more detailed discourse can be found in [Bax97] and [Zan05].

the capacitance are not in opposite position, but in parallel next to each other. Thus, the area of the plates and the distance between the plates is fixed and the relative permittivity ϵ_r is the one key factor.

2.2.2 Capacitive Distance Measurement

A common technique for capacitive distance measurement uses one or more transmitter electrodes and one or more receiver electrodes. An example with one transmitter and one receiver is shown in Figure 2.5(a). Depending on the used electronic circuitry, the displacement current through the coupling capacitance C_D or the potential of the capacitance C_D (between the transceiver electrode A and the receiver electrode B) is determined. Both, the displacement current and the potential, are proportional to the coupling capacitance C_D. The measurement circuitries used in Chapter 3 are based on the displacement current technique to measure the capacitance. Thus, only this measurement technique is mentioned further on. More information on the displacement current technique and the potential technique can be found in [Bax97].

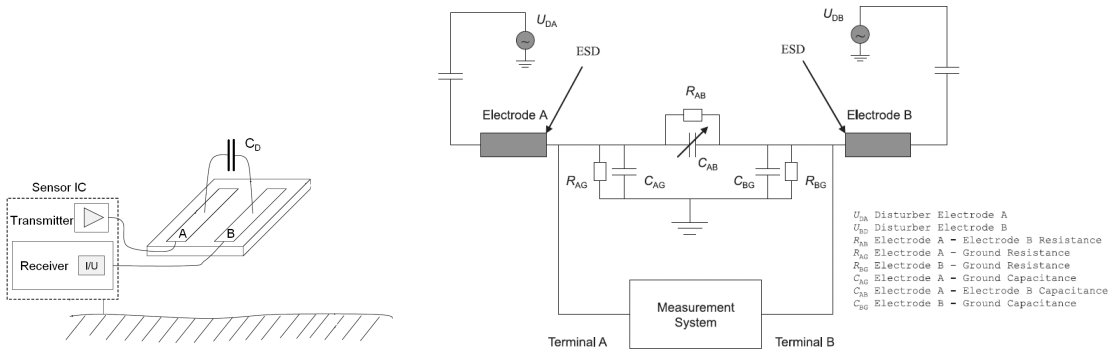

(a) Capacitive distance sensor with two plates.

(b) Equivalent circuit diagram of a capacitive sensor front end.

Figure 2.5: Capacitive distance measurement with two electrodes [Zan05]. (a) The capacitance is measured by means of the displacement current through the capacitance C_D from the transmitter electrode A to the receiver electrode B. (b) Equivalent circuit diagram of a capacitive sensor front end. The measurement system is influenced by electrostatic discharge, external disturbances, and parasitics to ground.

In order to work out the advantages and disadvantages of the used measuring technique, an understanding of the parasitic effects in the sensor front end is essential. The capacitance, which is measured between the transmitter electrode and the receiver electrode is also exposed to external disturbances and stray (coupling) capacitances to other objects and ground. Figure 2.5(b) shows an equivalent circuit diagram of a capacitive sensor front end.

According to [Zan05], the effects, which influence the measurement, are

- Shunt capacitors C_{AG} and C_{BG} between the electrodes and ground. These capacitances may be much higher than the actual measurement capacitance C_{AB},
- disturber crosstalk (U_{DA} and U_{DB}), and
- Electrostatic Discharge (ESD).

The measurement system must not be influenced by these disturbances in order to achieve accurate measurement results and robustness. Different circuitries with different characteristics, benefits, and drawbacks can be found in [Bax97], [BZH+08], and [Zan05].

For distance measurement applications, the influence of an approaching object on the electric field is utilized. As shown later, at least three electrodes are necessary for unambiguous distance measurements. If an approaching object comes in the vicinity of the electrodes, the capacitance C_D changes due to a change in the electrical field between the electrodes (among other things, the effect depends on the object size and the relative permittivity ϵ_r of the object). An exemplary simulation is shown in Figure 2.6. In far distance an approaching object (with $\epsilon_r = 80$) only influences the farther receiving electrode (referring to the transmitting electrode). When the object comes closer, the electric field of both electrodes is influenced by the approaching object (depending on its volume and ϵ_r). Thus, the coupling capacitance C_D between the transmitter electrode and the participating receiver electrodes (due to the position of the approaching object) changes.

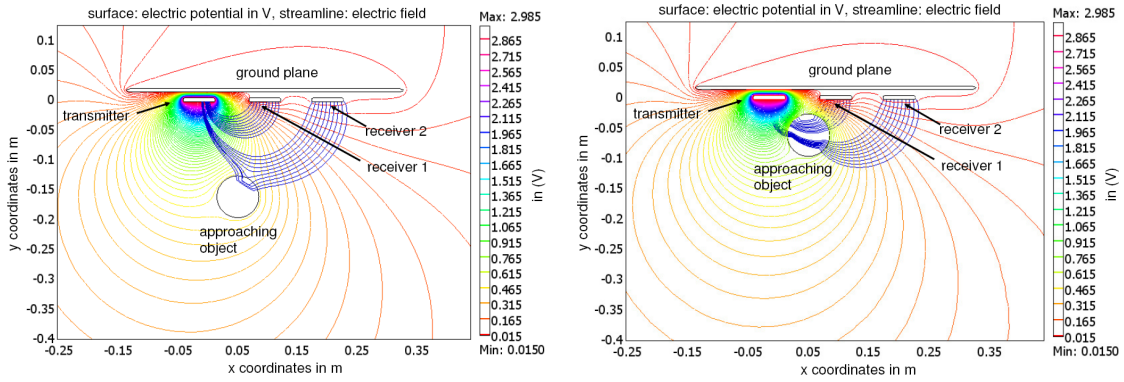

Figure 2.6: Exemplary simulation of an approaching object ($\epsilon_r = 80$) with a capacitive distance measurement system with two receiving electrodes and one transmitting electrode. In far distance only the electric field of the second receiver is influenced. When the object comes closer, the electric field of both receivers change, according to the volume and ϵ_r of the object. For unambiguous distance measurement at least two receiving electrodes are necessary (refer to subsection Distance Measurement). No shielding mode is considered in the simulation, because the approaching object has no connection to ground.

This change can be observed by means of measuring the displacement current through C_D and be converted into a distance between the object and the sensor electrodes. Also a ground plane is used at the backside of the electrodes. This ground plane prevents an influence of the electric field due to objects from the backside. Two modes of operation have to be distinguished for distance measurements of an approaching object in real world application:

- Shielding mode, for objects farther away from the sensor electrodes.
- Coupling mode, for objects very close to the sensor electrodes.

Both modes are described below. The simulation in Figure 2.6 does not consider the shielding mode, because the approaching object has no connection to ground.

Shielding Mode

Electric field lines are emitted by the transmitter T_1 and received from the receiver R. An approaching object in some distance from the sensor shields a part of the electric field lines from the receiver electrode R, as described in Figure 2.7.
Under these circumstances, as shown in Figure 2.7(b), the capacitance C_{GH} will typically stay approximately constant. With the approaching object (as shown in Figure 2.7(a)), the capacitance C_{TR} is lowered, while the capacitances C_{TH} and C_{RH} increase. As long as the capacitance C_{GH} has a higher influence than the capacitance C_{RH} the relevant capacitance is C_{TR} and the output signal v_0 decreases.
Thus, the received signal v_0 will get smaller compared to its value with no object in the sensor vicinity, due to the decreasing of the capacitance C_{TR}. This effect is called shielding [Zan05].

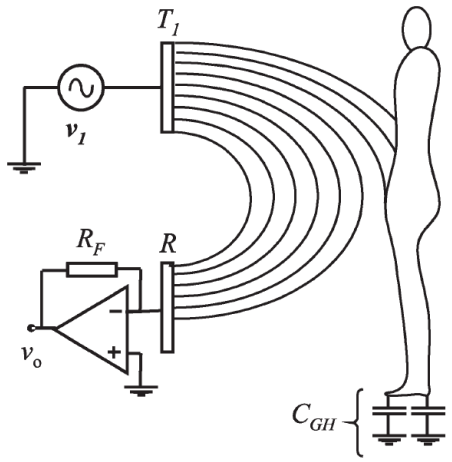

(a) Pictorial representation of the shielding mode.

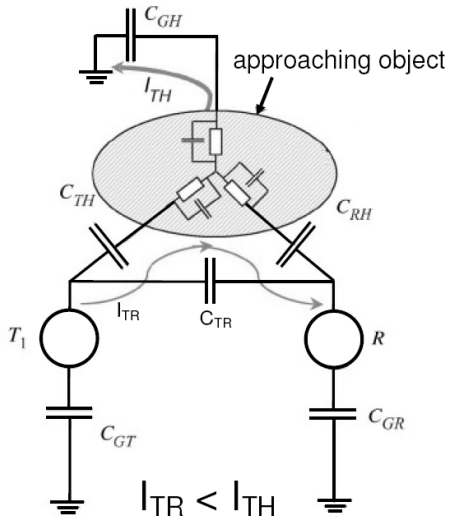

(b) Equivalent circuitry for the shielding effect.

Figure 2.7: Pictorial representation and equivalent circuitry for shielding mode [GZB08]. (a) In shielding mode an approaching object (e.g. a human body) in some distance to the sensor electrodes shields the electric field lines from reaching the receiver R. Thus, the measured displacement current decreases. The capacitance between the human body and ground is shown as C_{GH}. Electrical field lines between transmitter $T1$ and ground and between receiver R and ground are not shown. (b) The displacement current I_{TR} flowing from transmitter T_1 to receiver R is reduced by the increasing current I_{TH} through the approaching object (e.g. a human body).

Coupling Mode

If an approaching object comes very close to the sensor electrodes (refer to Figure 2.8(a)) the influence of the capacitance C_{RH} outranges the influence of the typically constant capacitance C_{GH}. Thus, the displacement current I_{TH} decreases, while the displacement current I_{TR} increases and the output signal v_0 increases.
At these distances, the approaching object does not shield the electric field lines from the receiver R, but changes the relative permittivity between the transmitter T and the receiver R. This effect is called coupling.

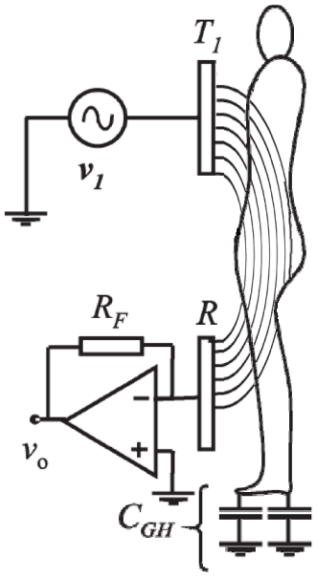

(a) Pictorial representation of the coupling mode.

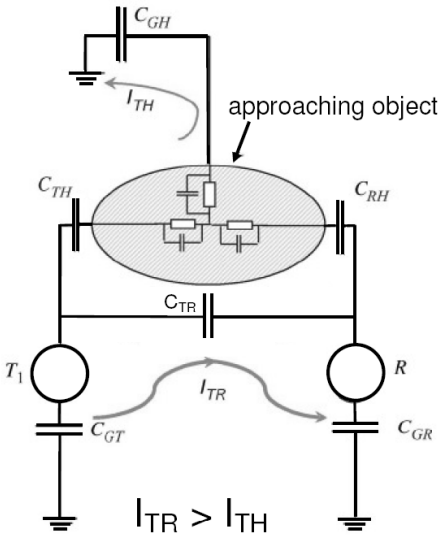

(b) Equivalent circuitry showing the coupling mode.

Figure 2.8: Pictorial representations and equivalent circuitry for coupling mode [GZB08]. (a) In coupling mode an approaching object (e.g. a human body) works as a solid dielectric. Thus, the displacement current increases. The capacitance between the human body and ground is shown as C_{GH}. Electrical field lines between transmitter $T1$ and ground and between receiver R and ground are not shown. (b) The approaching object (e.g. human body) is very close to the sensor electrodes. The influence of the capacitance C_{GH} is smaller than the influence of the capacitance C_{RH}. Thus, the displacement current I_{TR} and the output signal v_0 increases.

Distance Measurement

A typical output signal v_0 for an approaching object is shown in Figure 2.9. For this measurement result, two receivers (R_1 and R_2 printed in red and blue, respectively) placed at different distances to the transmitter T, were used (planar arrangement as used in the simulation in Figure 2.6).

As can be seen in Figure 2.9, it is necessary to have at least two receivers to determine an unambiguous distance from the measurement values. With only one receiver, one value of v_0 provides two distance values according to the coupling effect and the shielding effect (as can be seen in Figure 2.9).

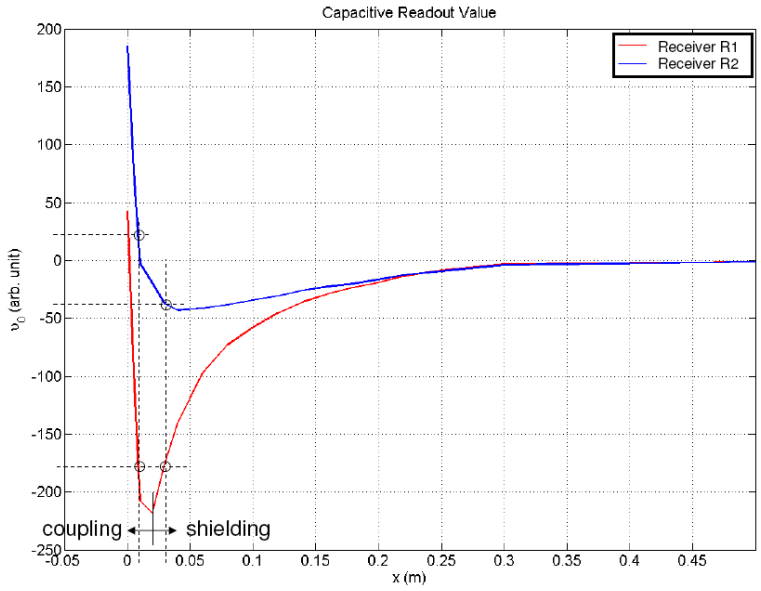

Figure 2.9: Output signal v_0 for an approaching object with two receiver electrodes R_1 and R_2 and one transmitter electrode T. R_1 is positioned closer to the receiver. Due to the shielding effect and the coupling effect, the capacitance change due to an approaching object is ambiguous (one output value v_0 belongs to two distance values x). Thus, at least two receiver electrodes are necessary to obtain an unique distance measurement.

Different objects will have different approaching signals (i.e. different values of v_0 for the same distance), due to their relative permittivity ϵ_r and their volume. Thus, with capacitive distance measurement, it is possible to distinguish between different objects. The more receiver electrodes are used, the better the distinction is, due to the unique footprint of every object class (e.g. humans, trees, fences, other cars, etc.).

2.2.3 Discussion of Benefits and Drawbacks

With the theoretical considerations of this section, benefits and drawbacks of the capacitive distance measurement for automotive applications are briefly discussed.

Benefits

- Object detection and classification is possible.
- Cheap sensors (a metal electrode can be used as a sensor).
- Independence of object surface (only the volume and the relative permittivity ϵ_r influence the electric field, produced by the electrodes).
- Easy integration into the test object (i.e. vehicle bumper), due to the possible flexible design of the sensor electrodes.

Drawbacks

- Short sensor range for parking aids ($< 0.3\,\mathrm{m}$), due to the short range of the electric field (with respect to EMC guidelines).
- Measurement sensitivity depends on object material properties (the influence on the electric field is, among others, depended on the relative permittivity ϵ_r of the object).
- Need of simulation (e.g. Finite Element Analysis (FEA)) or high number of fact finding measurements to observe all cross sensitivities.
- Sophisticated electronic circuitry for the sensor front to reduce all possible influences such as shunt capacitances, disturber crosstalk, or electrostatic discharge.

2.3 Concept for a Sensor Fusion System

With the theoretical background given in this chapter, expectations for a sensor fusion system consisting of ultrasonic and capacitive sensors are made. Table 2.1 lists requirements for automotive parking aids and how they are covered by the two different sensor systems and a sensor fusion system. It is assumed that the ultrasonic sensor configuration uses four sensors per bumper as it is common for automotive applications.

Expectations for a sensor fusion system for automotive parking aids			
	Ultrasonic	Capacitive	Sensor fusion [4]
Distance	$0.2 - 2\,\mathrm{m}$	$0 - 0.5\,\mathrm{m}$	$0 - 2\,\mathrm{m}$
Blind spots	Between sensors for $d < 0.3\,\mathrm{m}$	No	No
Measurement rate	Low	High	Depending on distance
Material classification	No	Yes (relative permittivity ϵ_r)	Yes
Dependent on object inclination	Yes	No	No
Influence of dirt on sensor	High	Low	Low
Influence of Rain	Low-Medium	Low	Low
Influence of Snow	Medium	Low	Low
Active pedestrian safety possible	No	Possible	Possible
Costs	Low	Low	Low

Table 2.1: Expectations for a sensor fusion system for parking aids.

As can be seen in Table 2.1 the sensor fusion of capacitive and ultrasonic sensors would solve many disadvantages of one single sensor system. Thus, this work provides a sensor fusion system and determines the expectations in this section through experimental investigations.

[4] The sensor fusion can use both measurements only in the overlapping range. Beyond this range the properties of the single sensor system apply.

Chapter 3

Rapid Prototyping Platforms

To prove the expectations in Chapter 2.3, an implementation of a Rapid Prototyping System is discussed in this chapter. For the capacitive measurement two techniques are used, which both will be presented in this chapter:

i) Capacitive Measurement with capacitive to digital converter (CapIC).

ii) Capacitive Measurement with Analog Devices IC AD7143.

The Rapid Prototyping System (RPS) is modularly designed and consists of the following modular constructed hardware components:

- Host computer with postprocessing Software.
- Micro controller board based on an Atmel AT90CAN128.
- Printed Circuit Board (PCB) with CapIC.
- PCB with AD7143.
- US sensors with an Electronic Control Unit (ECU) from Valeo.

The block diagram in Figure 3.1 shows the connection of the components and how they work together. The particular hardware parts are described in the following sections.

3.1 Design Software

The development of the hardware was done with the Computed Aided Design (CAD) software *Eagle-5.1.0*. All designed schematics, layouts, and list of components can be found in the Appendix B.

3.2 Prototype Requirements

In Table 3.1 the main properties and requirements for the developed system are shown. The whole rapid prototyping hardware was not only designed for test purposes of the sensor fusion system (described in Chapter 2), but also to implement it in an experimental vehicle (1 : 5 remote controlled model-car, refer to [SMG07]).

Prototype Requirements and Properties	
Supply voltage	12 V
Communication with host	Controller Area Network (CAN) protocol
Sensor range	$0 - 2$ m
Measurement rate	max. 25 ms for AD7143 (depending on decimation rate) $\approx 20\,\mu$s for CapIC (for one electrode measurement)
Number of electrodes for capacitive measurement	8 for AD7143 16 for CapIC
Resolution	16 Bit for AD7143 ($\Sigma\Delta$ ADC) 12 Bit for CapIC (successive approximation ADC)
Assembly	modular and easy demountable

Table 3.1: Prototype Requirements.

3.3 Prototype Design and System Overview

Figure 3.1 shows the concept of the measurement system. It basically comprises the host computer to analyze the measurement data and control the sensor devices. The capacitive measurement units (CapIC or AD7143) are connected to a micro controller board and the capacitive sensors. The micro controller board is connected to the host computer over a CAN bus. The US sensors are controlled through an ECU, which establishes the connection to the host computer.

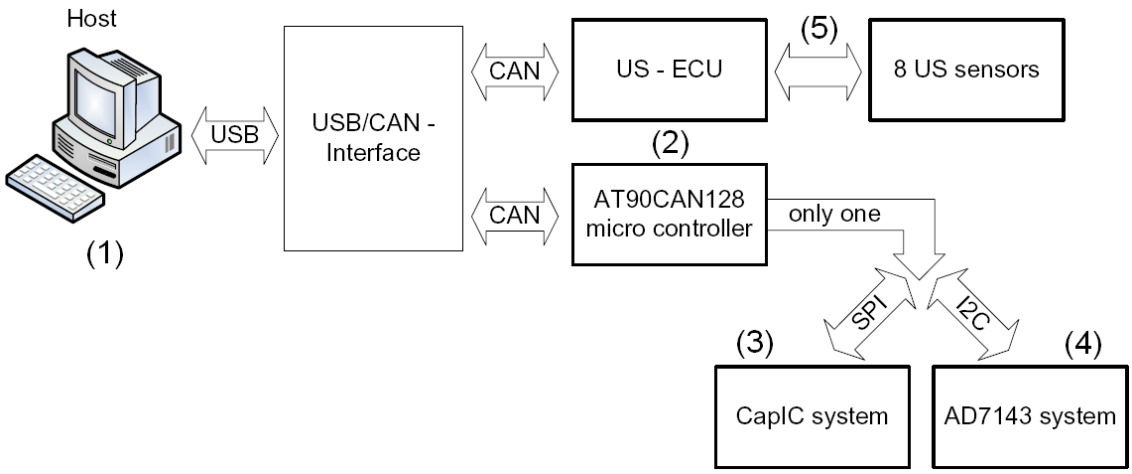

Figure 3.1: Block diagram of the constructed rapid prototyping system. Only one of the capacitive measurement systems can be used at one time. (1) Host computer for analyzing and combining the measurement results. (2) Main board with the micro controller, CAN, SPI, and I^2C transceivers for communication with the host and the capacitive measuring systems. (3) Capacitive sensor with CapIC. (4) Capacitive Sensor with AD7143. (5) Sensors and ECU for ultrasonic distance measurements.

3.4 Micro Controller Board

The micro controller board for the capacitive measurements is equipped with a micro-controller AT90CAN128 from Atmel [Atm07] and a CAN Transceiver for communication purposes with the host computer. All unused pins are connected with two male multipoint connectors for optional use. In Figure 3.2, the top view of the PCB with all its components can be seen.

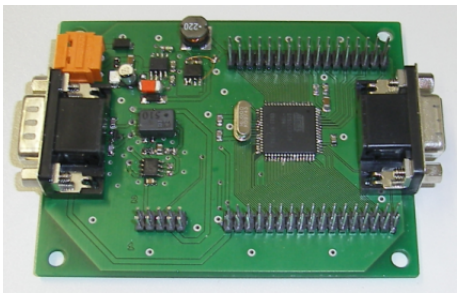

Figure 3.2: Photography of the micro controller board for capacitive measurements with equipped Atmel AT90CAN128, CAN Transceiver, two male multipoint connectors, and the power supply.

3.4.1 Hardware Requirements

The requirements for the main board are shown in Table 3.2.

Micro Controller Requirements	
Supply voltage	12 V
Communication with host	CAN Bus
Communication with clients	SPI (CapIC) I^2C (AD7143)
CAN Bus	Protection against noise and external disturbances
Assembly	Useable for an experimental vehicle (see [SMG07])

Table 3.2: Requirements for the micro controller board.

3.4.2 Major Circuitry Parts

A design constraint of the circuitry is to provide an interference free CAN-Bus. Thus, communication to the host computer with a high data rate (up to 1 Mbit/sec) independent from the environment should be possible.

As can be seen in Figure 3.3 the CAN transceiver and bus are protected by the following components (according to [NXP06]):

Common Mode Choke (CMC) Reduction of Electro Magnetic Interferences (EMI).

Electro Static Discharge (ESD) diodes Protection of the circuitry from ESD pulses up to 15 kV.

Bypass capacitors Avoidance of high current peaks.

Split termination Provides a higher reduction of emission than the usual 120 Ω bus termination.

Other components on the main board are:

- Step down converter MAX1649 for the 5 V supply voltage [Max05].
- Different multipin connectors for I/O pins, In System Programmer (ISP) [Atm07], and CAN connectors.

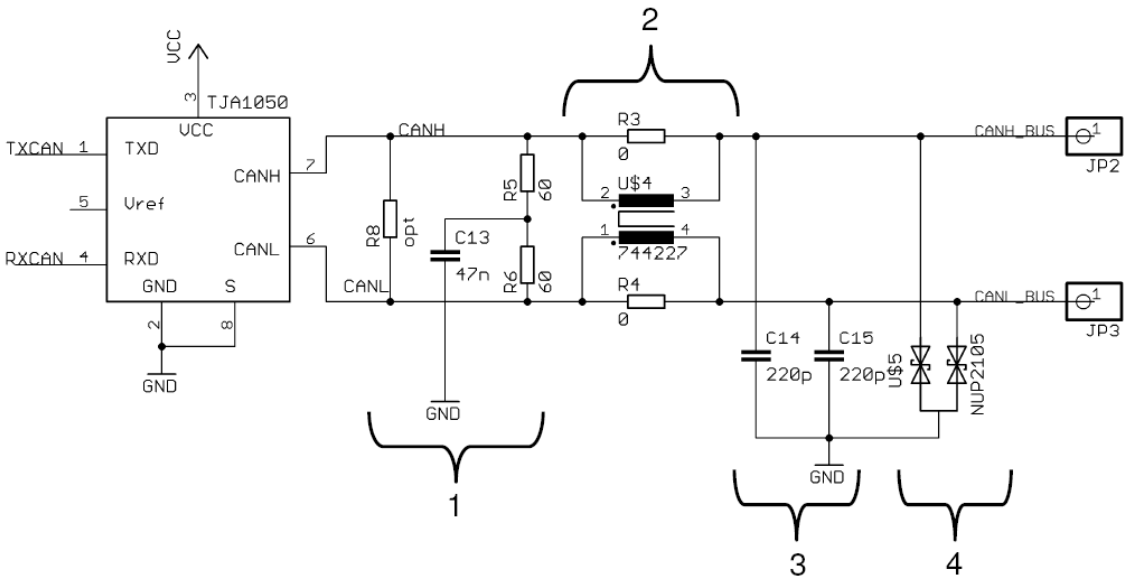

Figure 3.3: Schematic of the CAN transceiver with components required to provide robustness against external disturbances. (1) Split termination for an effective reduction of electro magnetic emissions. (2) Common mode choke to reduce electro magnetic interferences. (3) Bypass capacitors for avoiding high current peaks. (4) Electro Static Discharge diodes to protect the circuitry from voltage pulses up to 15 kV [NXP06].

3.5 Capacitive Front-End IC and External Electrodes

For capacitive measurement a new integrated capacitive sensor interface (CapIC) was developed at the Christian Doppler Laboratory for Automotive Measurement Research (refer to [BZH+08] and [BZM+08]). This capacitive to digital converter IC is used to implement a new way of distance and object measurement for automotive applications. This section gives an overview of the CapIC device and how it is used in this work.

3.5.1 System Concept and Theory of Operation

The block diagram in Figure 3.4 shows the capacitive measurement setup with CapIC. The power supply is done by the Low Dropout Regulator (LDO) MIC5235, which generates three voltages (5 V, 2.5 V, and 1.25 V) out of 12 V (from the micro controller board or a battery).

CapIC measures the displacement current through the coupling capacitance between the transmitter and the receiver electrode (compare Chapter 2.2).

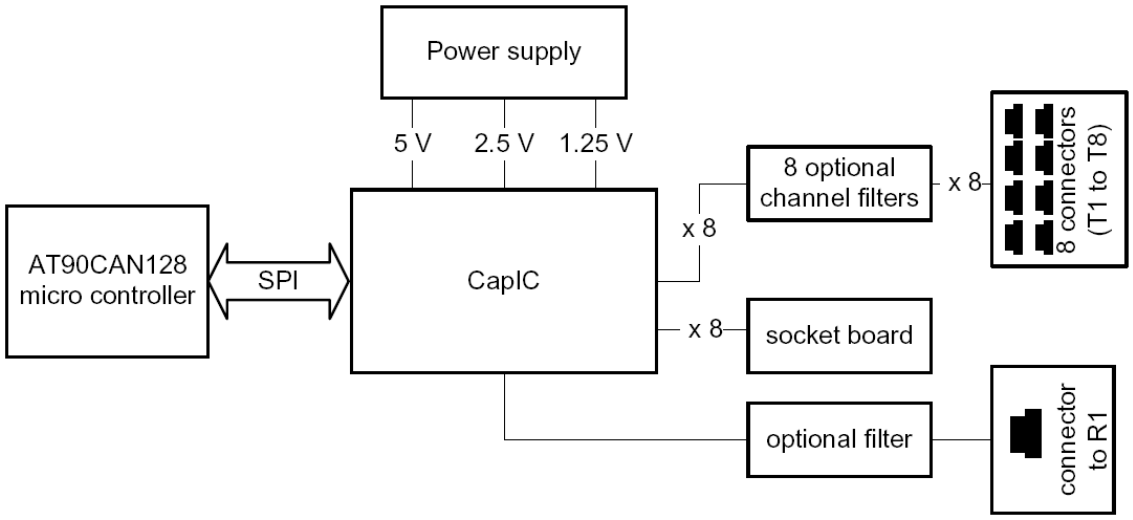

Figure 3.4: Block diagram of the distance measurement system using CapIC with one receiving electrode (R1), up to eight transmitting electrodes (T1 - T8), a socket board for the other eight (not used) transmitting electrodes, the power supply for CapIC, and the SPI connection to the micro controller AT90CAN128.

Figure 3.5 shows the demodulator circuitry of CapIC, which is attached to the sensor front end with several transmitting electrodes and one receiving electrode. The transmitting electrodes are selected with the excitation signal through a Time Division Multiple Access (TDMA) system. The LC filter shown in Figure 3.5 stands for a voltage to current converter. The virtual ground of this converter is connected to the receiver electrode. After the signal is pre amplified it is multiplied with the carrier for the I channel and with a 90° phase shifted carrier for the Q channel. With an offset compensation and a gain setting through a Programmable Gain Amplifier (PGA) the Full Scale Range (FSR) of a following Analog to Digital Converter (ADC) can be used [BZM+08].

3.5.2 Details of the Implementation

Figure 3.6 shows the developed PCB for CapIC. CapIC is able to handle up to 16 transmitting electrodes. The circuitry developed in this work is equipped with eight connectors. The other eight channels are connected to a socket board. The complete schematic and layout can be found in the Appendix B. In the following sections, the main parts of the circuitry are discussed.

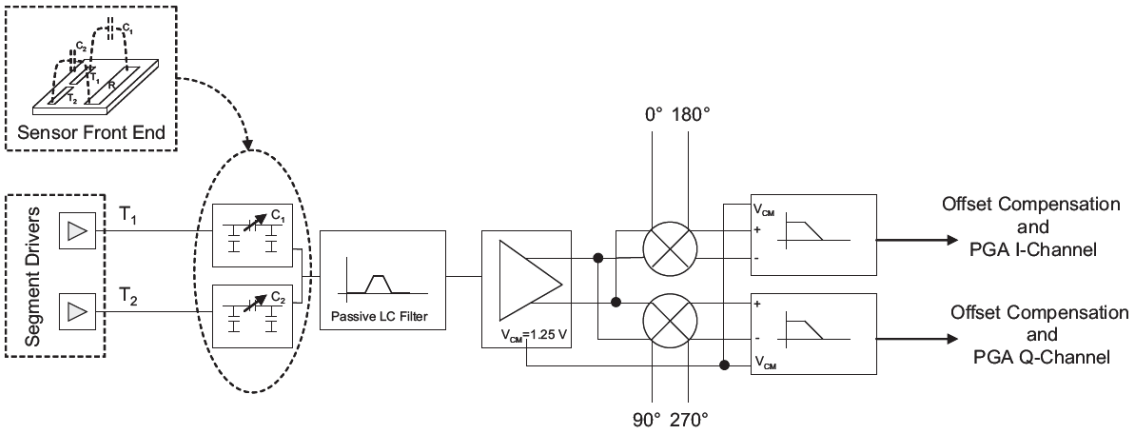

Figure 3.5: Block diagram of the demodulator circuitry for two transmitting electrodes (T1 and T2) and one receiving electrode (R1) [BZM+08]. For further details, refer to the text.

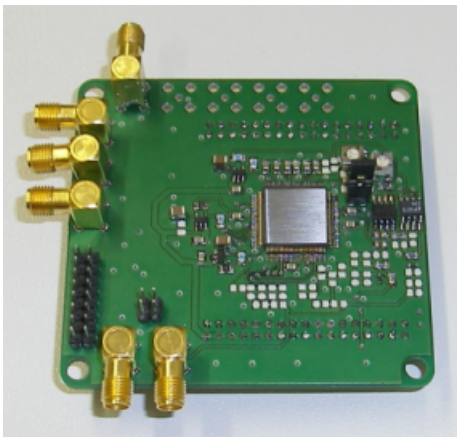

Figure 3.6: Photography of the developed PCB for CapIC.

Constant Current Source

Figure 3.7(a) shows the constant current source, which is used to provide an adjustable current in the I_{REF} pin. The LM334 IC [Lin01] is a widely used Constant Current Source and Temperature Sensor. The current of 50 μA is adjusted with the resistor $R29$.

CapIC Output Channel Filters

To obtain low costs and a high number of transmitter elements for CapIC, the elements have to be rather simple [ZBHW08]. Thus the transmitters elements are digital output stages. Harmonics of the carrier frequency (= 2 MHz in this work) due to the digital outputs are unwanted (e.g. distortion of the measurement) and have to be reduced. This

is achieved by means of output channel filters, which are shown in Figure 3.7(b). For each of the eight channels (transmitting electrodes) one filter is required. Such filter consist of a parallel resonant LC circuitry and a resistor that affects the bandwidth. Figure 3.8

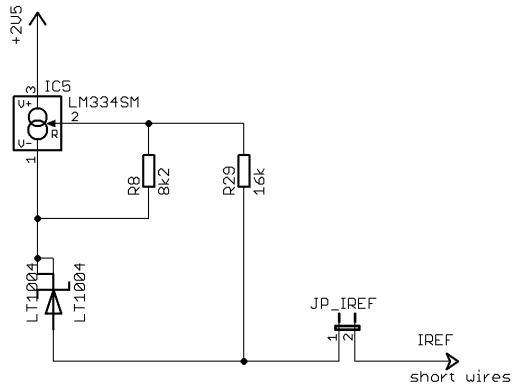

(a) Constant current source of the CapIC circuitry.

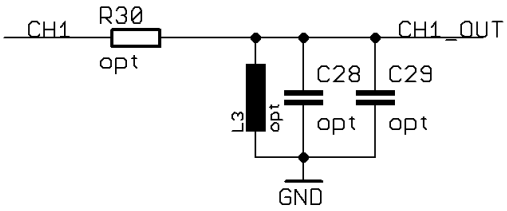

(b) Optional channel filters for CapIC.

Figure 3.7: Relevant parts of external circuitry. (a) Constant current source for CapIC circuitry for I_{REF} pin of the CapIC. (b) One output channel filter. CH1 is connected with CapIC output and CH1_OUT with the electrode. This circuitry is applied to each of the eight used channel inputs.

shows an AC analysis of the channel filter. As can be seen, the parallel resonant circuitry has a bandpass behavior with the resonance frequency at 2 MHz as desired (equals the carrier frequency of CapIC).

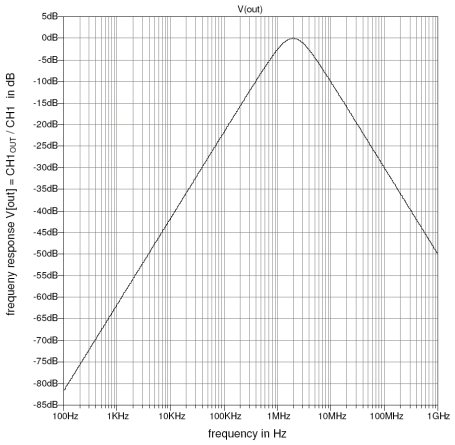

Figure 3.8: Frequency response of a channel filter. Resonance frequency is 2 MHz, which is also the frequency of the excitation source in this work.

Frontend Filter

The frontend filter, shown in Figure 3.9, protects the receiver (input pin `FRONTEND_IN`) from

- ESD voltages.
- External Disturbances.
- Bias currents.

and reduces harmonics from the excitation source.

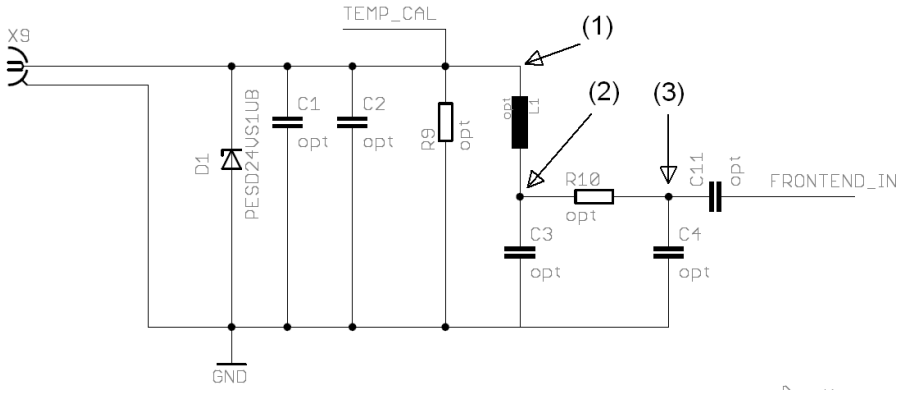

Figure 3.9: Frontend filter circuitry. (1) Voltage point after the parallel resonant circuitry. (2) With the capacitance $C3$ additional attenuation of higher frequencies is reached. (3) Final voltage point, which is connected to the CapIC receiver input (through the DC blocking capacitance $C11$). A low pass filter enforces the effect of $C3$.

$D1$ is a Transient Voltage Suppressor (TVS) diode, which protects the CapIC input from voltage spikes induced by external disturbances.

Figure 3.10 shows the frequency response of three voltages for a given excitation signal of the transmitter. $C1$, $C2$, $R9$, and $L1$ build a parallel resonant circuitry. With higher frequencies ($f > 4\,\text{MHz}$) the capacitances $C1$ and $C2$ behave like a short circuitry. This results in a static attenuation and $V[1]$ in Figure 3.10) for higher frequencies. With a capacitance $C3$ connected in series to $L1$ this effect can be minimized ($V[2]$) and the extinction increases with higher frequency (for $f > 4\,\text{MHz}$). The low pass filter provides additional attenuation as shown for $V[3]$ in Figure 3.10. The capacitance $C11$ works as a DC blocker for the amplifier input of the receiver.

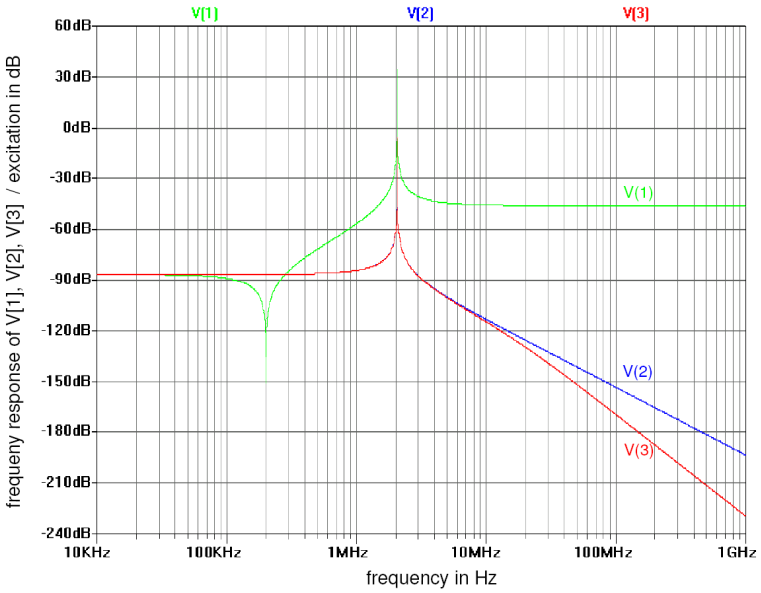

Figure 3.10: Frequency response of the frontend filter. Three frequency responses of interest according to the three measuring points V(1), V(2), and V(3) in the circuitry in Figure 3.9. V(1) shows the frequency response after the parallel LC circuitry. The first peak occurs from the serial LC circuitry ($L1$ and $C3$). In V(2) an additional capacitance is used to provide additional attenuation with higher frequencies. With a low pass filter, V(3) provides an even higher attenuation.

Implementation of Reference Capacitances for Temperature Calibration

Since the CapIC amplifiers are not temperature stabilized, a temperature calibration is necessary. Without calibration, the capacitance measurement would show a considerable offset and gain change. Figure 3.11 shows the effects. The gain of the amplifiers increases with higher temperature in the measurement range of CapIC ($C_{max} - C_{min}$). Thus, the CapIC measurement error increases for the measured capacitances.

To overcome this effect, a circuitry, which simulates two capacitances C_{nom1} and C_{nom2} is connected to CapIC. Figure 3.12 shows this circuitry part. The digital values for C_{min} and C_{max} are measured at room temperature and stored. Before every measurement, CapIC performs the temperature calibration through the following steps (according to [BZB09]):

i) Excitation at pin `SEG_OUT8`.

ii) Measurement of C_{min} at pin `FRONTEND_IN` (connected with the net `TEMP_CAL` in Figure 3.12 and 3.9).

iii) Excitation at pin `SEG_OUT9`.

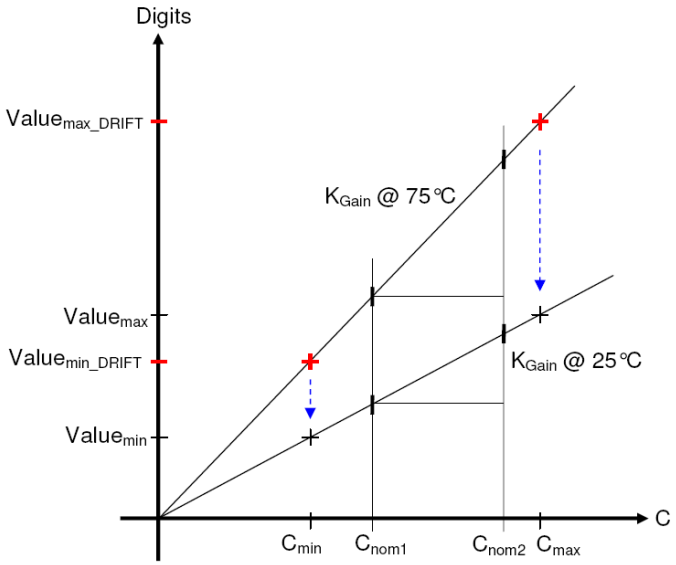

Figure 3.11: Gain characteristic curve of CapIC as function of input capacitance for two temperatures.

iv) Measurement of C_{max} at pin `FRONTEND_IN`.

v) Calculation of gain correction with respect to room temperature (see Figure 3.11).

After the temperature calibration every measurement is corrected and thus, independent of the ambient temperature.

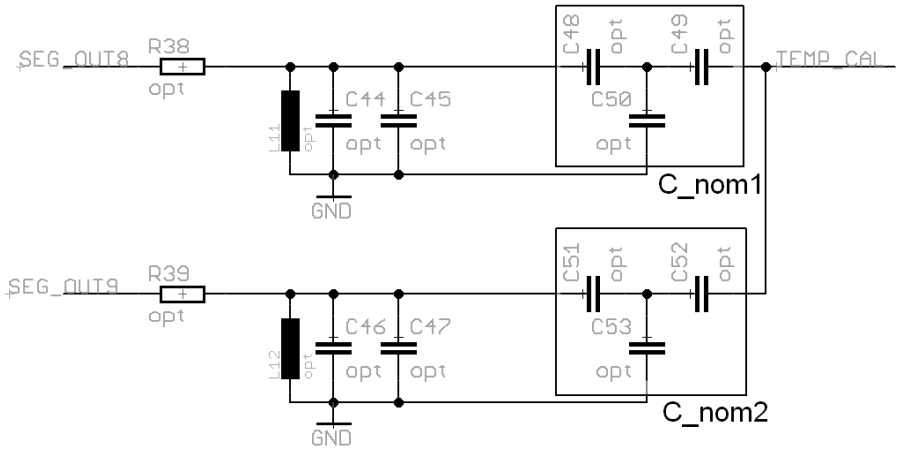

Figure 3.12: Schematic of the optional temperature calibration.

For a temperature calibration on the same terms with measurement conditions, the same channel filters have to be used, as are used for the output channels (Figure 3.9 and 3.12). The six capacitances $C48$,$C49$,$C50$ and $C51$,$C52$,$C53$ which form C_{nom1} and C_{nom2}, have

to be stable for temperature changes. Otherwise, the measured capacitance will change due to temperature changes. As can be seen from Figure 3.11 an offset change (due to temperature change) must not occur to get a correct temperature calibration [BZB09].

3.6 Analog Devices IC AD7143 with External Electrodes

Analog Devices provides capacitive measurement ICs. In this work the AD7143 (according to [Ana07]) is used similarly to CapIC in Section 3.5. The board of the Analog Devices IC AD7143 comprises of following components:

- AD7143 IC [Ana07].
- Low Drop-Out (LDO) Regulator [Mic05].
- Different plugs to connect to the main board and the electrodes.

3.6.1 System Concept and Theory of Operation

According to [Ana07], the AD7143 is a capacitive to digital converter (CDC) with environmental calibration integrated in the chip. The most important properties are listed in Table 3.3. As can be seen in Figure 3.13 the eight sensor inputs are connected to a

AD7143 Properties	
Supply voltage	$2.6\,\mathrm{V} - 3.6\,\mathrm{V}$
Communication with host	I^2C Bus
Update Rate	25 ms
Number of sensor inputs	8
Resolution	16 Bit
FSR	$\pm 2\,\mathrm{pF}$
Excitation Source frequency	250 kHz
Capacitive to Digital Converter (CDC)	250 kHz Sigma Delta ($\Sigma\Delta$) converter

Table 3.3: Properties of the Analog Devices IC AD7143.

switch matrix in the AD7143. This switch connects each input to a 16 Bit $\Sigma\Delta$-CDC, which stores the value in the on-chip registers. The host (e.g. a micro controller) reads the stored value over the I^2C interface. Additionally, the chip can be configured through the on-chip registers for averaging, offset compensation, and different gains.

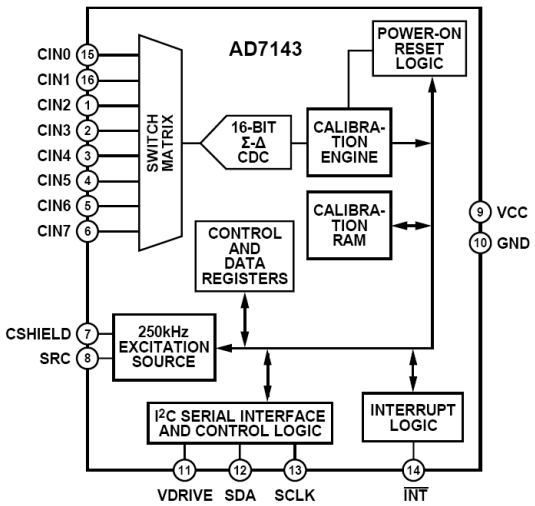

Figure 3.13: Functional block diagram of the AD7143 IC. Explanation of the function can be found in Section 3.6.1 (according to [Ana07]).

Capacitive-to-Digital Converter

As explained above, the AD7143 has the possibility for an offset and average control. The two options and the depending times for a capacitive to digital conversion of one electrode can be seen in Table 3.4. The more sensors are used the more time one measurement

CDC Averaging Properties	
Averaging Samples	CDC Output Rate Per Sensor
384	1.525 ms
768	3.072 ms

Table 3.4: AD7143 CDC averaging properties and depending output rate of one electrode.

cycle needs (also depending on the number of sample averages). The maximum time one measurement cycle needs to complete is shown in calculation 3.1 for a decimation rate of 256 and the usage of all eight sensors.

$$Time_{max} = Count_{Sensors} * Outputrate_{CDC} = 8 * 3.072 = 24.576\,\text{ms} \tag{3.1}$$

The times above are only valid when operating the AD7143 in full power mode. There is also the possibility to run the chip in different low power modes. For further details see [Ana07].

3.6.2 Details of the Implementation

A photography in Figure 3.14 shows the developed PCB for the capacitive distance measurement system with the AD7143 IC.

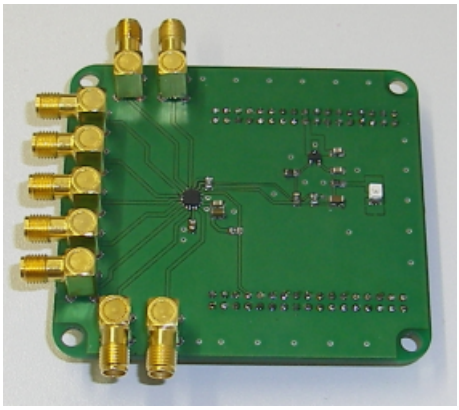

Figure 3.14: Photography of the developed PCB for the AD7143.

The main part of the AD7143 schematic is shown in Figure 3.15. The interrupt function (pin INTQ) of the AD7143 is not used in this work because the host (micro controller) initiates the readout of the measurement (for more information refer to Chapter 4.3). The receiving electrodes are connected to CIN0 to CIN7. SRC is the connection for the transmitting electrode (CDC excitation source output) and CSHIELD (CDC shield potential output) has to be connected to GND through a 10 nF capacitor. The two I^2C bus lines are connected to SCLK and SDA with two pull up resistor to +3.3 V.

3.7 Ultrasonic Sensor and Evaluation Hardware

For the ultrasonic measurements a sensor system from Valeo, which is commercially available e.g. in systems from the vehicle manufacturer BMW, was used. The following sections give an overview of the system, describe the major parts of the test arrangement, and the principle of operation.

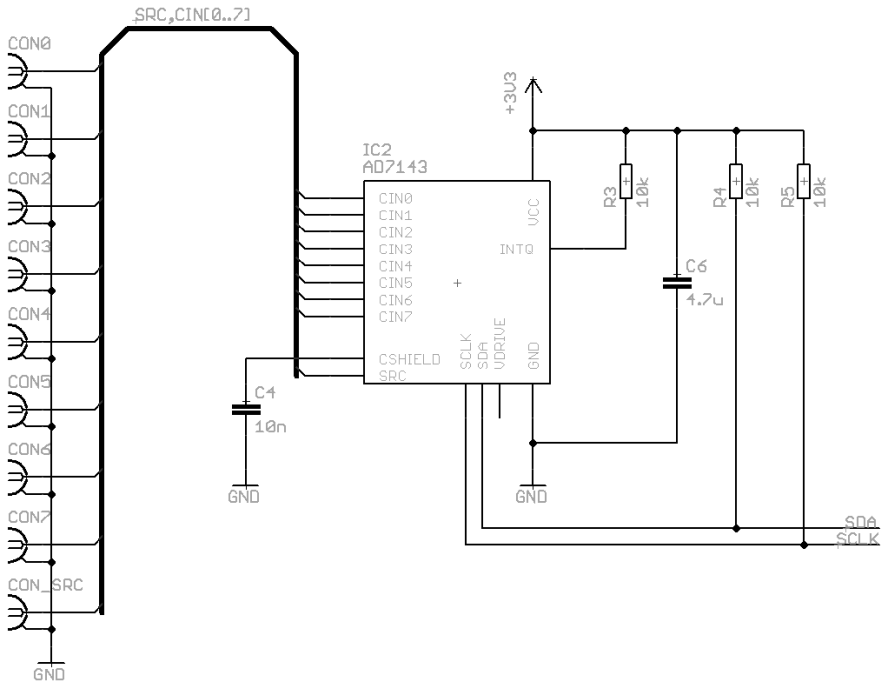

Figure 3.15: Part of the schematic of the AD7143 implementation. CIN0 to CIN7 are connected to the electrodes, which operate as receivers and SRC connects to the electrode operating as transmitter. The pin CSHIELD connects the CDC shield potential output to ground through a 10 nF capacity. SDA and SCLK are the two I^2C bus lines and INTQ is the interrupt output of the AD7143, which is not used.

3.7.1 System Overview

As can be seen from the block diagram in Figure 3.16 the ultrasonic measurement system comprises of

- 8 ultrasonic sensors.
- Ultrasonic Electronic Control Unit (ECU).
- Interface to connect the CAN bus of the vehicle with a host.

3.7.2 Theory of Operation

As described in Chapter 2.1 the ultrasonic measurement system works with a time-of-flight method. The BMW system has eight ultrasonic sensors for park distance control (PDC). Four sensors are used for the front side and four for the back side. These eight sensors are required to cover the whole working range for parking aids with vehicles.

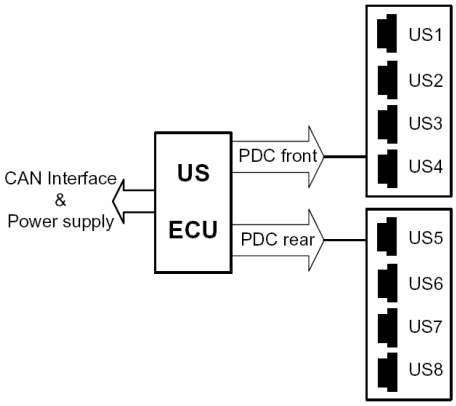

Figure 3.16: Block diagram of the ultrasonic measurement system. Four ultrasonic sensors are used for one Park Distance Control (PDC) at a time (front and rear).

In this work different impacts on the ultrasonic and capacitive measurement are tested, which is why mostly only one sensor out of the eight is used. This sensor is located at the front center right position (Figure 3.17). For blind spot detection the sensor at the front center left position is used additionally. Since the ultrasonic ECU does some signal

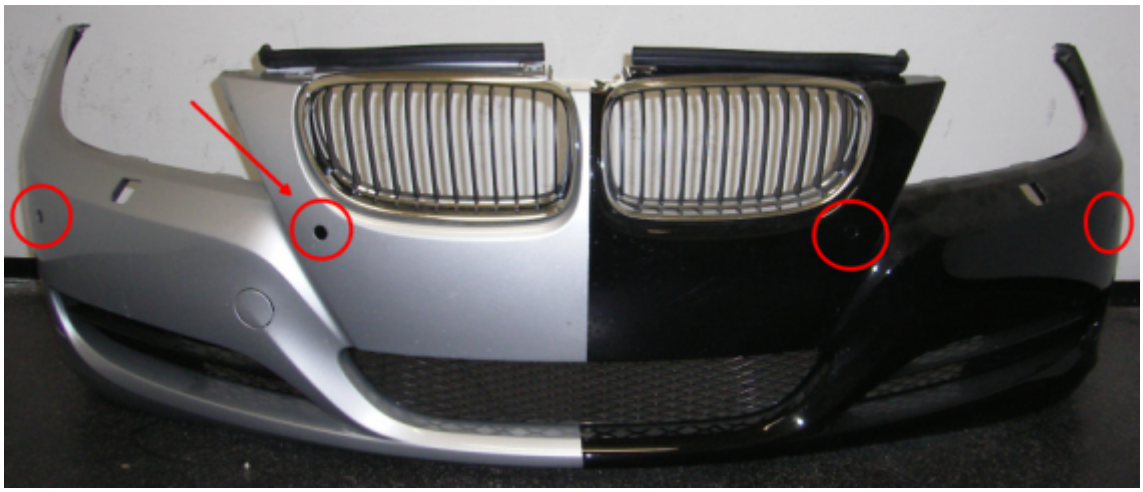

Figure 3.17: Vehicle bumper with the four front ultrasonic sensors. The measurement tests were done with the front center right sensor, which is marked.

processing and plausibility checks, the other three sensors on the side of the tested one (back or front) must not have an object in their measurement range during the investigations. Otherwise the ECU corrects the distances based on the plausibility checks. The ECU converts the time-of-flight data from the sensors to a distance. This distance value is transmitted using a CAN bus, where it can be read out under specified circumstances (explained in Chapter 4.4).

3.7.3 Details of the Implementation

Since the sensor arrangement originates from a vehicle, the original CAN interface has to be simulated. Otherwise the ultrasonic ECU will send error messages on the CAN bus and no distances can be read out from the host computer. To connect the ultrasonic ECU to a host computer, a NI USB-8472 from National Instruments ([Nat08]) is used.

The NI USB-8472 is connected to the ultrasonic ECU through the CAN Interface and connected to a host by the universal serial bus (USB). By applying the correct communication protocol with the US ECU, the ECU puts the calculated distances on the CAN bus. The values and their meaning are described in Table 3.5. The communication protocol of the host with the US ECU is described in Chapter 4.4.

Ultrasonic Distance Codes	
Code	Description
0...253	Distance to an object in cm.
254	Object is out of measurement range.
255	Sensor signal is not valid.

Table 3.5: Distance codes from the ultrasonic ECU, which are send over CAN bus.

Chapter 4

Implementation of the Software Framework

This chapter discusses all software aspects of this work. Two programs are needed to control the capacitive measurement system:

- Micro controller program (running on the Atmel AT90CAN128).
- LabView program (running on the host computer).

An overview of both programs is given and major parts of the implementation are discussed.

4.1 Description of the Framework

The framework comprises the functions to communicate with the AD7143 IC and CapIC over I2C bus and SPI bus, respectively. Also a CAN communication stack for communication with the host computer is implemented. A program overview is provided and detailed information on the implementation can be found in the Appendix A.

4.1.1 Program Overview

The flow diagram of the framework is depicted in Figure 4.1. After the program start and completion of all initialization processes, the main program waits for a CAN message. When a CAN message is received, the first byte of the eight byte long message is analyzed. The definition of the codes is described in Table A.2 in the appendix. The other seven bytes are not used.

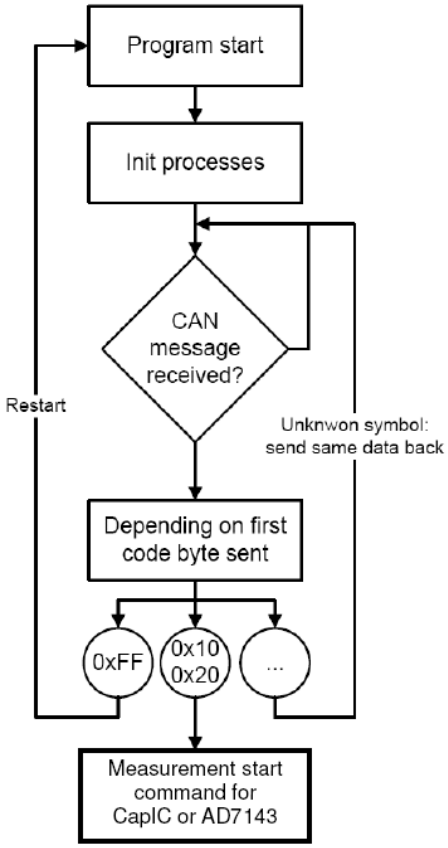

Figure 4.1: Block diagram of the software framework. After a CAN message has been received, the transmitted code is analyzed. Depending on this code and which IC is used (CapIC or AD7143), further commands are executed.

4.1.2 Major Parts of the Implementation

The CAN communication stack is the most important part of the framework. The parameter for the CAN bus, which have to be the same on the host computer and the micro controller, can be found in Table A.1 in the appendix. To implement the CAN protocol on the used micro controller AT90CAN128, the CAN library from Atmel is used. According to [Atm07] the four most important elements used from this library are summarized below.

- Structure `st_cmd_t`, which is the CAN message descriptor.
- Function `u8 can_cmd(st_cmd*)` to perform actions on the CAN bus.
- Function `u8 can_get_status(st_cmd*)` to get the status of the CAN message descriptor (described in the appendix in Figure A.1).
- Function `u8 can_init(u8 mode)` to initialize the CAN bus.

The message descriptor contains all information for the communication over the CAN bus. Figure A.1 in the appendix shows the structure of the message descriptor. It is the most important structure used in the main program.

4.2 CapIC Measurement Routines

In this section, the micro controller program for controlling the CapIC and the LabView host program to postprocess the capacitive values are described.

4.2.1 Software Concept

Figure 4.2 shows the main parts of the micro controller program flow. After the initialization of the CAN and the SPI bus, the micro controller sends the ready signal (hex command `0x22`) over the CAN bus.
Now the micro controller program waits for an user interaction. If the start command (hex `0x10`) is received from the host computer, the instruction for starting the measurement is send to CapIC. In addition, the interrupts are enabled. With the restart command (hex `0xFF`) the micro controller and CapIC are restarted. All other commands are send back and ignored. With the start command, the measurement sequence in CapIC is started. After the micro controller has read out all measurements (I and Q parts of all segments), it sends the data to the host computer. A more detailed description can be found in the following section and the Appendix A.2.1.

The LabView program, running on the host computer, is implemented as a state machine. Further details on the implementation of a state machine in LabView can be found in the Appendix A.2.2.

4.2.2 Details of the Implementation

Micro Controller Program

A major part of the micro controller program is the interrupt handling. CapIC always sends three interrupt signals if one measurement (I or Q part) is done. The signals arrive too fast at the micro controller to catch all of them. Hence, only the first and the second are catched (refer to [Atm07]).

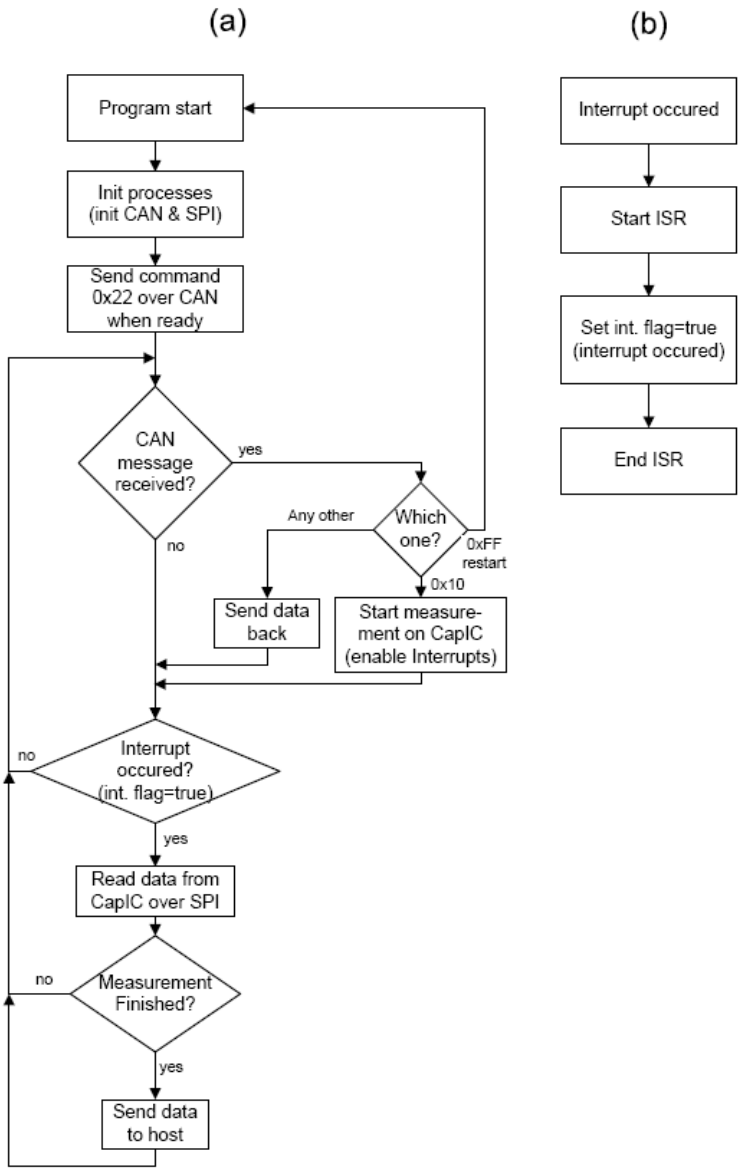

Figure 4.2: Program flow of the CapIC micro controller software program. (a) Main program procedure. (b) Interrupt service routine procedure.

After a finished measurement (I or Q part) CapIC waits for an acknowledge command over the SPI bus. Not till then the next measurement is started. This gives the micro controller program the time to read out the value of the measurement from CapIC. The acknowledge signal is send after the measurand was read out and temporally saved. Right after the measurement is finished (all segments are read out), the micro controller sends the data to the host computer over the CAN bus.

Because no other interrupts can be catched while the ISR is running, it is important to keep the ISR code very short. The listing of the ISR and the functions used to control CapIC can be found in the Appendix A.2.1.

Host Program for Analysing Results

The LabView programm is organized as a state machine. After the initialization state the program executes the following steps to get the capacitive measurements:

i) Write the command for `start measurement` on the CAN bus.

ii) Wait 100 ms.

iii) Read out all data from the CAN bus.

After the read out, all measurements are shown in a waveform chart. More details and a part of the listing of the LabView program can be found in the Appendix A.2.2.

4.3 AD7143 IC Measurement Routines

This section gives an overview of the software procedures to control the AD7143 IC. Important details on the software code are discussed in the following.

4.3.1 Software Concept

Figure 4.3 shows the program flow of the micro controller program. Different to the CapIC program, no interrupts are used in the AD7143 software. The measurement rate is defined by the host computer (limited by the AD7143 specifications defined in [Ana07]). With every `start measurement` command, one measurement value is read out and send back over the CAN bus.

The LabView program on the host computer works within a state machine similar to the CapIC software (refer to Figure A.3 in the appendix). The important differences are shown in the following section.

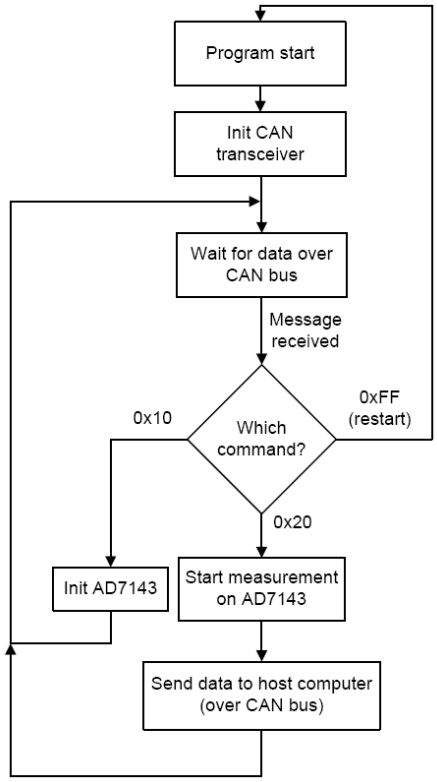

Figure 4.3: Program flow of the AD7143 micro controller software process. No interrupts are used and the measurement rate is defined by the host computer over the CAN bus.

4.3.2 Details of the Implementation

Description of the Micro Controller Program

An important part of the micro controller program is the initialization of the AD7143. A listing of this function can be found in the Appendix A.3.1. According to [Atm07] the I^2C bus is called Two Wire Interface (TWI) but has the same functionality. After the initialization step the program waits for the `measurement execute` command from the host computer. After this execute command (hex `0x10`) was send over the CAN bus, the micro controller sends commands to the AD7143. In a next step the capacitive measurement results are read out over the TWI and send back to the host computer.

Description of the Host Program for Analyzing Results

The procedure of the LabView program to control the micro controller and the AD7143 is described in Appendix A.3.2. Because the AD7143 needs an initialization step, the state diagram in the LabView program comprises the of following parts:

- Initialization (for CAN bus).
- Wait (waiting for user interaction).
- InitAD7143 (initialization step for AD7143).
- MeasureAD7143 (measure and reading command for capacitive measurements with the AD7143).
- Stop (close all connections and the program).

The major part of the LabView implementation is described in the Appendix A.3.2 and in Figure A.4.

4.4 Ultrasonic Measurement Routines

The US measurement is performed with an US system from Valeo on a BMW bumper. (compare Chapter 3.7). The following section describes the host software concept and the CAN bus to simulate this car environment.

4.4.1 Host Software Concept

The host computer is connected to the US ECU via a CAN interface (refer to Chapter 3.7.1). A LabView program is running on the host computer, which simulates the vehicle CAN bus environment. The reason for the necessariness and an example of a simulation of the car environment is given in the following section. An exemplary frame of the LabView program is shown in Figure 4.4. First, the CAN bus has to be initialized. In a second step all CAN data frames are send to simulate the car environment (refer to Appendix A.4.1). Accordingly, the CAN bus is read out for the measurement data (also called Park Distance Control (PDC) values). This is repeated until the program is stopped and the CAN bus is closed through a user interaction.

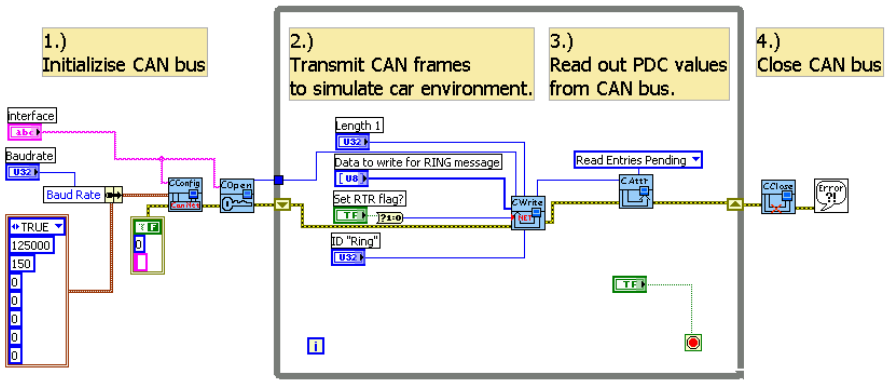

Figure 4.4: Exemplary Frame of a LabView program with four steps to simulate a car environment and read out the measurement data from the US ECU.

4.4.2 Significant Parts of the Implementation

The used ultrasonic sensors and the ultrasonic ECU from Valeo are for commercial use, e.g. in the car bumpers from BMW. As already described in Chapter 3.7, the ECU does some signal processing and plausibility checks. One plausibility check tests the functionality of the CAN bus in which it is normally used (a car CAN bus with other members). Therefore, a token ring message is received and send from member to member on the car CAN bus. To use the ultrasonic ECU as a stand alone device, this token ring message has to be generated by the host computer and send to the ECU in defined intervals to keep the ECU alive. Otherwise the ECU would generate error messages and and stop sending the distance measurements from the sensors.

The most important LabView implementations and all messages, to keep the ultrasonic ECU alive, can be found in the Appendix A.4.2.

Chapter 5

Measurement Results and Validation

This chapter describes the experimental investigations of the ultrasonic and the capacitive measurement principle. Impacts on the measurements due to external disturbances are discussed. The sensor fusion concept, which is based on a Kalman filter is explained and its results are provided and discussed. An evaluation of the proposed novel concept closes this chapter.

5.1 Measurements with the Ultrasonic Sensor

For the experimental investigations on the ultrasonic sensors, different measurement setups and different test objects were used. In the first section, a description of the measurement setup is given, followed by the measurement results and their discussion.

5.1.1 Measurement Setup

For distance measurement, one ultrasonic sensor of the sensor array is used (compare Figure 5.1). The influences of external disturbances (e.g. rain, ice, dirt, etc.) on the ultrasonic sensors are also tested with the same sensor. The blind spot detection test is carried out with the two sensors nearest to the center. Both measurement setups are shown and explained in Figure 5.1. For a detailed explanation of the electronics of the measurement setup refer to Chapter 3.7. For distance measurements, different objects were used to test the ultrasonic sensor.

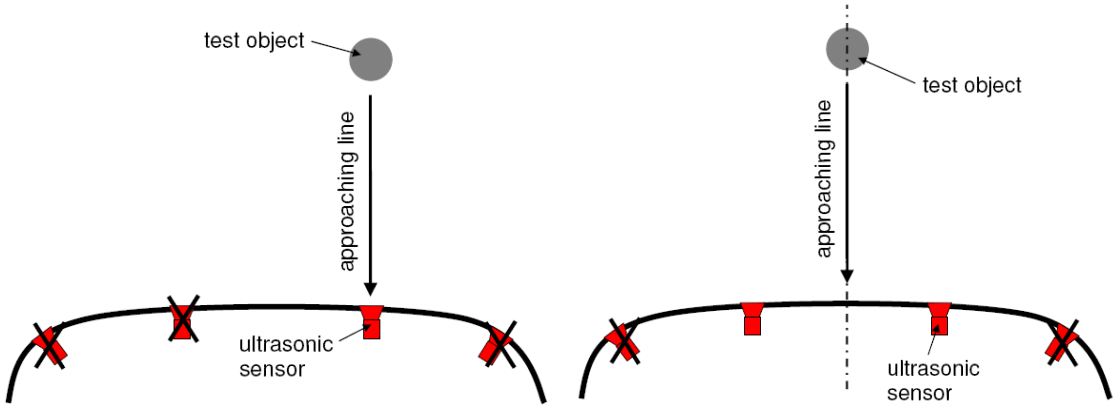

(a) Ultrasonic distance measurement setup.

(b) Ultrasonic measurement setup for blind spot detection.

Figure 5.1: Ultrasonic measurement setup (not in scale). (a) Setup for distance measurements and measurements with external disturbances. One ultrasonic sensors is used. (b) Measurement setup for blind spot detection. Two ultrasonic sensors are used to search for blind spots.

The following test cases are considered:

- Plastic pipe, empty (diameter: 0.07 m, height: 1 m).
- Plastic pipe filled with gravel.
- Plastic pipe filled with water.
- Round kerbstone (diameter: 0.25 m, height:0.3 m).
- Metallic trolley (*length* × *width* × *height* - 0.5 m × 0.6 m × 0.7 m).
- Metallic trolley, same as above, 45° inclination with respect to the approaching line.
- Wire mesh fence (*length* × *height* - 1 m × 1.5 m, electrically floating, fence tile of 50 mm × 100 mm, a wire diameter of 2 mm).
- Snow pile (height ≈ 1 m, diameter ≈ 0.2 m).

Figure 5.2 shows photos of the different test cases. The distance from the ultrasonic sensor on the vehicle bumper to the approaching object was determined with a measuring tape.

5.1.2 Measurement Results

The different measurement results for the different approaching objects are shown in Figure 5.3. As pointed out in Chapter 2.1, ultrasonic distance measurements are influenced by the surface of an approaching object, but are not influenced by the material of the

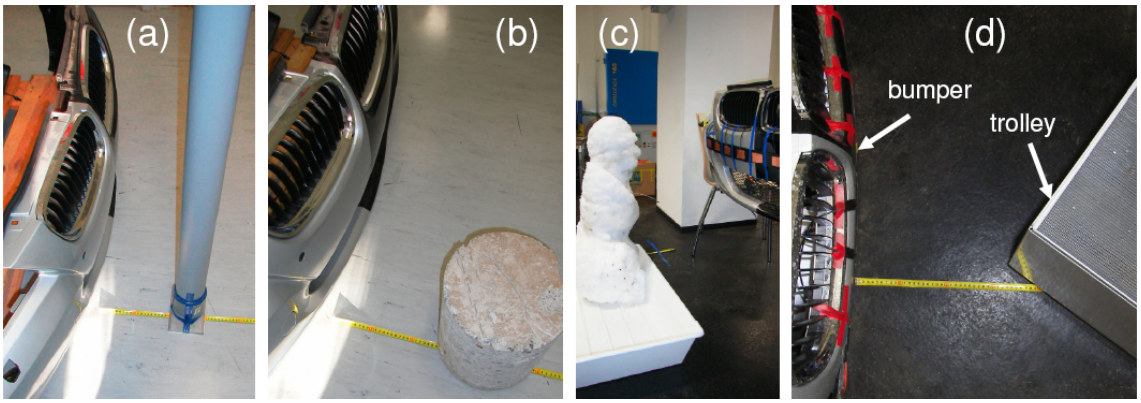

Figure 5.2: Photographs of the different measurement setups. (a) Measuring the distance to an approaching pipe. (b) Distance measurement with a kerbstone. (c) Setup with a snow pile. (d) Setup with a metallic trolley with 45° of inclination.

object. Thus, as can be seen in Figure 5.3, the measurement results for a plastic pipe with different content (air, stones, or water) are nearly the same. Also the measured trolley with metal surface provides the same measurement results. Below a distance of 0.2 m, no US measurement can be taken (compare also Chapter 2.1).

As shown in Figure 5.3, with the fence or the kerbstone in front of the bumper, the US measurement system does not provide very accurate measurement results. With the kerbstone, the provided distances are always longer than the true distances. This is because the kerbstone has not the same height as the sensor interface. Because of the height difference, the sound wave has to travel a longer distance and a longer travel time is measured (which results in a longer distance). For the fence, accurate distance measurements are only delivered for distances below 0.5 m. The thin wires, the fence is made of, prevent an accurate measurement for farther distances.

For the 45° inclined trolley (refer to Figure 5.1) the maximum measurement range reduces to 0.6 m. Due to the inclination, the main axis of the propagation direction of the ultrasonic waves does not point back to the sensor, but in some distance away from the sensor (as shown in Figure 2.4). Thus, the maximum sensing range reduces (the theoretical background was discussed in Chapter 2.1). The standard deviation of the measurements shows high values for distances between 0.5 m and 0.6 m. At these distances the US ECU is not able to calculate a stable distance.

A snow pile can be detected up to 0.8 m. The snow prevents a good reflection of the ultrasonic waves. The waves are scattered at the surface of the snow pile and only a part of the echo reaches the transceiver. Thus, a reduced sonic pressure reaches the receiver and the maximum sensing range is reduced. At distances between 0.6 m and 0.8 m, the standard deviation is higher for the same reason as for the inclined metallic trolley.

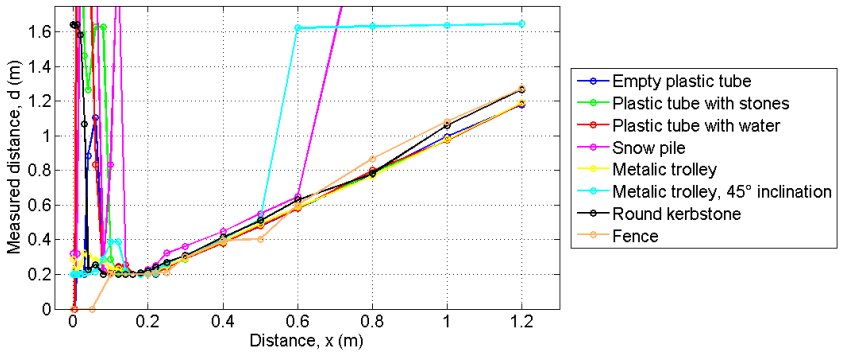

(a) US distance measurement results for different approaching objects.

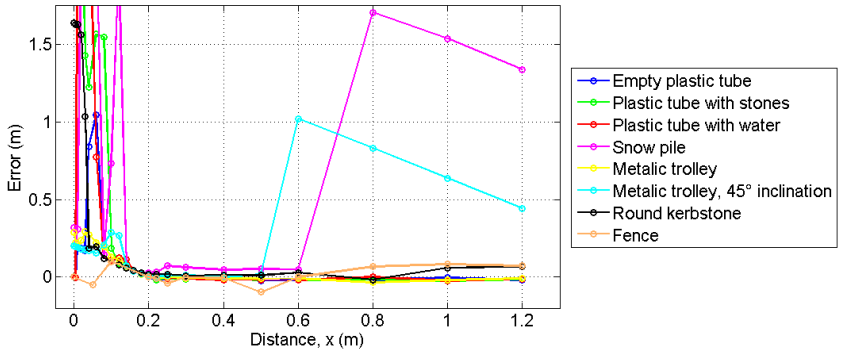

(b) Error of the measurement for different approaching objects.

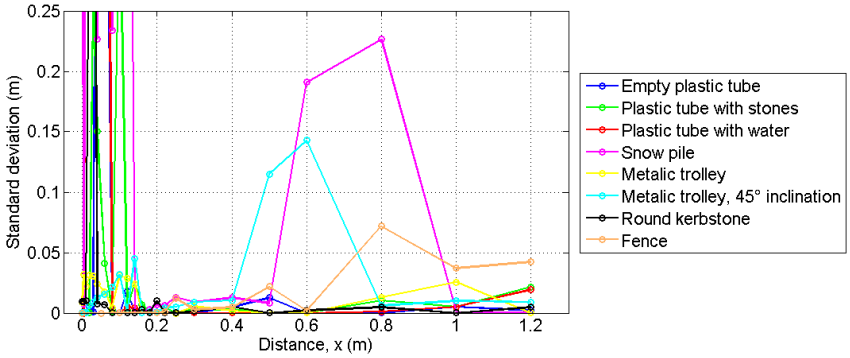

(c) Standard deviations of the measurements for the different approaching objects.

Figure 5.3: Ultrasonic distance measurement results, error and standard deviations for the different approaching objects. At distances lower than 0.2 m no distance measurements are possible, due to the sensor limitations (refer to Chapter 2.1). For the snow pile and the inclined trolley the maximum detection range is 0.5 m and 0.6 m, respectively. This depends on the objects form (trolley) and its material (snow pile). Due to the thin wires of the fence, it delivers slightly wrong measurement results with a higher standard deviation for distances larger than 0.4 m. The kerbstone provides slightly wrong distance measurement results for distances above 0.8 m, due to the different height of the US sensor and the kerbstone. For further explanation refer to the text.

Blind Spot Detection

For blind spot detection two US sensors were used (Figure 5.1(b)). For the used vehicle bumper with fixed distances of the US sensors, blind spots only occur for small objects below 0.3 m. The measurement setup was made with a small metallic pipe (diameter of 15 mm, refer to Figure 5.4). If the sensors are put farther away from each other, or the

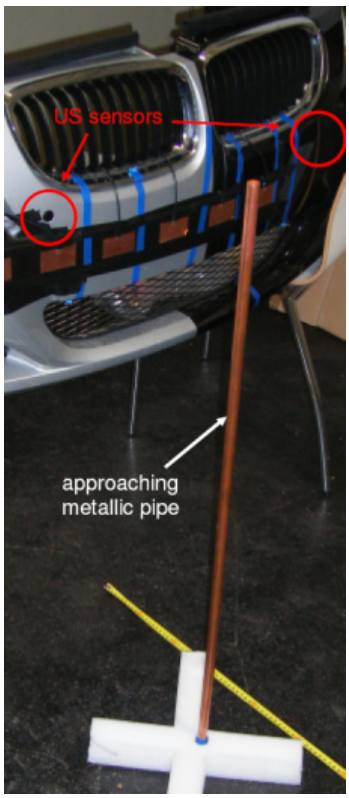

Figure 5.4: Photograph of the blind spot test for US sensors. A thin metallic pipe is approached between two US sensors. For distances below 0.3 m the metallic pipe was not detected.

bumper has a bending at the mounting position of the US sensor, the blind spot area may increase. The reason is the limited opening angle γ of every US sensor (refer to Chapter 2.1 for further explanation).

Influence of Water

To analyze the effects of water on the ultrasonic sensors, two experiments were carried out. In the first, which is shown in Figure 5.5, water was sprayed on the sensor during the measurements. The peaks in the measurement trace originate from water drops flowing over the sensor interface. Each water drop causes multiple reflections between the sensor

and the approaching object. Thus, the sensor provides wrong distance measurements during times when a water drop is directly on the sensor surface (as shown in Figure 5.5(b)). For larger drops, a significant deterioration of the sensor performance is observed.

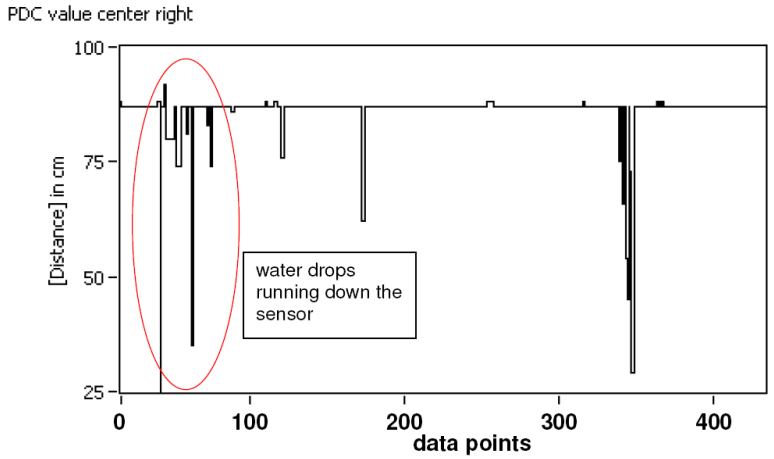

(a) Ultrasonic distance measurement with water on the sensor.

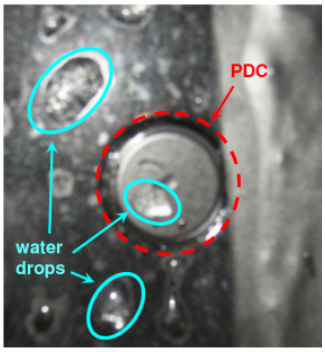

(b) Photograph of the sensor element with water drops.

Figure 5.5: Ultrasonic distance measurement and photograph of sensor with water. (a) Ultrasonic distance measurement results. A fixed distance of 0.8 m to the reference object (plastic tube) is measured. During the measurements, water was sprayed on the sensor. The peaks in the distance measurements result from water drops flowing over the sensor interface. (b) Photograph of the ultrasonic sensor with a typically sized water drop touching the sensor surface.

In further experiments two types of rain with two different intensities were simulated. The first type of simulated rain does not touch the bumper, whereas the second type touches the bumper (with included ultrasonic sensors). For the experiment a garden hose was placed 3 m above the bumper and water was sprayed down. Two levels of intensities were used and controlled by a regulating screw on the garden hose:

i) Normal rain with a rain gauge of 5 $\frac{\text{mm}}{\text{m}^2\ \text{min}}$.

ii) Heavy rain with a rain gauge of 10 $\frac{\text{mm}}{\text{m}^2\ \text{min}}$.

The measurement setup and measurement results are shown in Figure 5.6. In the first measurement in interval (i) an object was placed in a distance of 2 m. Afterwards it was replaced at a distance of 0.5 m (interval (ii)). In the first and the third interval ((i) and (iii)) no rain was simulated. In the second and the fourth interval ((ii) and (iv)) normal rain was simulated but prevented from touching the bumper. As can be seen in Figure 5.6(b) this type of rain simulation has only a small influence on the distance measurement (about ± 0.04 m). In the second measurement in Figure 5.6(b) heavy rain

was simulated and the water touched the bumper. This measurement was done with no object in front of the sensor. Heavy rain leads to unemployable distance measurements. The high number of rain drops flowing over the sensor have a too high impact on the measurement as described above. For this case the US ECU has to detect the high change in the standard deviation and report an error to the user.

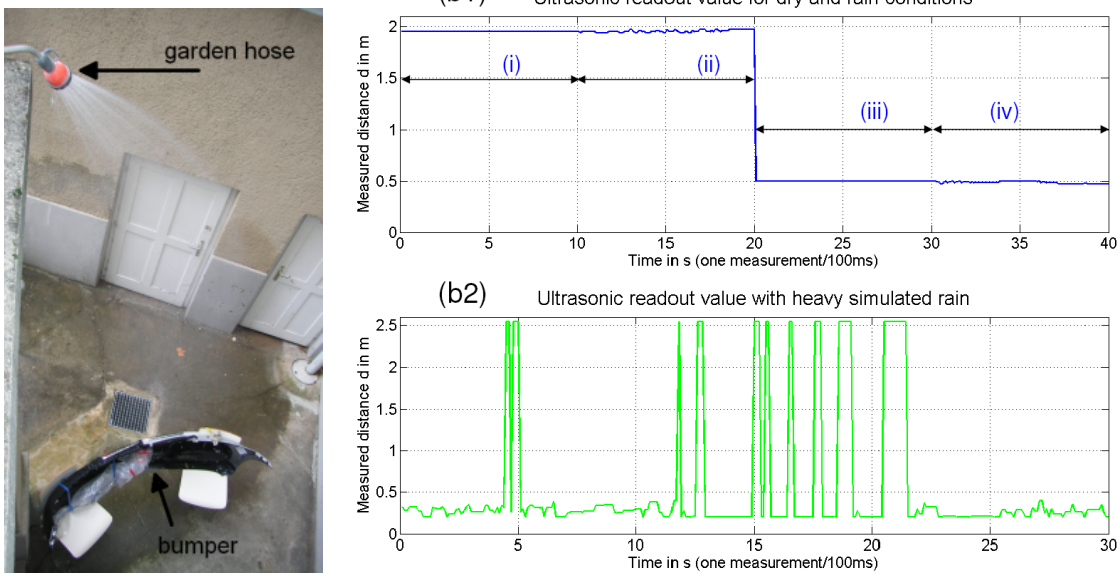

(a) Photograph of the sensor setup for rain simulation.

(b) US distance measurement with simulated rain.

Figure 5.6: Photograph and US measurements for a rain simulation. (a) Experimental setup for rain simulation. The garden hose was placed approximately 3 m above the bumper and the intensity of the rain was adjusted with a regulating screw on the garden hose. (b) US measurement results for different rain cases. (b1) For the time interval (i), an object (plastic tube) in a distance of about 2 m is placed and the distance is measured. (ii) Normal rain condition, which does not touch the bumper. ((iii) and (iv)) The plastic tube is approached to a distance of 0.5 m, without rain for the first 10 s and with rain for the second 10 s. (b2) Heavy rain is simulated and water is allowed to touch the bumper. No object was placed in front of the bumper. However, a distance measurement is not possible, due to the high variance of the measured signal.

Measurement Impacts due to Contamination

The ultrasonic sensors were also tested in the presence of external disturbances such as

- Dirty water (water and soil mixture), dried.
- Surface active agents (as can be found in e.g. screen wash), dried.
- Salted water ($20\,\mathrm{g}/liter$), dried.
- Snowfall.
- Layer of ice.

Photographs to the according measurement setups can be found in Figure 5.7. An exemplary photograph of an ultrasonic sensor polluted with salt water is shown in Figure 5.7(a). As can be seen in Table 5.1, all measurements, except the one with a layer of ice on the sensors, have no measurable influences on the distance measurements.

Impacts on the measurements due to contamination	
Test	Impact
Snow fall	minor
Ice	high [5]
Dirt	minor
Surface active agents	minor
Salted water	minor

Table 5.1: Effects on the US measurement system due to different types of contamination.

If the sensor is fully covered with ice (see Figure 5.7(b)), no measurements can be taken. The icesheet acts like an object directly in front of the sensor and thus, prohibits distance measurements of an approaching object.

5.2 Measurements with the Capacitive Sensor

Different measurement setups for capacitive distance measurement are tested on a car bumper. Furthermore, distance measurements for different approaching objects are presented and discussed. The measurement setup is also exposed to external disturbances and resulting measurement impacts are evaluated.

[5] High impact means, that no more measurement can be taken.

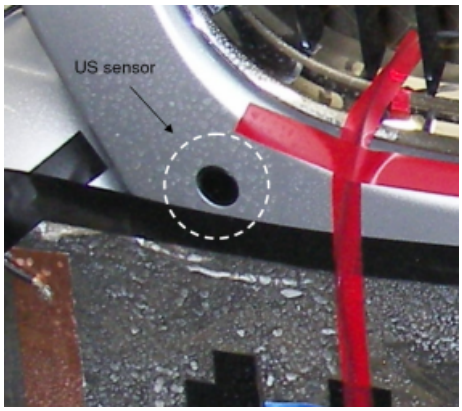

(a) Ultrasonic sensor fouled with dried salt water.

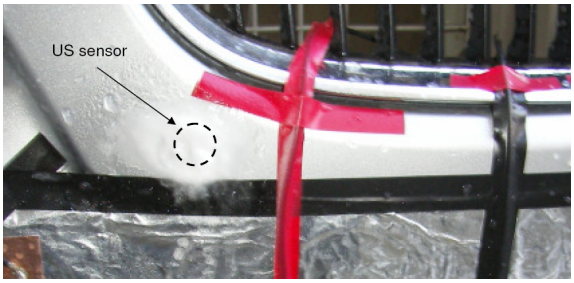

(b) Photograph of the ultrasonic sensor with a layer of ice.

Figure 5.7: Ultrasonic sensors, mounted in a vehicle bumper and polluted with different external disturbances. (a) US sensor fouled with salt water. This contamination has no influence on the distance measurements. (b) US sensor element is sheeted with a layer of ice. No distance measurements can be taken.

5.2.1 Experimental Setups

In all setups the electrodes were realized by means of copper plates, which exhibit a thickness of 100 μm, a width of 60 mm and a length of 30 mm, and with a distance of 50 mm between the electrodes. The size of the electrodes was chosen with respect to the fitting on the vehicle bumper. The reference test object was a plastic tube with a diameter of 75 mm and a height of 1 m, according to ISO 17386 (standardized test object for parking aids), which was filled with water to approximate a relative permittivity of a human. The measurement results are shown in Section 5.2.2. For all presented measurements the Analog Devices IC AD7143 was used. For the distance measurements used in this work, it does not matter, which capacitive IC is chosen (AD7143 or CapIC). Prior experiments show the same results for this type of measurement. For every measurement the test object was positioned in a fixed distance to the bumper and 1000 measurements were taken. After averaging and removing the offset the measurement value and its standard deviation were saved.

For the first setup the electrodes were mounted on a cardboard, to get a reference measurement with very low cross sensitivities. These measurements were compared with the other two setups to identify impacts of the bumper material.

In the second setup the capacitive sensor unit uses three electrodes, which were mounted on the inner side of the bumper and were connected to the evaluation circuitry. Figure 5.8(a) shows the electrodes, the measurement circuitry, and the connection to the CAN bus. As

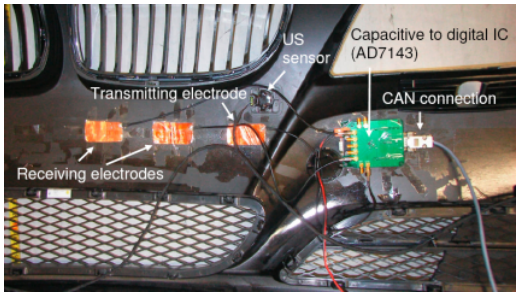

(a) Photograph of the setup on the inner side of the bumper.

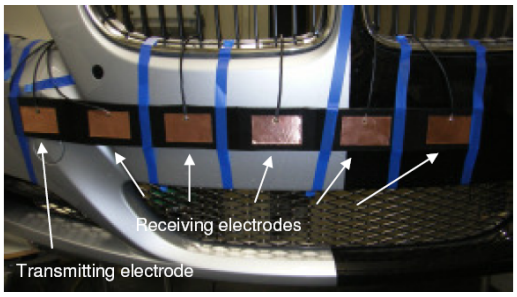

(b) Photograph of the setup on the outer side of the bumper.

Figure 5.8: Photographs of the used capacitive measurement setups. The printed circuit board carries the evaluation circuitry and the micro controller and is mounted on the inner side of the bumper. One transmitting electrode and two or more receiver electrodes are used for the capacitance based distance measurement. (a) The measurement setup is mounted on the inner side of a bumper. According to Section 5.2.2, the measurements are highly influenced by cross sensitivities. (b) To reduce cross sensitivities the sensor is mounted on the outer side of the car bumper. Similar measurement results are obtained as for the reference setup (electrodes on a cardboard). In this setup no influences through the mounted material are observed.

shown in Figure 5.9, the measurement setup with the electrodes placed on the inner side of the bumper can not be used due to high cross sensitivities. The material of the bumper or its coating influences the produced electric field due to its conductance. Thus, the electric field is propagated to undesired positions and the electrode area is undefinedly increased. To describe these effects more closely, detailed investigations on the bumper material have to be carried out.

To reduce the cross sensitivities, a third measurement setup was used. In the third setup (Figure 5.8(b)), the electrodes were mounted on the outer side of the bumper. The evaluation circuitry is again placed on the inner side of the bumper. The back side of the electrodes is covered with a ground plane, which is connected to the surface of the bumper and the ground potential of the evaluation circuitry. The ground plane prevents influences on the measurement by objects from behind the bumper (compare Figure 2.6). As can be seen in Figure 5.9, the bumper has no measurable influence on the distance measurement with the electrodes mounted on the outer side of the bumper. Thus, the third measurement setup is used for all further measurements. For readability, only the two receiving electrodes, which are nearest to the transmitting electrode, are shown in Figure 5.9.

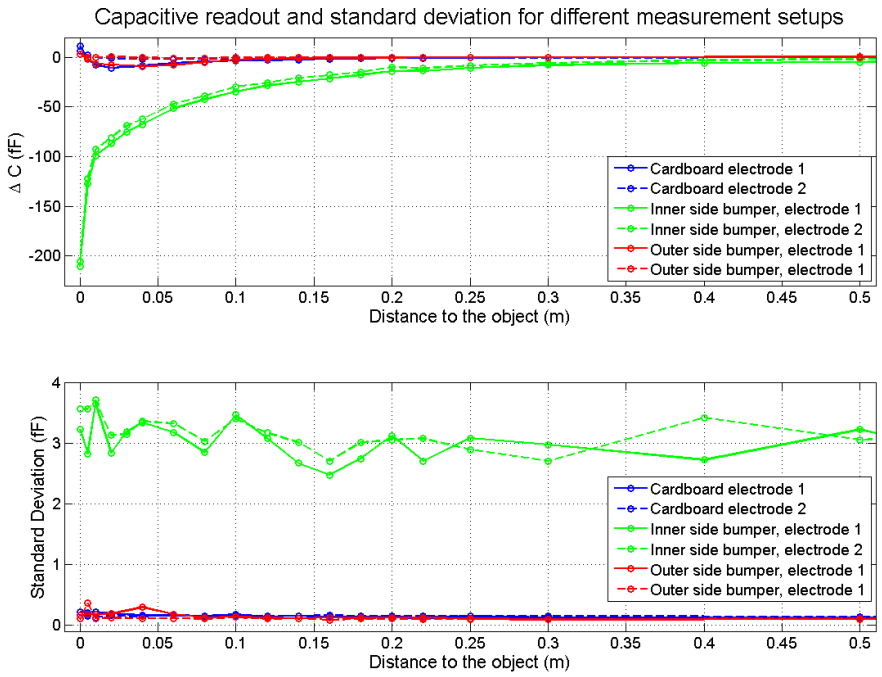

Figure 5.9: Capacitive distance measurement with different measurement setups. The distance to an approaching plastic tube filled with water is determined by means of different capacitive measurement setups. The measurement setup with the electrodes placed on the inner side of the bumper is influenced by the bumper material and provides unpredictable different results compared with the electrodes placed on a cardboard or the outer side of the bumper. Thus, for further measurements the measurement setup with electrodes placed on the outer side of the bumper is used.

5.2.2 Measurement Results for Different Approaching Objects

In this section, measurement results for capacitive distance sensing are presented. Figure 5.10 shows the relative change of the capacitance for an approaching human (1.85 m tall and 80 kg of weight) for the different receiving electrodes. With the capacitance change of the first and second receiver electrode (nearest and second nearest to transmitter electrode, respectively) an unambiguous distance measurement is possible (refer to Chapter 2.2.1). Also the change between shielding mode and coupling mode at a distance of approximately 0.04 m can be seen for the first receiving electrode. Due to the different distances of the receiver electrodes with respect to the transmitter electrode, different capacitance traces are observed between the receivers and the transmitter for an approaching human. Thus, the second receiver electrode changes to coupling mode at a farther distance compared with the first receiver electrode and the shielding signal is lower. The increase of the standard deviation for very low distances (< 0.02 m) occurs from undesired small movements

of the test object (human), which result in high differences in the measurement results.

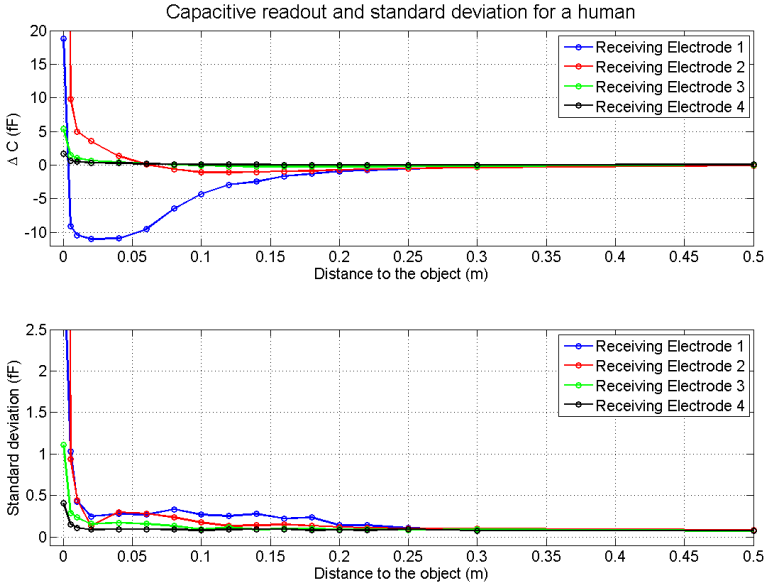

Figure 5.10: Capacitive distance measurement results for an approaching human. Electrode 1 is the nearest receiving electrode with respect to the transmitting electrode and electrode 4 the farthest one. A distance measurement starting at a distance of $\approx 0.3\,\mathrm{m}$ is possible.

Different objects with different relative permittivities ϵ_r and different volumes result in different capacitance changes when approaching to the measurement setup. Figure 5.11 and 5.12 show the capacitance change for different objects. The higher standard deviation of the measurements with the fence can be explained by Electro Magnetic Interferences (EMI), which originates from laboratory devices. During the experiments the fence was kept electrically floating. The most challenging object to detect is the empty plastic tube. Due to its low relative permittivity ϵ_r and its low volume, the electric field is marginally influenced. Other objects such as fences, kerbstones, or snow piles can easily be detected.

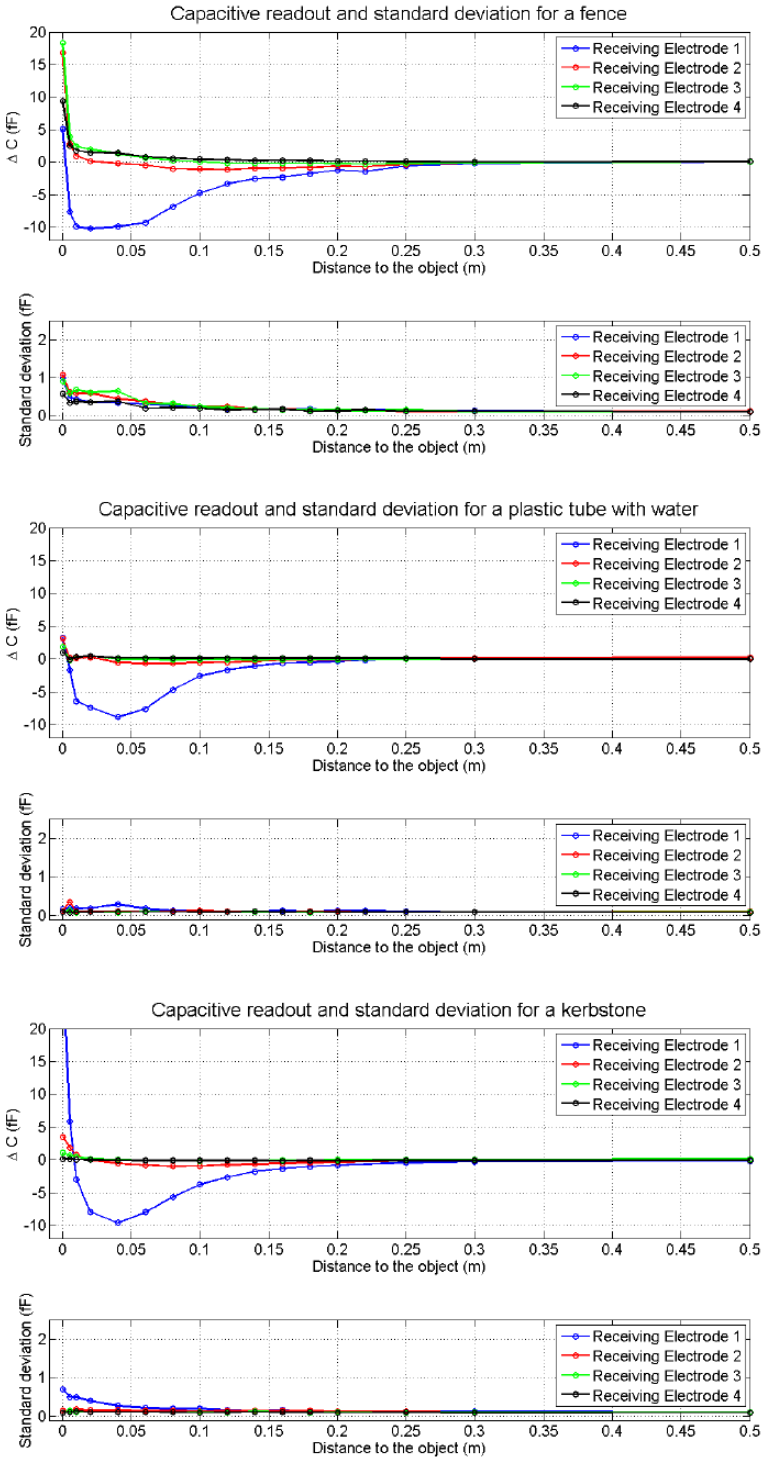

Figure 5.11: (I) Capacitive distance measurement results for different objects. For every object the capacitive change and the standard deviation of the four receiving electrodes is shown. All objects (fence, plastic tube with water, and kerbstone) individually change the coupling capacitance. For detailed discussion of the results refer to the text.

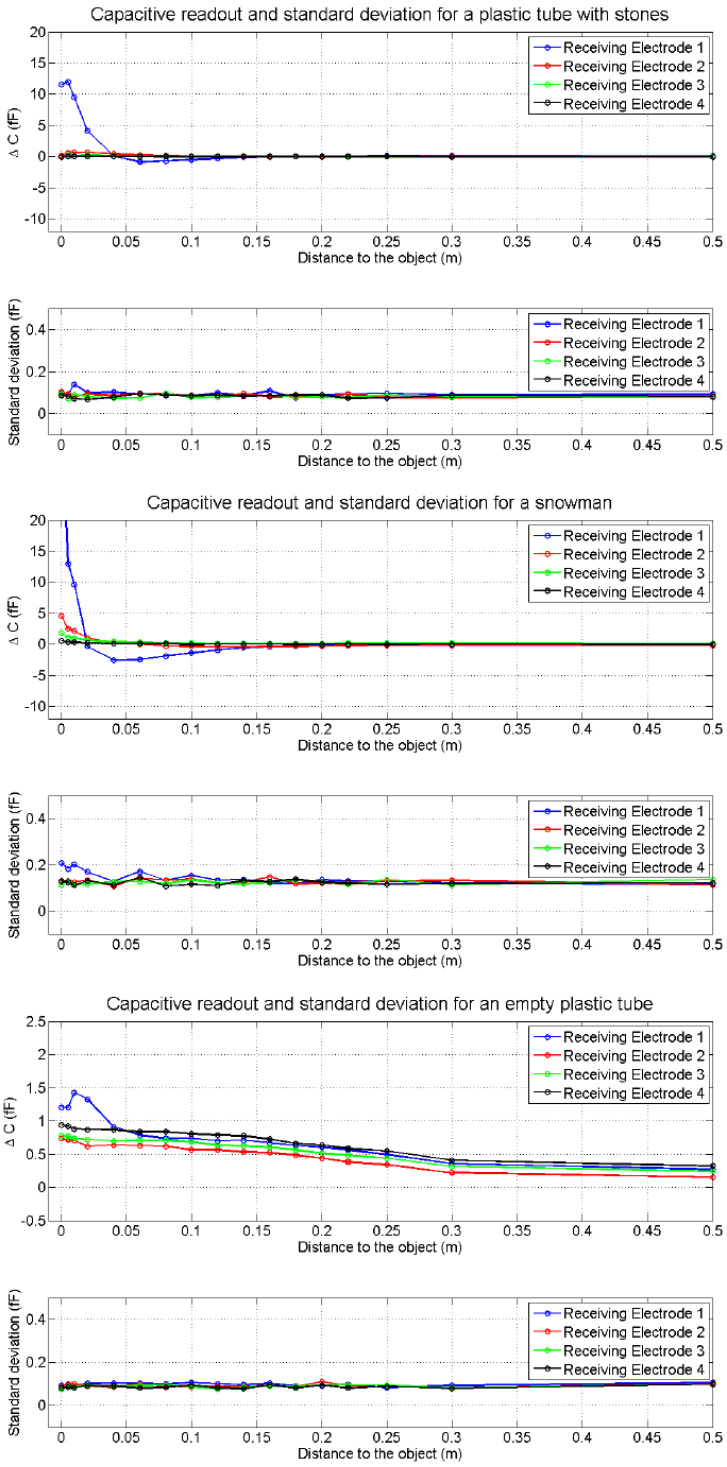

Figure 5.12: (II) Capacitive distance measurement results for different objects. For every object (plastic tube with stones, snow pile, and an empty plastic tube) the capacitive change and the standard deviation of the four receiving electrodes is shown (changed in scale for readability). The most challenging object to detect is the empty plastic tube. The measured capacitance changes marginally (changed in scale), due to the pipes' low ϵ_r and small volume.

Objects must also be detected if they approach in different angles γ, as defined in Figure 5.13(a). A sensitivity map was created with the reference plastic tube filled with water. As can be seen in Figure 5.13(b), a capacitance change due to the approaching angle γ is not measurable. Thus, the maximum detection range of approximately 0.2 m stays the same for all approaching angles γ.

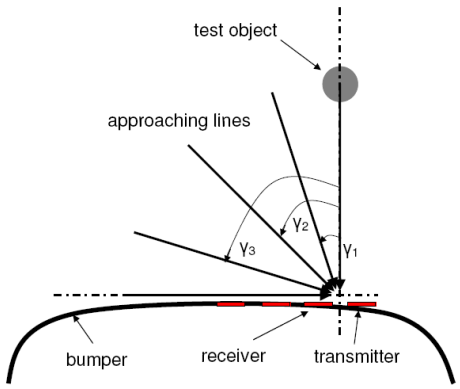

(a) Sketch (not in scale) of the capacitive measurement setup with objects approaching in different angles γ.

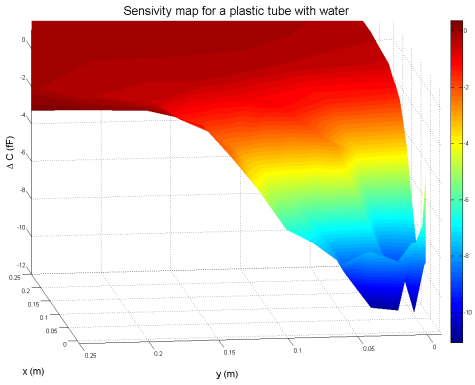

(b) Sensitivity map of a plastic tube filled with water.

Figure 5.13: Sensitivity map for different approaching angles. (a) The object (plastic tube filled with water) approaches the sensor setup from different angles γ. (b) The measured capacitance changes are plotted. With larger angles γ, no significant change in the maximum detection range is measurable.

5.2.3 Measurement Impacts due to External Disturbances

For real world operation on a car bumper it is very important to know how the measurement system reacts on external disturbances such as:

- Dirty water (water and soil mixture), dried.
- Surface active agents (as can be found in e.g. screen wash), dried.
- Salted water (20 g/*liter*), dried.
- Layer of snow.
- Layer of ice.

Contamination with Dirt

For every investigation, a reference measurement with an approaching plastic tube with water was taken. Afterwards the liquids mentioned above were directly sprayed on the electrodes and dried. After the drying process, measurements were taken at different places and conditions:

- In the laboratory at room temperature of approximately $20\,°C$.
- Outside (at approximately $0\,°C$).
- Outside with a breeze (made by a fan at level 2 of 3, $\approx 0\,°C$).
- Outside with a gale (made by a fan at level 3 of 3, $\approx 0\,°C$).

Only the nearest receiver was used to compare the measurement results. For the other receiving electrodes, no significant changes could be observed. Table 5.2 gives an brief overview of the measurement results and the effects due to the contamination of the electrodes. A photograph of the tested bumper fouled with dirty water is shown in Figure 5.14. The distance measurement results and the calculated standard deviations for the different test cases are shown in Figure 5.15, 5.16, and 5.17. By contaminating the bumper with dried salted water and dried wash water, a slightly difference in the capacitance change and a higher standard deviation (higher noise level) can be observed. A possible reason is the hygroscopic layer on the sensor electrodes. It probably changes its moisture content very fast, due to the air circulations. This fast changes results in a higher measurement noise. To be confident, more experiments under replicable conditions and without any other disturbances have to be made, but are out of scope of this work.

Measurement results with contamination of the measurement setup				
Test case	Inside fouled	Outside fouled	Outside fouled and breeze	Outside fouled and gale
Dirty water	minor	minor	minor	minor
Salted water	minor	high diff. in std. dev. [6]	high diff. in std. dev. and higher shielding.	
Surface active agents	small diff. in std. dev. and higher shielding		high diff. in std. dev. and higher shielding	

Table 5.2: Effects on the measurement system due to different types of contamination. The results are compared with the measurement results of a clean bumper at $20\,°$ in the laboratory. The measurements outside were all taken at a temperature of approximately $0\,°$. For further discussion refer to the text.

[6] 'diff. in std. dev.' ... difference in standard deviation

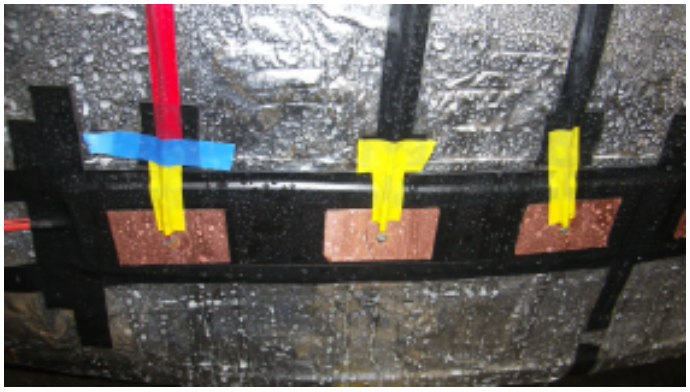

Figure 5.14: Photograph of the fouled bumper with dried dirty water containing the sensor electrodes and the electronic circuitry at the inner side of the bumper.

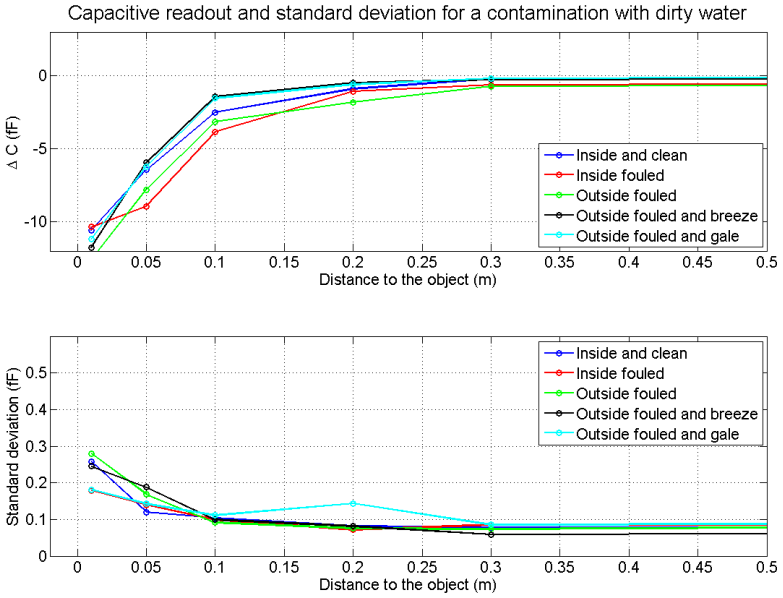

Figure 5.15: Measurement results for contamination with dirty water. The electrodes are fouled with a mixture of water and soil. A minor change of the measurement results can be observed.

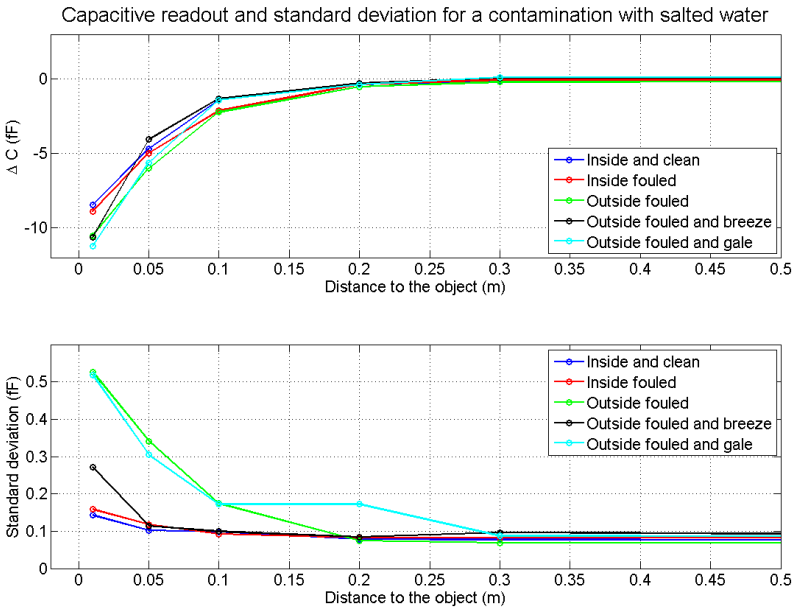

Figure 5.16: Measurement results for contamination with salted water. When fouled with salted water, the capacitance changes in a farther distance (shielding occurs farther away from the sensor electrodes) if the bumper is exposed to simulated wind. Additionally the standard deviation increases.

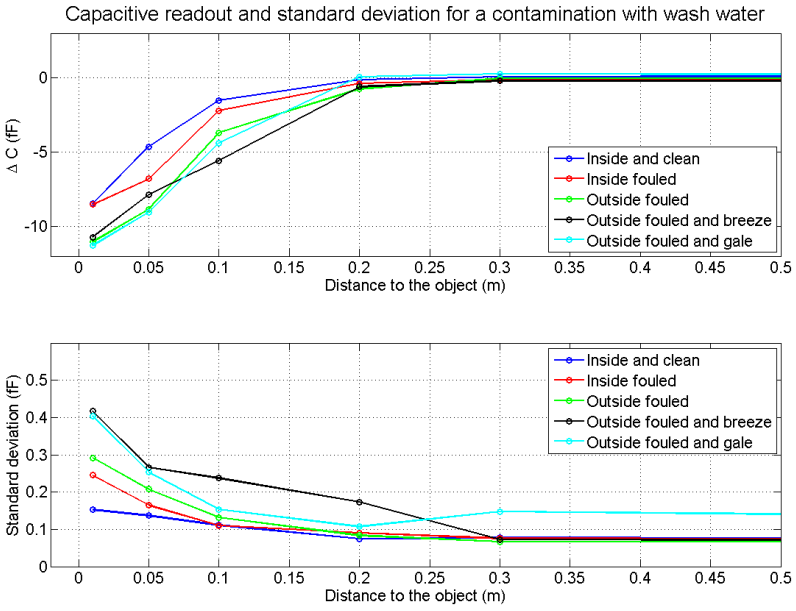

Figure 5.17: Measurement results for contamination with surface active agents (e.g. wash water). In this case a significant change in the measurement results occur. Shielding occurs farther away from the sensor electrodes and the standard deviation increases significantly.

Influence of Snow

To determine the impacts of snow, two layers of snow (approximately 10 mm and 20 mm) were used to cover the electrodes. A photograph of the measurement setup is shown in Figure 5.18(a). A structure made of styrofoam was used to hold the snow layer on the bumper. Due to the nearly similar relative permittivity ϵ_r of styrofoam and air, no influences are expected from the structure. A plastic tube filled with water was used as reference object.

As can be seen in Figure 5.18(b), changes of the relative capacitance, due to the snow, are only observed with the thick ($\approx$ 20 mm) snow layer. The snow on the sensor electrodes leads virtually to an increase of their size. Thus, the electrode field lines spread farther away from the bumper (compare Figure 2.6(a)). Now an approaching object influences the electric field at a farther distance. However, the standard deviation increases for both snow layers. The comparatively low influences of such thick layers can be explained by the low ϵ_r of fresh fallen snow ($\approx$ 1.5 according to [Bax97]). The used structure also has a slight influence on the measurement (ϵ_r of styrofoam has to be slightly different to 1). Thus, no difference between the test case with only the styrofoam structure and with the thin snow layer can be observed.

Influence of Rain

To simulate rain scenarios, the measurement setup as shown in Figure 5.6(a) was used. A garden hose was place 3 m above the bumper and water was sprayed down (similar to the setup described in Section 5.1.2).

In the first setup, the electrodes were fully exposed to the environment with no protection (same setup as used for the measurements above). As can be seen from Figure 5.19(b), no distance measurement is possible, due to the high capacitance changes, while water is running down the sensors.

To reduce this effect, a sheet of styrofoam was used to cover the electrodes and protect them from direct contact to the water. Figure 5.19(a) shows the modified electrode setup and the occurring water films during rain. The results for capacitance measurements are shown in Figure 5.19(b). The measurement noise decreases by approximately 75%. However, reliable measurements are not possible under heavy raining conditions.

A model of the test setup under raining conditions is described in Figure 5.20. Coupling capacitances occur between the electrodes and the water film and between the water film and the ground plane. This coupling capacitances influence the measurement of the capacitance between the receiver electrode and the transmitter electrode in a way, that an

(a) Photograph of the measurement setup with a layer of snow in front of the bumper.

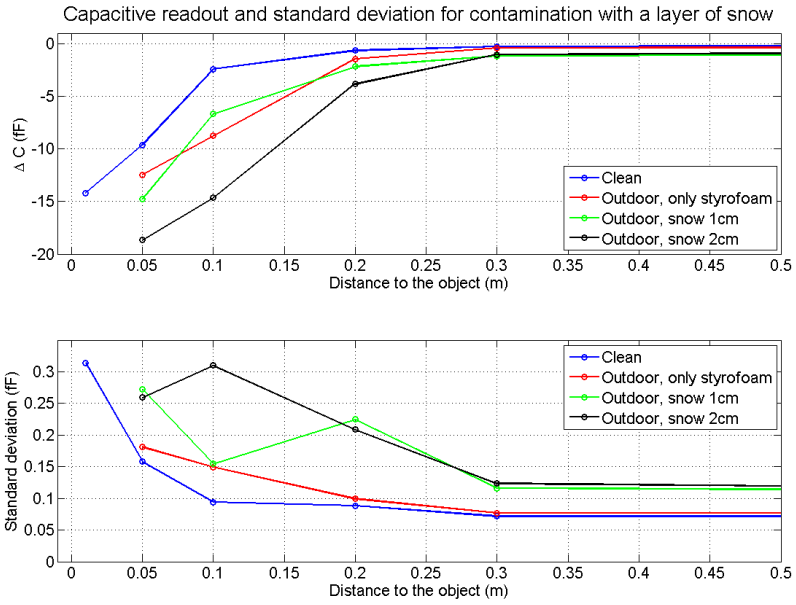

(b) Measurement results for contamination with two different layers of snow.

Figure 5.18: Measurement setup and results for contamination with snow. (a) With a structure made of styrofoam, two layers of snow (approximately 10 mm and 20 mm) where applied on the bumper. (b) Only for the thick snow layer (≈ 20 mm), significant deviations can be observed. The low influence can be explained by the low ϵ_r of fresh fallen snow. The structure made of styrofoam slightly influences the measurement. Additionally the measurement setup slightly changed, due to the construction limitations.

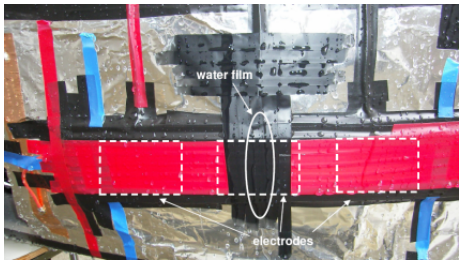

(a) Photograph of the wet bumper with water films on the protected electrodes.

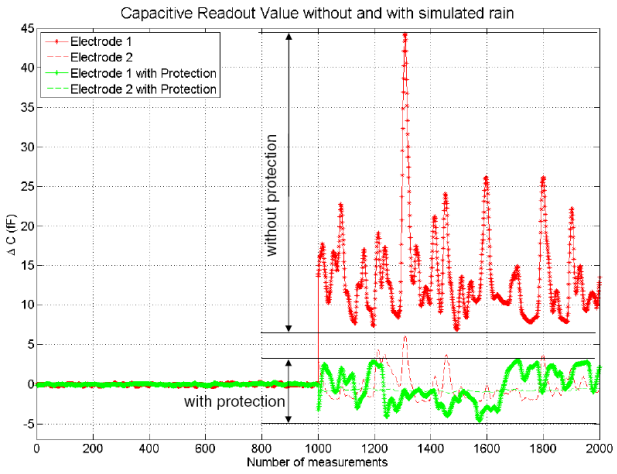

(b) Measurement results with and without simulated rain for an electrode setup with and without protection.

Figure 5.19: Capacitive measurement setup and results for simulated rain. (a) Photograph of the bumper with a styrofoam layer on the electrodes and a water film on the electrode. (b) Measurement results for the two used setups. With a styrofoam layer the measurement noise decreases by approximately 75%. However, no measurement can be taken with these influences.

approaching object can not be detected any more. Depending on the conductivity σ of the water film, different effects can occur. If the conductivity σ is high, the water film is kept on the ground potential and thus, virtually increases the ground plane. This effect reduces the measured capacitance between the receiver electrode and the transmitter electrode. If the conductivity σ is lower, the water film follows the potential of the transmitting electrode. This virtually increases the surface of the sensor electrodes. Thus, the measured capacitance between the receiver electrode and the transmitter electrode is increased.

Solutions to this problem may be:

- Use of a differential measurement setup which reduces common mode currents to ground ([ZBH08]).
- Special surface construction, that no water films can occur.
- Use of an additionally technique to detect occurring water films (e.g. IQ modulation principle).

The mentioned possibilities are out of scope, but give ideas how to overcome the challenging problems with rain and the capacitive measurement system for future investigations.

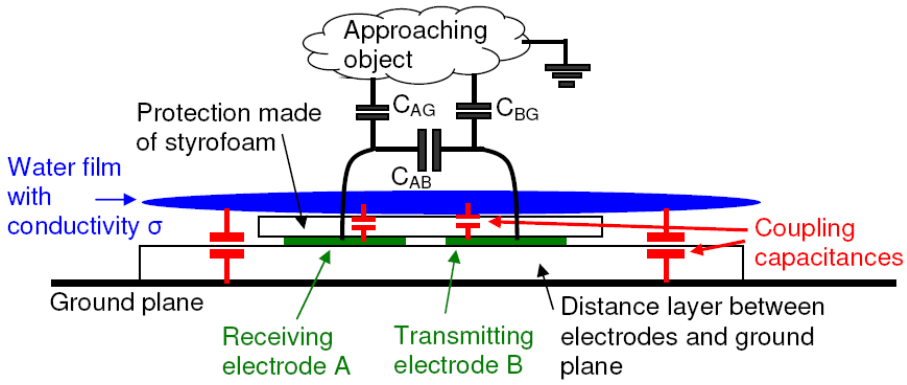

Figure 5.20: Sketch of the rain setup with occurring coupling capacitances. C_{AB}, C_{AG}, and C_{BG} are the coupling capacitances between the two electrodes and between the electrodes to ground (effected by the approaching object). Due to the water film, coupling capacitances occur between the electrodes, the water film, and the ground plane. Depending on the conductivity σ of the water film, different effects occur. For higher values of σ, the water film will virtually increase the ground plane. Thus, the measured capacitance between transmitter electrode and receiver electrode reduces. If σ is lower, the water film is kept on a potential similar to the transmitting electrode and thus, virtually increase the electrode surface (measured capacitance is increased).

5.3 The Sensor Fusion Concept and Case Study

Sensor fusion denotes the concept of combining several measurements taken from the same quantity such that the combined result is better than for single measurements. For the proposed system, the properties of the capacitive sensor (e.g. high resolution for short measurement ranges) and the ultrasonic sensor (e.g. ability to measure long distances) are combined in order to use the benefits of both sensor systems and reduce their drawbacks. In the following section the fusion approach based on a Kalman filter is presented and the measurement results are discussed.

5.3.1 Kalman Filtering

As it is tried to measure the distance of a moving object in front of the sensor plane, one is dealing with the identification of the parameter vector $x_k = [d\ v]^T$, where d denotes the distance to the object and v denotes the velocity of the object. A Kalman filter is appropriate for the fusion concept, as it is particular useful for the estimation of states in a dynamic system.

The state space model can be written as

$$x_k = \begin{bmatrix} d_k \\ v_k \end{bmatrix} = \begin{bmatrix} 1 & T_s \\ 0 & 1 \end{bmatrix} \cdot \begin{bmatrix} d_{k-1} \\ v_{k-1} \end{bmatrix} \tag{5.1}$$

$$z_k = \begin{bmatrix} d_{US} \\ C1 \\ C2 \end{bmatrix} = \begin{bmatrix} d_k \\ f1(d_k) \\ f2(d_k) \end{bmatrix} \tag{5.2}$$

Equation 5.1 describes the dynamic behavior of the moving object (state vector x_k) at step k and T_s denotes the sampling period. Equation 5.2 represents the measurement vector z_k at step k. As the ultrasonic measurement system provides direct information about the distance, a linear relation is given for the first entry in the measurement vector. However, the measured capacitances depend on the encountered distance (C_1 and C_2 denote the nearer and farther receiver electrode respectively with respect to the transmitter electrode). As can be seen from Section 5.2.2, $f1(d_k)$ and $f2(d_k)$ are non linear functions of d_k. Thus, at least a linearized Kalman Filter has to be used to estimate the state vector x_k [GA08].

Two receiving electrodes are used for the sensor fusion concept, in order to get unambiguous results for the investigated test cases (refer to Chapter 2.2.2).

Implementation of the Discrete Linearized Kalman Filter

To test the sensor fusion system, a parking scenario is simulated in the numerical computing environment Matlab. The measured capacitance changes for the two nearest receiving electrodes for different approaching objects are interpolated with spline functions (shown in Figure 5.21 for the first receiving electrode). As can be seen, for the interpolation of the human approaching measurements the difference between the measurement results and the interpolation can be kept small, except for very near distances ($< 0.03\,\mathrm{m}$). Due to the interpolation with spline functions, a tradeoff has to be made between a smooth function and a function which fits the measurement result. These interpolating functions are used as the measurement functions ($f1(d_k)$ and $f2(d_k)$) in Equation 5.2 and are numbered in Figure 5.21 for later reference (referenced as fct_nbr for the first receiving electrode).

For a given approaching scenario, the ultrasonic values and the capacitance values (depending on the different objects) are calculated according to the interpolated functions above and white Gaussian noise is added (determined by the standard deviations of the measurements in Sections 5.1.2 and 5.2.2). These noisy values are used as measurement values z_k in Equation 5.2.

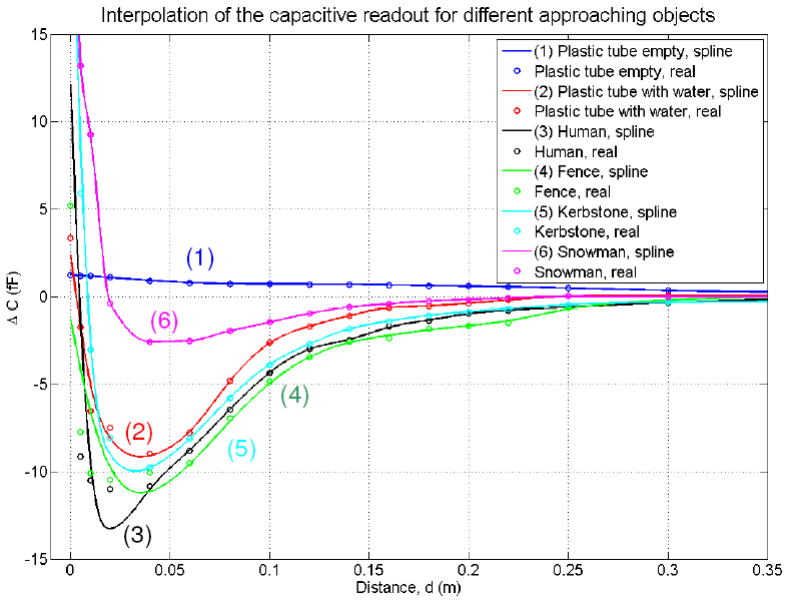

Figure 5.21: Piecewise spline interpolation of the measured capacitance values of different approaching objects for the first receiving electrode, nearest to the transmitter electrode. A tradeoff between a smooth function and a function, which fits all measurement points, has to be made.

Figure 5.22 shows the parking scenario, the ultrasonic measurements, and the capacitance measurements. If the approaching object comes closer than 0.2 m, the ultrasonic value is set to zero because no US measurement can be taken below this distance. A change of the capacitance values can be observed for a distance below 0.3 m (also depending on the approaching object).

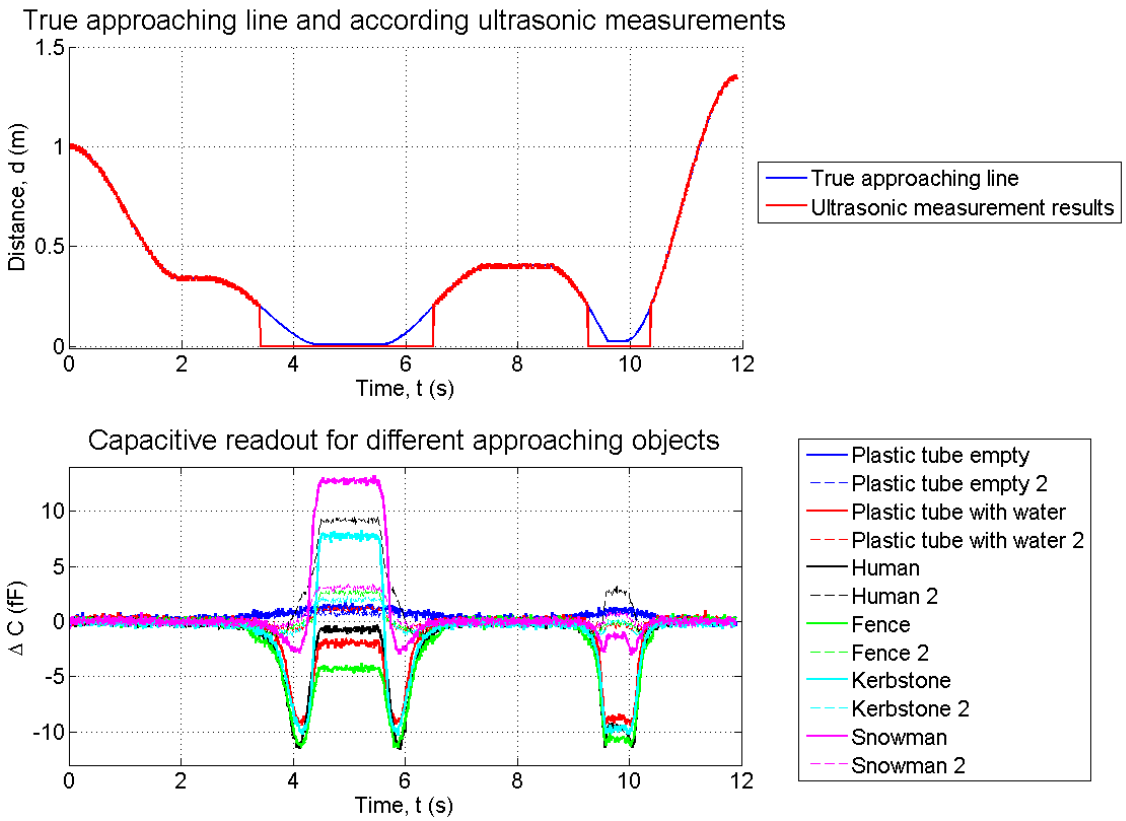

Figure 5.22: Simulation of a parking scenario with observed ultrasonic and capacitance measurements. The US sensor is not able to measure distances below 0.2 m and is set to 0 during these distances. For distances below 0.3 m, the relative capacitance changes are high enough to use them for a distance measurement.

After the generation of the datasets, a linearized Kalman filter is used to combine the distance measurements from both sensors with following steps:

i) For every distance x, calculate the probability that x belongs to a certain object type (defined by fct_nbr) with the detector described below.

ii) Initialize Kalman filter parameters.

iii) For every time step k of simulating the approach of an object:

- Get measurement values $z_k = [d_{US}\ C_1\ C_2]^T$.
- Perform optimal prediction $\delta x_k = \Phi_{k-1} * \delta x_{k-1}$ and $x_k = x_{k-1} + \delta x$.
- Get the fct_nbr with the highest probability for the current distance x_k.

- Get the matrix
$$H_k \approx \frac{\partial h_k}{\partial x}|_{x_k} = [1\ 0; K_1\ 0; K_2\ 0] \tag{5.3}$$
where K_1 and K_2 are the slopes of the used measurement functions for C_1 and C_2 respectively. H_k relates the current state x_k to the measurement z_k.

- Calculate $x_{k,lin} = [x_k, C_{f1}, C_{f2}]^T$, where C_{f1} and C_{f1} are the capacitance values out of the chosen measurement function $f1(d_k)$ and $f2(d_k)$, respectively.

- Depending on x_k, set the measurement noise covariance matrix R. For US values below 0.2 m and for capacitance measurements above 0.3 m set the measurement noise to a high value. Thus, below 0.2 m the US measurement is turned off.

- Compute the a priori covariance matrix
$$P_k(-) = \Phi P_{k-1}(+)\Phi^T + Q \tag{5.4}$$
where Q is the process noise covariance matrix.

- Compute the Kalman gain
$$K_k = P_k(-)H_k^T(H_k P_k(-)H_k^T + R_k)^{-1} \tag{5.5}$$

- Conditioning the change of the predicted estimate state
$$\delta x_k(+) = \delta x_k + K_k(z_k - x_{k,lin} - H_k \delta x_k) \tag{5.6}$$
where $(z_k - x_{k,lin} - H_k\delta x_k)$ is the measurement residual, which denotes the difference between the actual measurement z_k and the predicted measurement $x_{k,lin} + H_k\delta x_k$.

- Compute the a posteriori covariance matrix
$$P_k(+) = (I - K_k H_k)P_k(-) \tag{5.7}$$

- If the distance $x_k < 0$, it is set to 0, since in real world operation a negative value of x_k is not possible.

iv) Plot the results.

Measurement Trace Decision and Object Classification

As described above, every object type has a different measurement trace, when approaching to the sensor (compare with Figure 5.21). With the measurements for different approaching objects, done in Chapter 5.2, a collection of measurement traces is known and stored. It is not possible to measure all kinds of approaching objects and store their measurement traces (endless number of traces). Thus, in real world applications the measurement trace of an approaching object will typically not exactly match a known (stored) trace (object type).
If an object is approaching, a decision (based on the measurement results) has to be made, which object type out of the stored ones should be chosen, to predict the trend of the measurement trace of the approaching object.
This decision is necessary, because the Kalman filter needs the measurements and the measurement trace to estimate the state vector x_k, as described above. With this decision an object classification is made additionally.

To take the measurement trace (decide for an object type), which delivers the nearest capacitance value to the measurement value seems obvious, but is not the safest decision. For example, a measurement trace with a capacitance value larger or smaller than the measurement value will provide a distance nearer or farther away than the true one. Thus, for safety reasons, it should be considered to take a measurement trace which provides a distance value closer to the bumper than the true distance. Otherwise a contact with the bumper can occur before a contact is estimated. A tradeoff has to be made, between the size of error, which is made due to the decision for a possible not nearest function, and the safety aspect, if choosing a measurement trace (object type), which delivers a distance farther away than the true one.

Bayes Risk Decision

In this work, the decision for the object classification (decision for a measurement trace) described above, is made by a Bayes Risk decision, which is a generalization of the Maximum Likelihood (ML) detector and assigns costs to each decision [Kay98].

According to the problem stated above, two hypothesis and their costs are defined:

- H_0: Measurement trace, which delivers a distance farther away.
- H_1: Measurement trace, which delivers a distance closer to the bumper.
- C_0: Costs for decision for H_0.
- C_1: Costs for decision for H_1.

Both hypothesis have equal prior probabilities. The decision is made by comparing the probabilities (considering the costs) with a chosen threshold γ:

$$\frac{p(x|H_1)}{p(x|H_0)} > \frac{C_1\ P(H_0)}{C_0\ P(H_1)} = \gamma \tag{5.8}$$

The decision threshold γ stands for the mentioned tradeoff between a safety decision (object type that delivers a closer distance than the true one, H_1) and the error (higher distance error, due to choosing an object type which has not the nearest measurement trace).

Figure 5.23 shows an example of the decision process. x stands for the current measurement value, $p(x[0]|H_1)$ is the probability of the object type (measurement trace), which provides a closer distance, and $p(x[0]|H_0)$ the probability for the object type with the farther distance function. The threshold is chosen by $\gamma = \frac{1}{10}$. Even if the object type with the farther measurement trace (H_0) is more likely, the detector chooses H_1, as it is the safer decision.

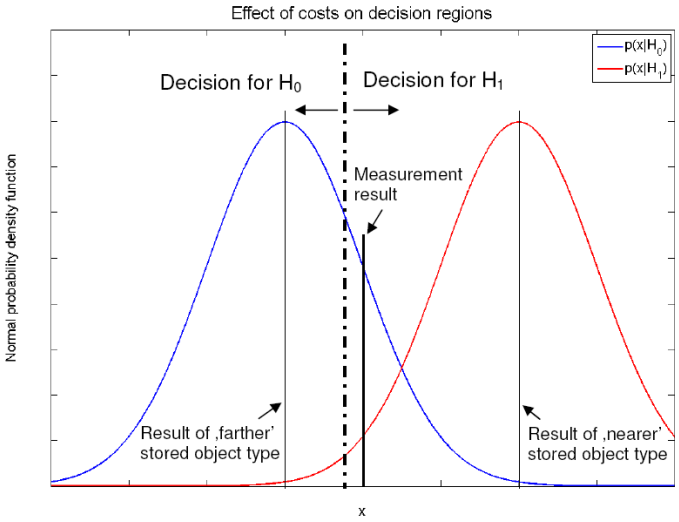

Figure 5.23: Effect of costs on decision regions. With applying costs (e.g. $C_0 = 10$ and $C_1 = 1$) for the two decisions, the decision region of one hypothesis (H_1) is increased while the other (H_0) is decreased. Thus, even if H_0 has a higher probability for the measurement result, H_1 is chosen, because it delivers the nearer distance value. This is the saver decision.

The implementation in this work also takes the second receiver electrode into account for the probability calculation. Therefore, the probabilities of the measurement traces of the first receiving electrodes are multiplied by the probabilities of the second receiving electrodes.

5.3.2 Results for Different Test Cases

For the following test cases a human acts as the approaching object. Figure 5.24 shows a test case, where all measurement traces (i.e. all known object types) of the stored collection are used (including the object type of the human). As described above, this is an ideal case, which probably will not occur in real world applications. However, the Kalman filter works as expected. It chooses the right measurement function over the whole measurement time and estimates the approaching line nearly perfect. When the US sensor is turned off the first time, a small difference ($\approx 0.03\,\mathrm{m}$) can be found for one step.

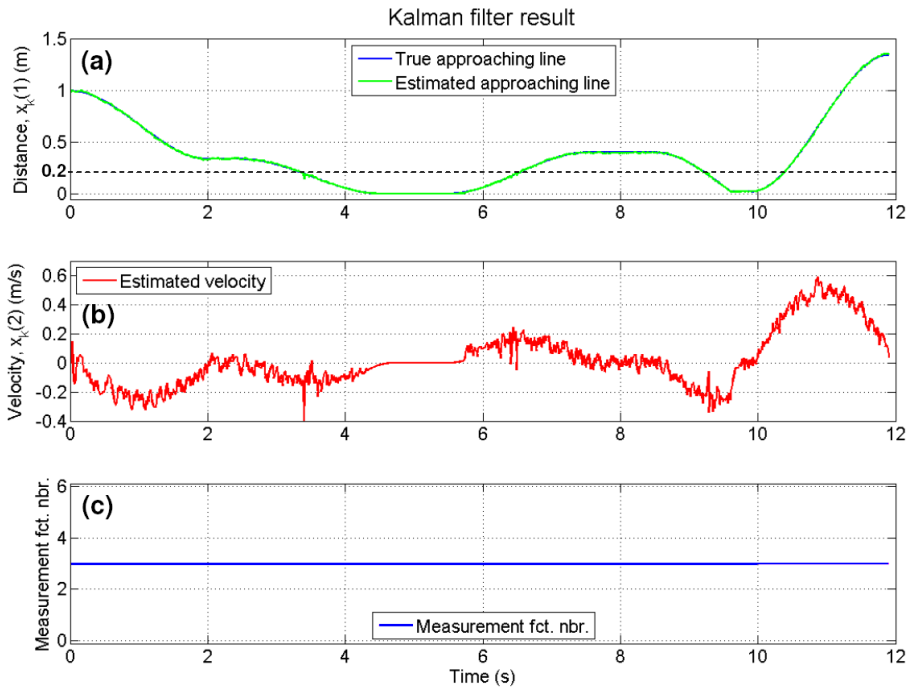

Figure 5.24: Simulation results for an approaching human. All measurement traces (object types) of the stored collection are used (including the human). (a) The estimated distance of the Kalman filter coincides in nearly all points. Only at the time step 3.4 s, where the US sensor is turned of ($x_k < 0.2\,\mathrm{m}$), the estimated state is not correct. (b) The trace of the estimated velocity is shown. When the US sensor is turned of, a short peak occurs, due to the same reason as above. (c) The correct object type (measurement trace, $fct\_nbr = 3$, for an approaching human) is chosen over the whole simulation time and thus, the detector works properly.

Figure 5.25 shows the result of the Kalman filter in absence of the object type of an approaching human ($fct\_nbr = 3$). If the simulated human enters the region below a distance of 0.04 m (the measurement value has the largest difference to the value of the chosen object type), the Kalman filter estimates a distance closer than the true one.

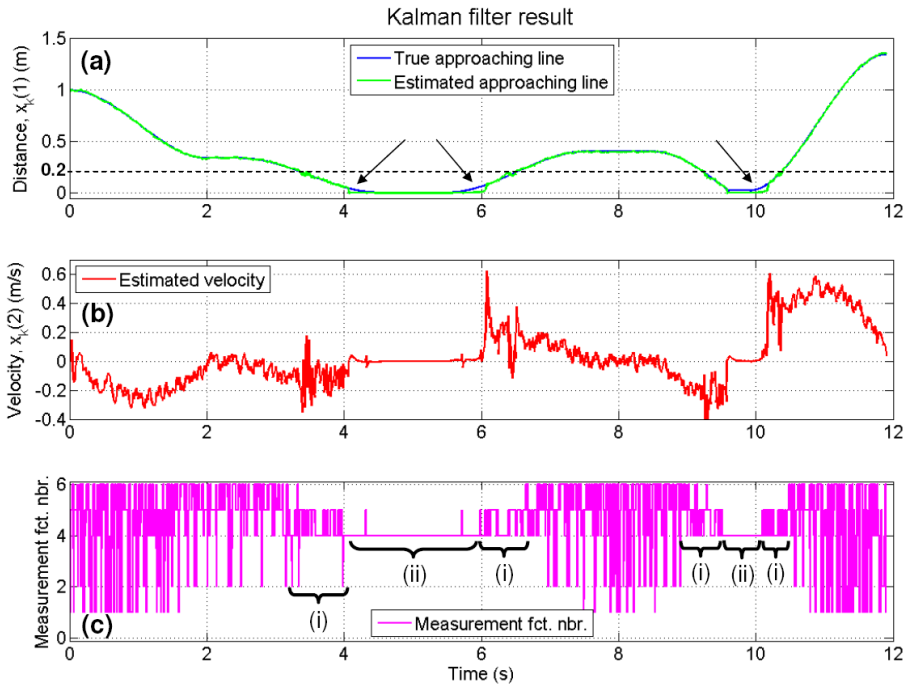

Figure 5.25: Result of the Kalman filter for an approaching human, where the collection of object types does not contain the humans' measurement function. (a) For distances below 0.04 m the estimated distance is shorter than the true one (marked by arrows). Thus, the detector works as expected. (b) The estimated velocity shows peaks at situations, where the estimated state differs from the measurements, because the Kalman filter tries to correct these differences. (c) For distances above 0.25 m it is nearly random, which object type is chosen, due to the similar capacitance values. In cases of (*i*) the Kalman filter switches between object type number 4 and 5 (fence and kerbstone, refer to Figure 5.21). In cases of (*ii*) object type number 4 is chosen, which is the nearest one.

As can be seen in Figure 5.25(c) the detector switches between the object types number 4 and 5 (fence and kerbstone) for estimated distances between 0.2 m and 0.04 m. For distances below 0.04 m, the object type number 4 (fence) is used. Obtained from Figure 5.21 these are the correct decisions. Thus, the detector works properly and the Kalman filter provides the expected estimate values.

Figure 5.26 and Figure 5.27 show zoomed views of the simulation shown in Figure 5.25, for time segments between 9 s and 10.6 s. The human comes close to the bumper, stops, and moves away again. Figure 5.26 also shows the measurement residual, which is the difference between the measurement and the predicted measurement, and the Kalman gain, which is an indicator for the weight of the prediction. Both parameters are plotted for the US part of the filter. As can be seen, when the object (human) reaches a distance lower than 0.2 m, several effects occur:

- The US measurement provides a distance of 0 m because no measurement can be taken by the US sensor for these distances.
- The measurement covariance matrix R for the part of the US measurement is set to a high value. This causes the Kalman filter not to use the US measurements for distances below 0.2 m.
- At this point the Kalman gain reduces to 0. This means, the Kalman filter takes only the prediction into account and rejects the US measurement value.
- The absolute value of the measurement residual increases very fast, because the difference between the prediction x_k and the US measurement value, which is set to 0, increases that fast.
- The peaks of the Kalman gain at time steps 9.25 s and 10.35 s, occur from switching the measurement noise of US measurements high and low (around a distance of 0.2 m).

Therefore the Kalman filter works as expected for the US part of the measurement system.

Figure 5.27 shows the measurement residual, the Kalman gain, and the object type number (fct_nbr) of the used object type (refer to Figure 5.21) for the capacitive part of the measurements. Only the parameters of the first receiving electrode are shown, as it is sufficient for the explanation and prove of the Kalman filter working principle. Since the collection of the object types does not contain the object type of the human in this simulation, the detector has to choose another object type.

As can be seen in Figure 5.21, for distances below 0.03 m the difference between the human measurement values and the other object types reach a maximum. Thus, below a distance of 0.03 m, the estimated distance is 0. The chosen object type number 4 (fence) provides higher measurement values for the same distances. This shows, that the detector chooses the right object type number. Since no negative values for the distance are allowed, the output of the Kalman filter is clipped below 0 m. After the human stopped at a distance of 0.025 m, it departs again. This is the worst case for the Kalman filter. As shown in

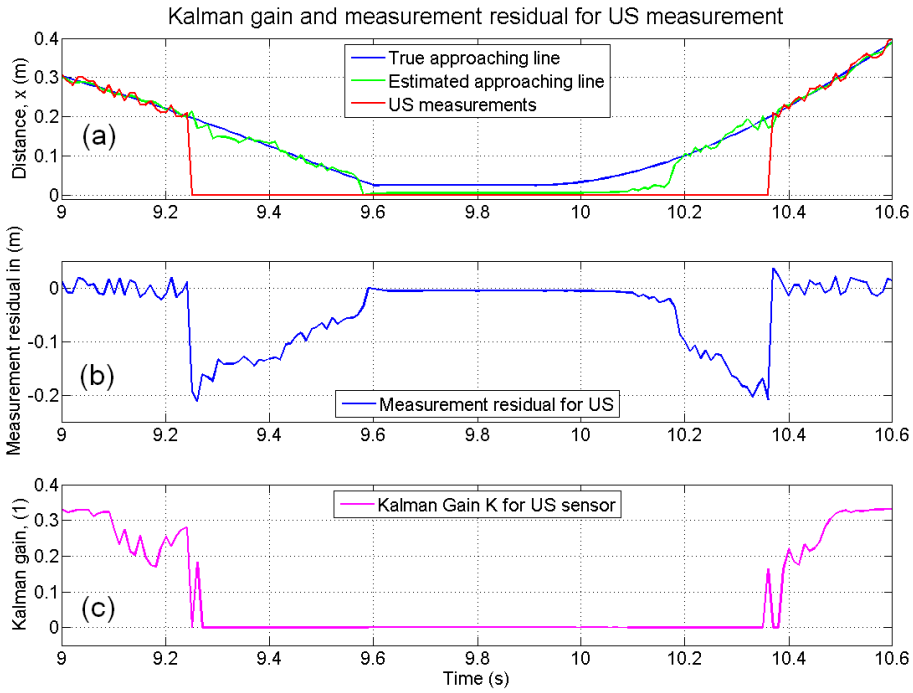

Figure 5.26: Kalman filter behavior for the US part of the measurement system for a zoomed segment. (a) Resulting distances for the true approach, the estimated approach, and the US measurement. Below 0.2 m the US measurement is set to 0. (b) Trace of the measurement residual, which is the difference between the measurement (for the US sensor) and the prediction. For distances below 0.2 m it is high, due to the clipping of the US sensor. (c) The Kalman gain weights the measurement residual. It is shown for the US part, where the residual is set to 0 for distances below 0.2 m. Thus, the US measurement is not taken into account.

Figure 5.21, this is the distance where the measurement trace of the object type has a very small slope and the moving direction of the object is not clear (due to the stop). Additionally the detector switches between two object types (marked by arrows), which results in a change of the residual. Thus, the Kalman filter slowly approaches the true distance (at a distance of 0.08 m). This false estimate for several millimeter occurs only for departing objects and thus, is no problem for the distance measurement system for approaching objects.

Objects for which no proper object type can be found, are difficult to detect (e.g. an approaching object like a snow pile in Figure 5.21). However, if the whole approaching area in Figure 5.21 is covered by measurement traces of different object types, and one is chosen from the detector, an object detection and a distance estimate with safety concerns is possible. As shown in the experiments above, the sensor fusion system is suitable for closing the existing gap in state of the art distance measurement systems for parking aids.

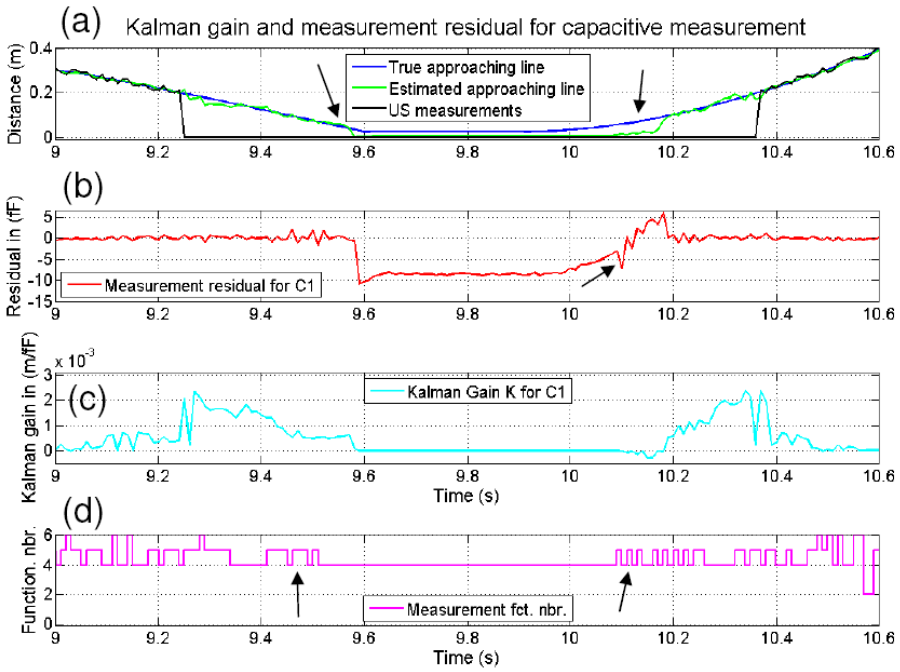

Figure 5.27: Kalman filter behavior for the capacitive part of the measurement system for a zoomed segment. The object type for the approaching object is not used in this simulation. (a) Resulting distances for the true approach, the estimated approach, and the US measurement. (b) Trace of the measurement residual, which is the difference between the capacitive measurement and the prediction. (c) The Kalman gain weights the measurement residual. It is shown for the capacitance part. (d) The detector switches between the object types 4 and 5 for distances above 0.055 m because those two object types deliver similar values. For further explanation refer to the text.

5.4 Evaluation of the Sensor Fusion Concept

Table 5.3 shows a summary of the properties and abilities of each sensor system (US and capacitive distance measurement system) and the improved results for a sensor fusion system developed and tested in this work. The sensor fusion exploit both measurement results in the overlapping range (between 0.2 m and 0.3 m). Beyond this range the properties of the single sensor system apply. However, a higher maximum distance range for the capacitive measurement system can be reached (by retaining the evaluated properties) by e.g. larger sized electrodes, optimized electrode configuration, or higher excitation power. On the other side the implementation constraints on a car bumper and the maximum allowed EMC have to be minded and a tradeoff has to be found, which was not part of the investigations in this work. As can be seen from Table 5.3, the sensor fusion system provides better results for the distance measurement system, than the single measurement systems.

Results for a sensor fusion system for automotive parking aids			
	Ultrasonic	Capacitive	Sensor fusion [7]
Distance	$0.2 - 2\,\mathrm{m}$ [8]	$0 - 0.3\,\mathrm{m}$	$0 - 2\,\mathrm{m}$ [8]
Blind spots	for $d < 0.3\,\mathrm{m}$	minor	minor
Measurement rate	low	high	depending on distance
Material classification	no	yes (volume and relative permittivity ϵ_r)	yes
Dependent on object form (e.g. inclination)	yes	minor	minor
Active pedestrian safety possible	no	no	yes
Costs	low	low	low
Influence of disturbances			
Dirt	minor	minor	minor
Surface active agents	minor	low	minor
Salted water	minor	low	minor
Heavy rain	high	high	high
Snow fall	minor	minor	minor
Layer of ice on the Sensor interface	high	low	low
Layer of snow on the Sensor interface	high	low	low
Object detection			
Objects not in sensor height	longer distance measurement	max. detection range reduces	reduced possible
Fence	short detection range, higher std. deviation	possible	possible
Snow pile	max. detection range reduces	possible	possible

Table 5.3: Results for a sensor fusion of an US and a capacitive measurement system.

[7] The sensor fusion can use both measurements only in the overlapping range (between 0.2 m and 0.3 m). Beyond this range the properties of the single sensor system apply.

[8] For future US sensors the maximum sensing range will be 4 m [Bos07]. However, the lower bound is still 0.2 m.

Chapter 6

Conclusion and Outlook

The developed sensor fusion of the US distance measurement system and the capacitive sensor system was successfully implemented and tested under laboratory conditions. A gapless detection of an approaching object is possible up to 2 m.
Investigations on the US sensor system show, that the system is well-suited for distance measurements between 0.2 m and 2 m. However, the measurement uncertainty increases in the presence of contaminations of the sensor with water. This can be a problem for real world operation under harsh conditions. The capacitive measurement system was evaluated for distance measurements in automotive applications (e.g. mounted on a car bumper). It is well-suited for distances below 0.3 m for nearly all types of objects. Challenging objects to detect are objects, which are small and have a low relative permittivity ϵ_r. However, different object types lead to different signal traces of the approaching objects. Thus, this can be used for object classification. Under harsh conditions, e.g. when the sensor is covered with a water film, the measurement noise can significantly increase. Further investigations have to be made in order to overcome this drawback.
For combining both measurement systems (US and capacitive sensing technique), the used Kalman filter works as expected. Approaching objects can be detected whereby blind spots are avoided. Even challenging objects (e.g. empty plastic pipe) for one technique are reliably detected with the use of the Kalman filter. It is also shown that the Kalman filter and the used detector provide means for a coarse object classification of approaching objects. Further investigations on the influences due to harsh conditions (e.g. water films or mud layer on the sensor electrodes) would be of interest. The use of a differential measurement setup, a special surface of the electrodes to avoid water films, or an additional technique to detect water films, can further enhance immunity to external disturbances. Future work for using the developed distance measurement system also for an object classification and thus, in active pedestrian safety systems, is designated.

Appendices

Appendix A

Software related Implementation Details

A.1 CAN Bus Details

In the following section important details of the CAN bus communication with the micro controller AT90CAN128 from Atmel are shown. The parameters in Table A.1 have to be adjusted to establish a connection between the host computer and the micro controller.

CAN Parameter Definition	
CAN baud rate	100 kBit defined in `config.h`
Sender ID (host)	Every ID will be received.
Receiver ID (micro controller)	`0x555` defined in `I2C.c` in function `can_start()`
Extended ID	Off

Table A.1: CAN parameters to achieve a communication with the host computer.

In Table A.2 the codes to control the main program are shown. There are codes for CapIC, for the AD7143, and for both. Refer to Chapter 4.2 and 4.3 for further details.

Command Codes	
0x10	CapIC start command, AD7143 init command (refer to 4.2 and 4.3).
0x20	AD7143 start command (refer to 4.3).
0xFF	Restart command for the micro controller and the used IC.
default (all others)	Same data is sent back.

Table A.2: Codes to control the main programm running on the Atmel AT90CAN128.

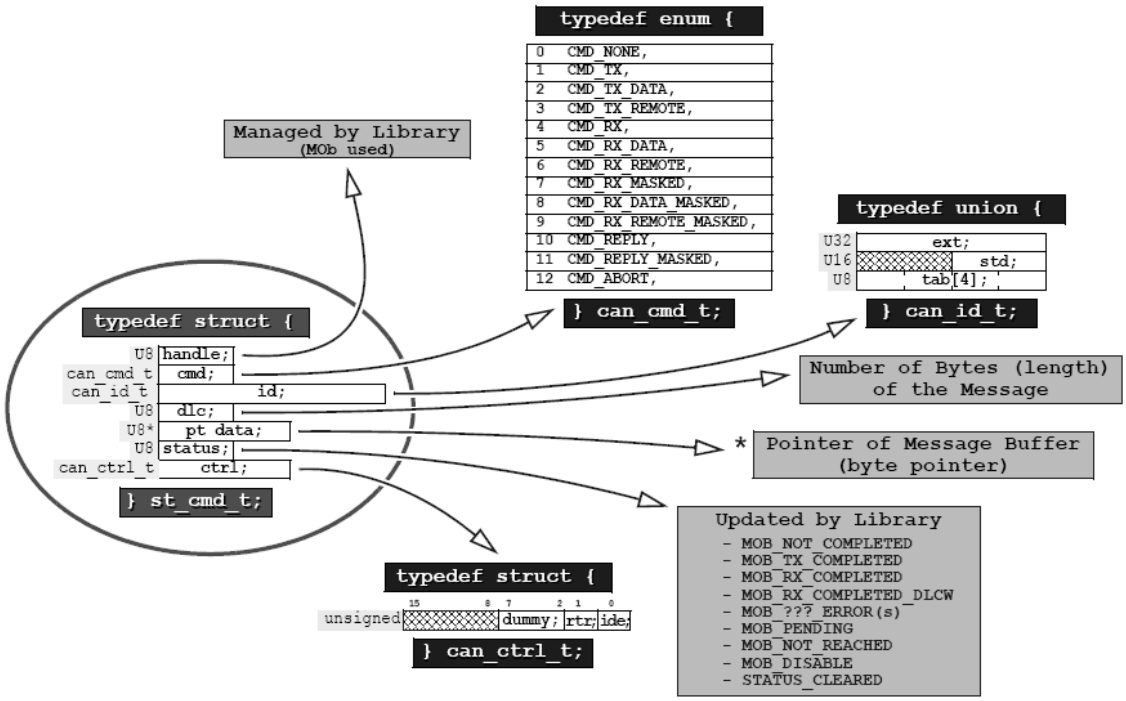

Figure A.1: CAN message descriptor structure, which contains all information about ongoing communication on the CAN bus [Atm07].

A.2 Details on the CapIC Implementation

A.2.1 Implementation of the Micro Controller Program

The following ISR code has to be very short to recognize the next arriving interrupts. Only two interrupts, which occur close behind one another, can be catched by the Atmel AT90CAN128 at one pin. If a third interrupt occurs at the same pin and the first execution of the ISR is not finished, this interrupt is ignored (refer to [Atm07]).

Listing A.1: ISR of the AD7143

```
1 ISR(INT7_vect)
2 {
3 count_int++;              // count the number of occurred interrupts
4 if ((count_int%2) == 0) // respond to every 2nd interrupt
5    int_data |= 0x01;
6 }
```

As can be seen above, only a counter is incremented and a variable is set every second time the ISR is called. With the counter the main program knows how many segments are already measured. The variable `int_data` gives the main program the command to read out the measurement values from CapIC.

Only if the variable `int_data` is set, the function `receive_seg_data()` will be called, as can be seen in line 3 in the following listing.

Listing A.2: Call for receiving data

```
1 ...
2 if (int_data&0x01)
3    receive_seg_data();
4 ...
```

This prevents the micro controller to measure data from CapIC before it sent the second interrupt.

A.2.2 Implementation of the LabView State Machine

A simple example of realizing a state machine in LabView is shown in Figure A.2. The initialization state is the starting state. The next state is chosen in the program code of the actual state.

The state machine for the CapIC measurement system consists of four states:

- Initialize.
- Wait.
- MeasureCapIC.
- Stop.

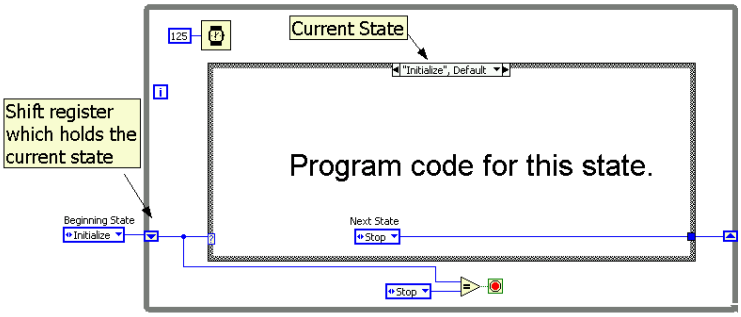

Figure A.2: Example of a LabView state machine with two states (Initialization and Stop state).

Figure A.3 shows the most important part of the CapIC LabView program. It is a extract of the `MeasureCapIC` state. The execute code `0x10` is put on the CAN bus in a first step. The wait command gives the micro controller the time to manage all measurements with CapIC. Afterwards the CAN bus is checked and all available data is received and shown in a waveform chart.

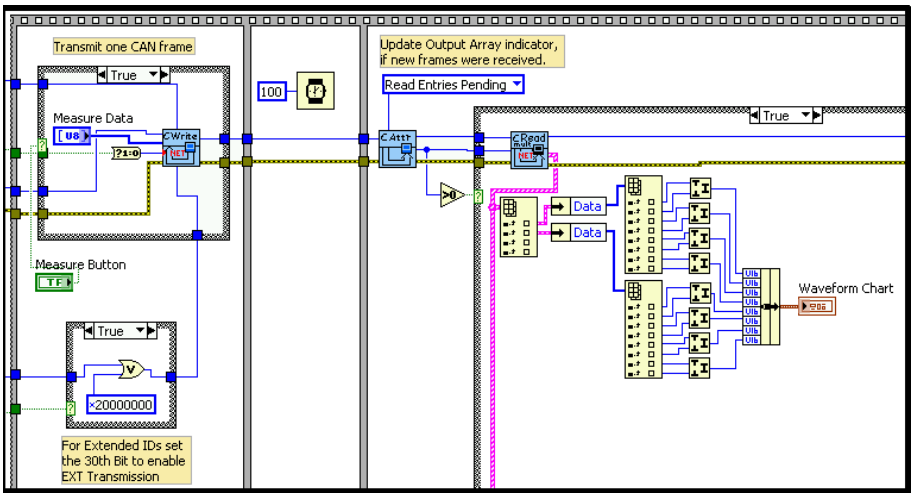

Figure A.3: Extract of the CapIC LabView program in the so called "MeasureCapIC" state.

A.3 Details on the AD7143 Implementation

A.3.1 Implementation of the Micro Controller Program

Listing A.3 shows the first part of the function to initialize the AD7143. The data written to the register banks 1 and 2 contain the configuration settings for the AD7143 (refer to [Ana07]). In line 7 of Listing A.3 the communication to write from a master (AT90CAN128) to a Slave (AD7143) is started. In a second step the whole data for one bank is written (lines 10 to 17). To finalize the storage procedure a `Stop condition` must be send, which is done in line 19.

Listing A.3: Initialization phase of the AD7143

```
1  unsigned short init_ad7143(unsigned short* ptrDataArray,...
2                             unsigned int size)
3  {
4     unsigned short returnVal;
5
6     // ---- send start condition for writing ----------------
7     if ((returnVal=send_twi_start(SLA_W)) != ALL_OK)
8        return returnVal;
9     // write data for bank (need for init) including address
10    for (i=0;i<(size+2);i++)
11    {
12       TWDR = ptrDataArray[i];
13       TWCR = (1<<TWINT) | (1<<TWEN);
14       while (!(TWCR & (1<<TWINT)));
15       if ((TWSR & TWI_MSK_PRE) != TWI_MT_DATA_ACK)
16          return TWI_ERROR_DATA_ACK;
17    }
18    // transmit STOP condition
19    TWCR = (1<<TWINT) | (1<<TWEN) | (1<<TWSTO);
20
21    // ---- now read back and check if they are the same ---
22    // send start condition and write address for reading
23    ...
24    return ALL_OK;
25 }
```

A.3.2 Implementation of the LabView Program

In the following the LabView program to read out the capacitive measurements is shown. Figure A.4 shows the LabView implementation of the `MeasureAD7143` state. After this state was reached and the command for measuring was send over the CAN bus, data

reading starts:

i) CAN bus is read out ((a) in Figure A.4).

ii) An optional filter operation (i.e. low pass filter) is applied (b).

iii) Data recording to a text file is possible (c).

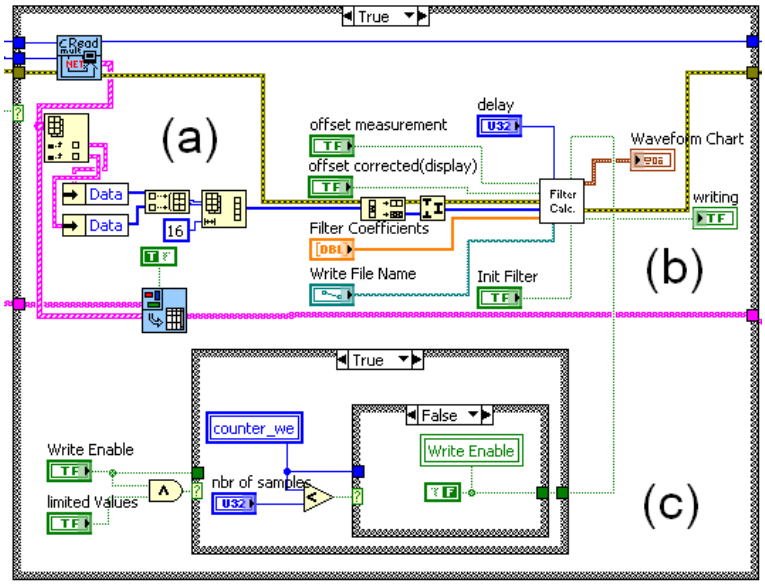

Figure A.4: Extract of the AD713 LabView program in the so called "MeasureAD7143" state. (a) Reading out the data from the CAN bus. (b) Possible post processing of the measurement data (i.e. low pass filtering). (c) Possible file storage of received data.

A.4 Details on the Ultrasonic Sensor Implementation

The CAN communication requirements are listed and major parts of the implementation are shown.

A.4.1 CAN Communication Requirements

All necessary requirements to communicate with the US sensors over the CAN bus are listed below:

100 kBit **Baudrate** Only with this data rate a communication is possible.

Periodic message "Klemmenstatus" This CAN message has to be send every 100ms and simulates the signal for ignition on.

Periodic message "Bedienung Taste PDC" A CAN message that simulates the PDC button.

Periodic message "Netzwerkmanagment K-CAN" Every ECU in the CAN environment of the BMW vehicle puts this message on the CAN bus after it received the same message from a predecessor (another ECU).

Only if this four conditions are kept, the US ECU puts the measurement data from the US sensors on the CAN bus. Otherwise an error message is reported and no distance measurement can be made.

A.4.2 Significant Parts of the LabView Implementation

Figure A.5 shows parts of the blockdiagram and the frontpanel of the LabView program, which simulates the car environment. All three periodic messages (according to the Appendix A.4.1) are send over the CAN bus every 100 ms. The fourth message is to give the user the possibility to put his own message on the CAN bus. After sending this three messages, the US ECU automatically puts alls PDC values (measurement values from the eight US sensors) on the CAN bus. All eight US sensors have to be connected to the US ECU. Otherwise the ECU would put error messages instead of the PDC values on the CAN bus.

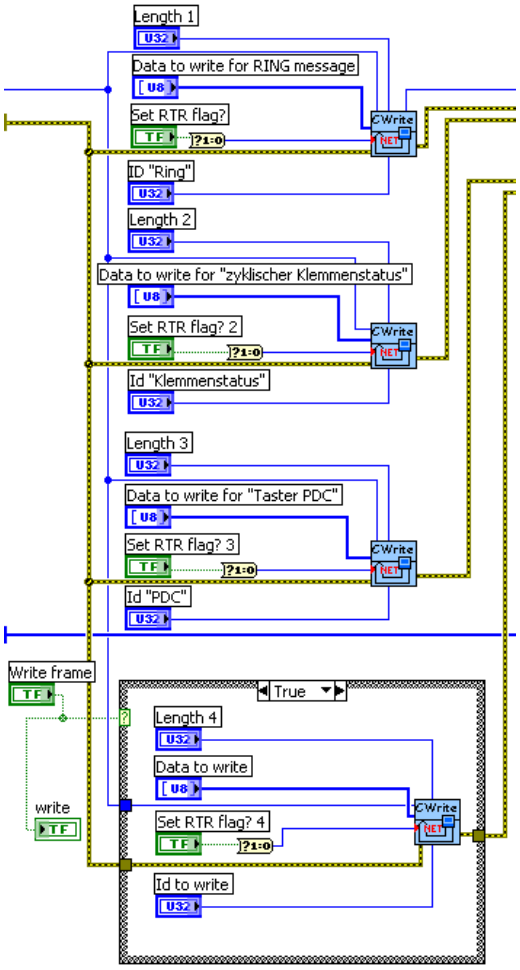

(a) LabView blockdiagram of the US program part.

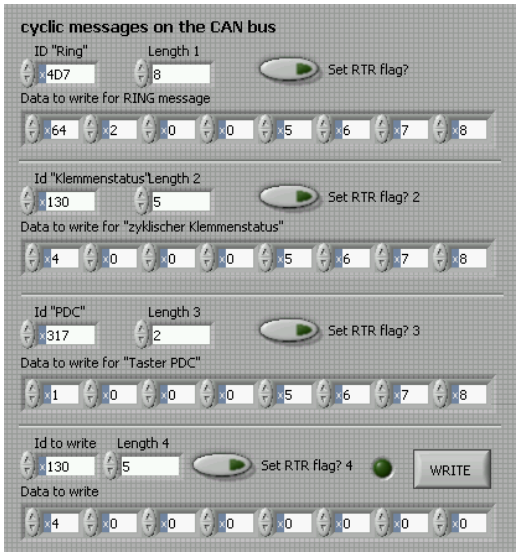

(b) LabView frontpanel of the US program part.

Figure A.5: Major part of the LabView program to measure data from the US ECU. (a) LabView blockdiagram of the three periodic messages, which have to be sent to simulate a car environment. (b) LabView frontpanel, which shows the data that every CAN frame has to contain.

Appendix B

Circuitry Diagrams and Layouts

B.1 Board for Micro Controller

B.1.1 Assembly Diagram

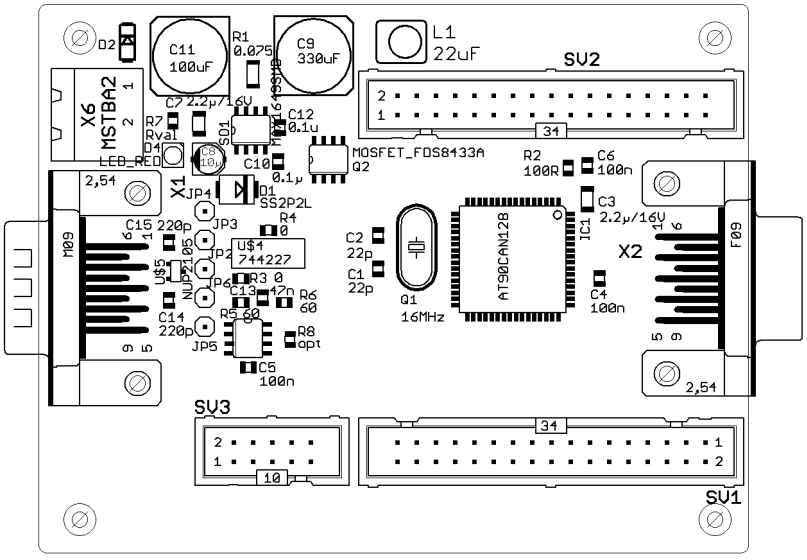

Figure B.1: Assembly diagram: Micro controller board with CAN transceiver.

B.1.2 Schematic

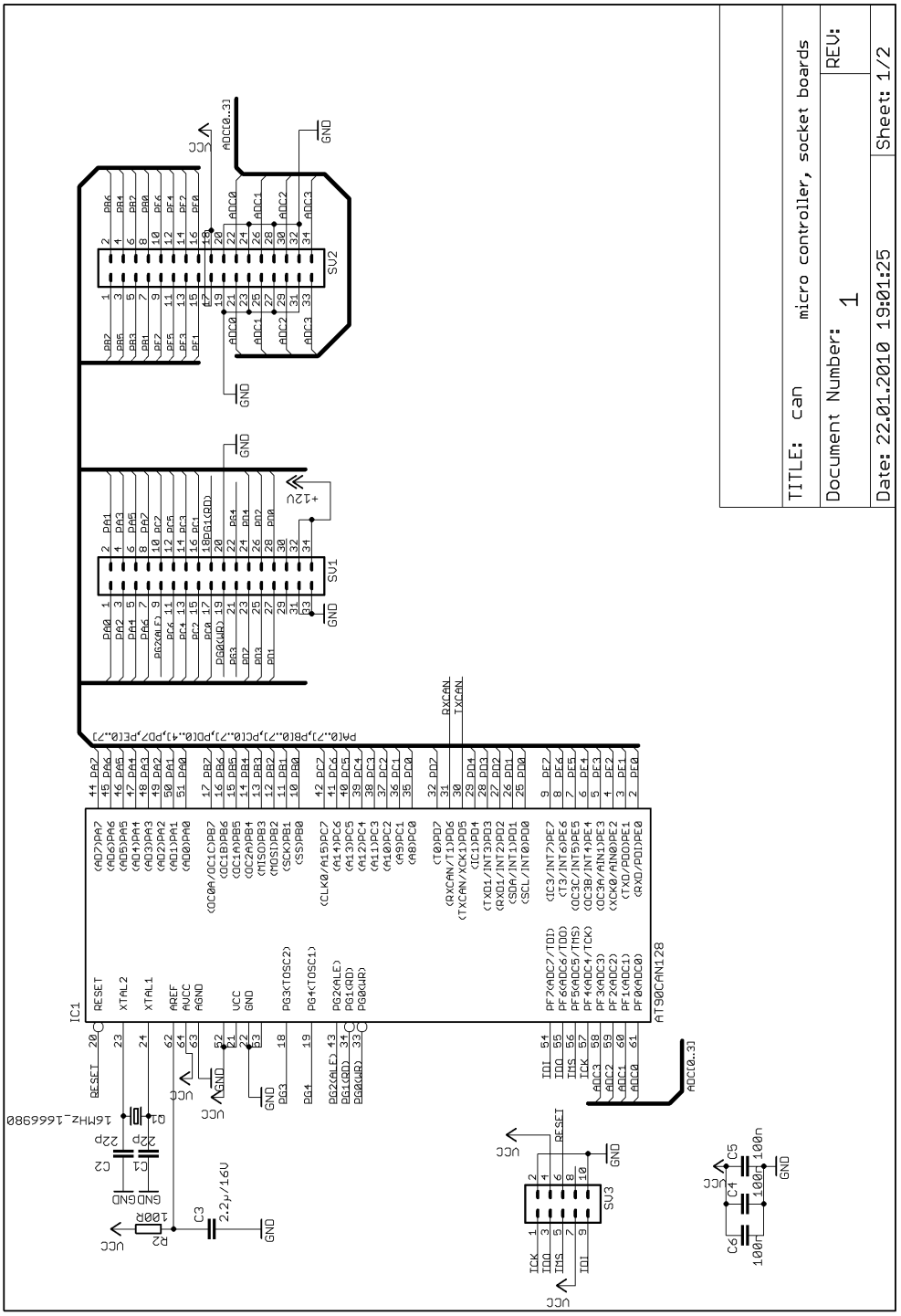

Figure B.2: Schematic: Micro controller board with CAN transceiver 1/2.

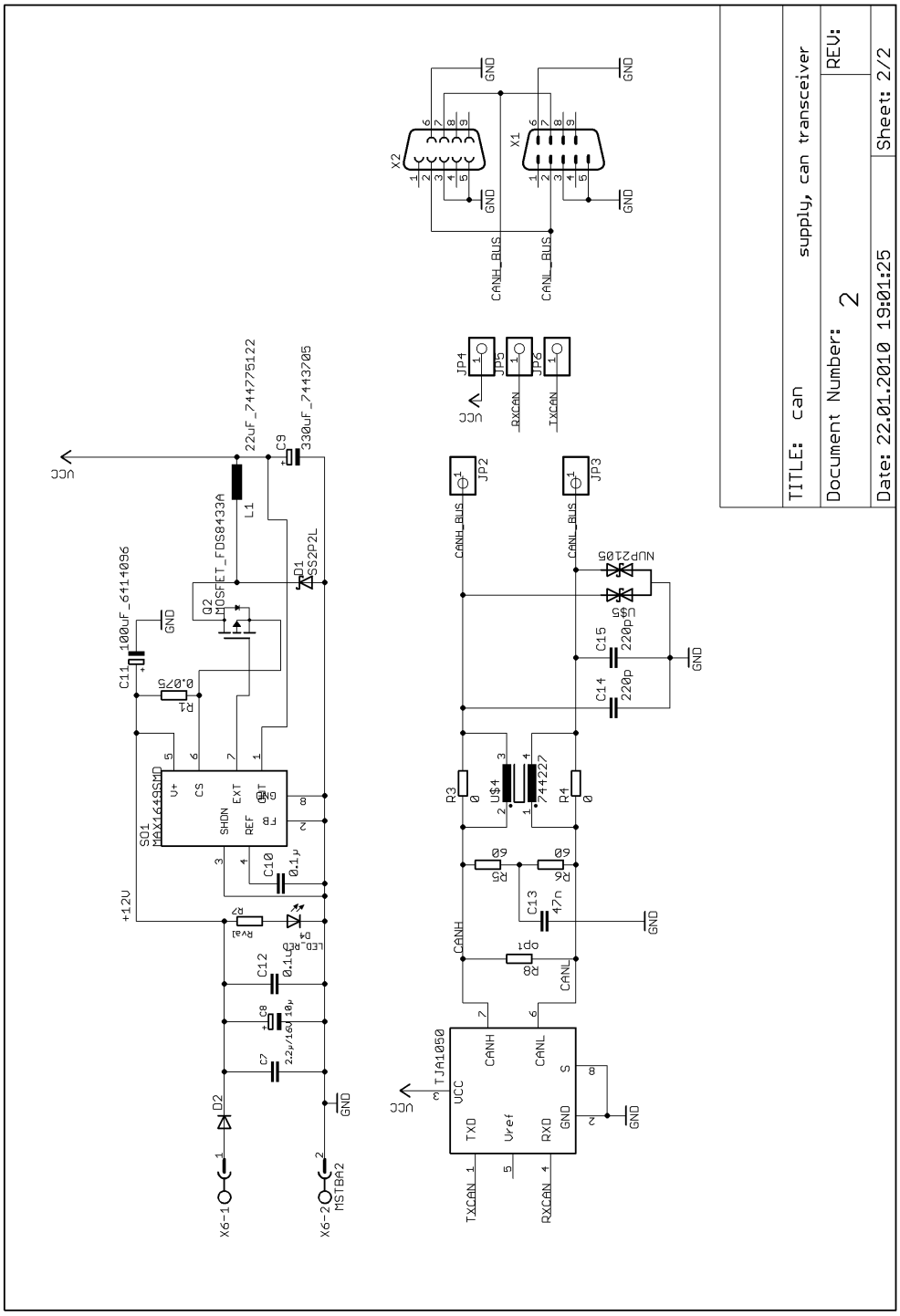

Figure B.3: Schematic: Micro controller board with CAN transceiver 2/2.

B.2 Board for Capacitive Front-End IC

B.2.1 Assembly Diagram

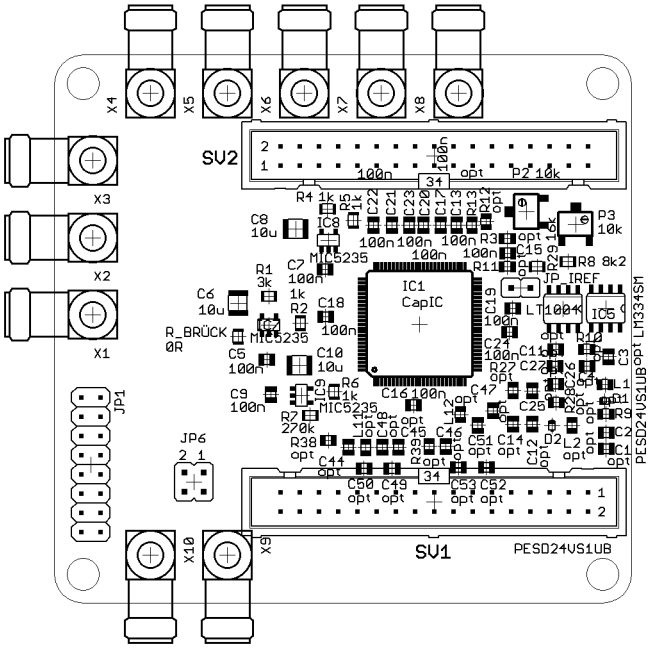

Figure B.4: Assembly diagram: Capacitive Front-End IC, CapIC, top side.

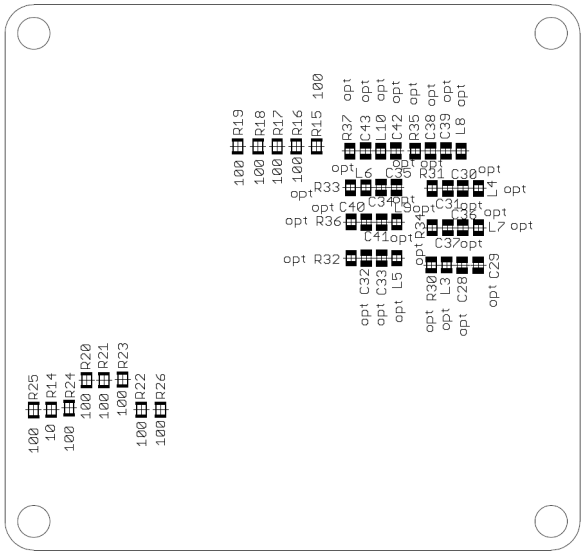

Figure B.5: Assembly diagram: Capacitive Front-End IC, CapIC, bottom side.

B.2.2 Schematic

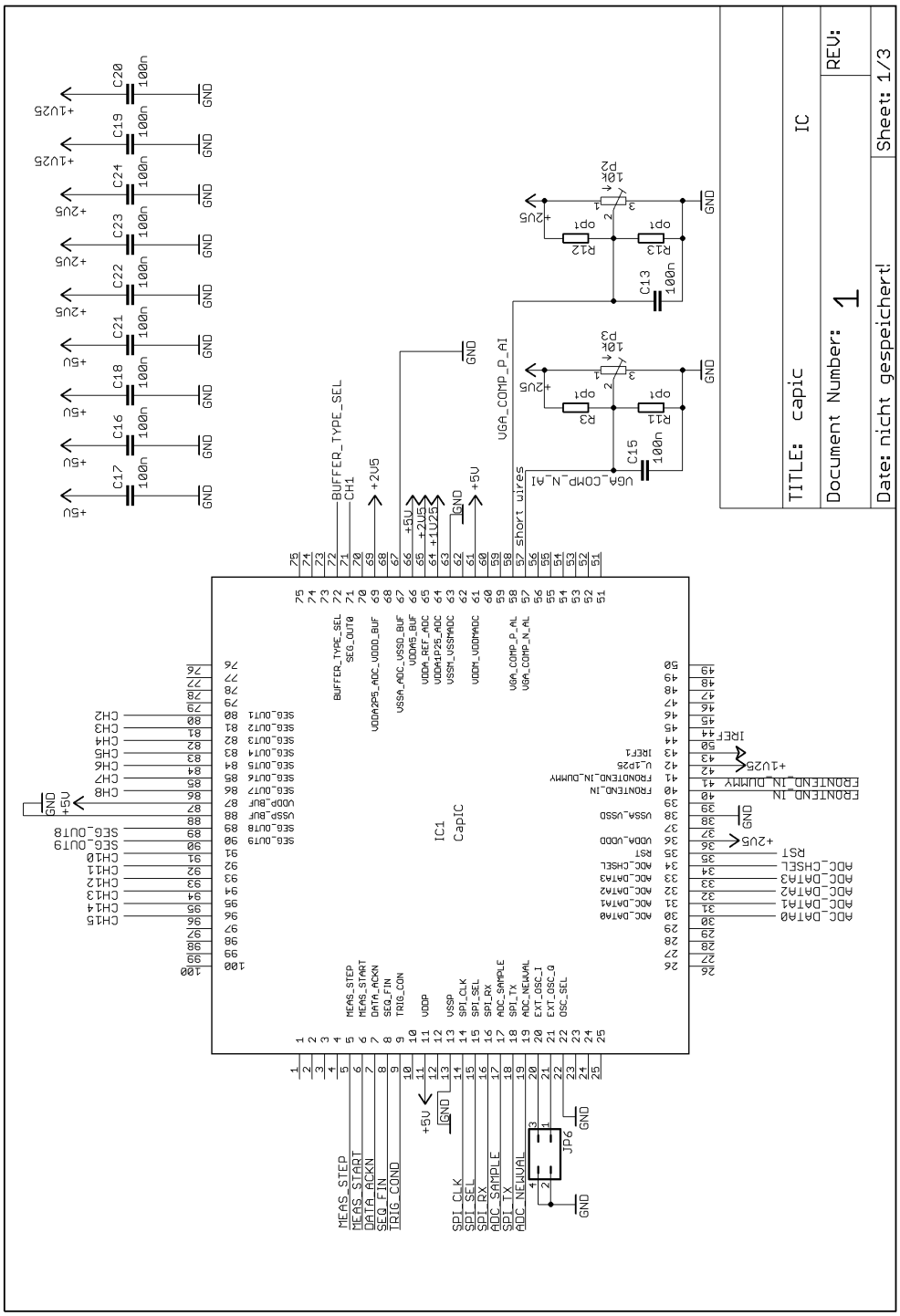

Figure B.6: Schematic: Capacitive Front-End IC, CapIC 1/3.

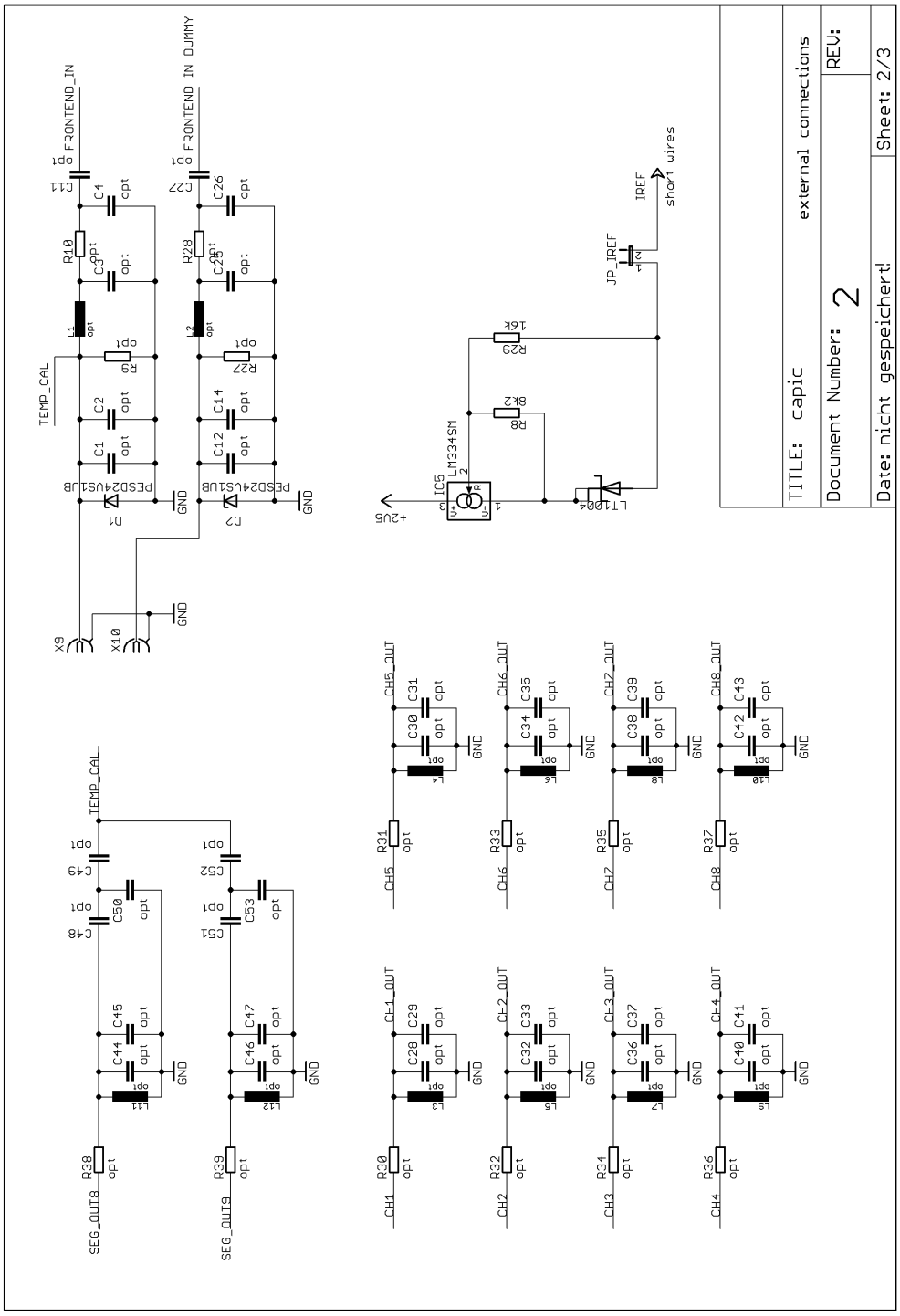

Figure B.7: Schematic: Capacitive Front-End IC, CapIC 2/3.

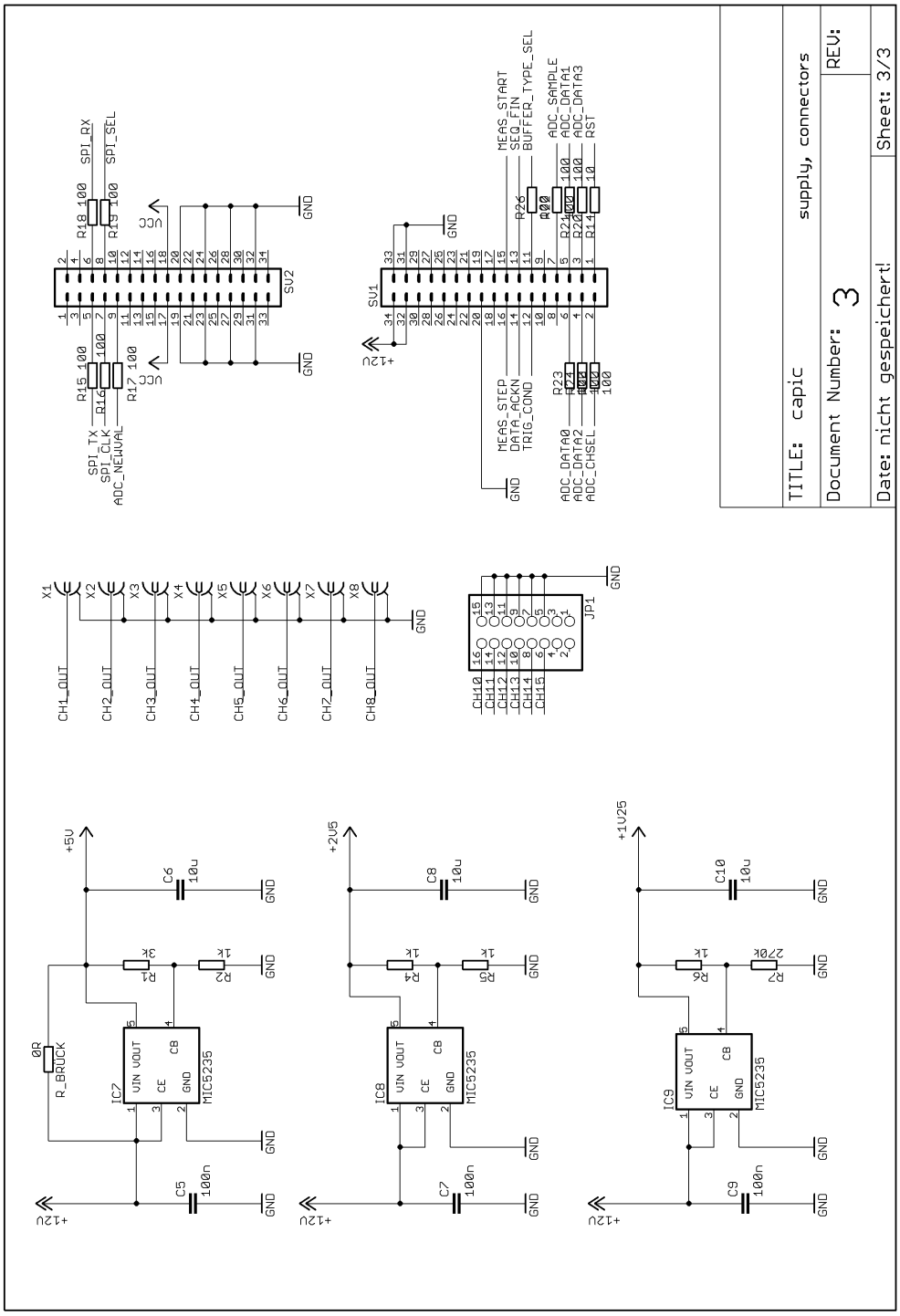

Figure B.8: Schematic: Capacitive Front-End IC, CapIC 3/3.

B.3 Board for Analog Devices IC AD7143

B.3.1 Assembly Diagram

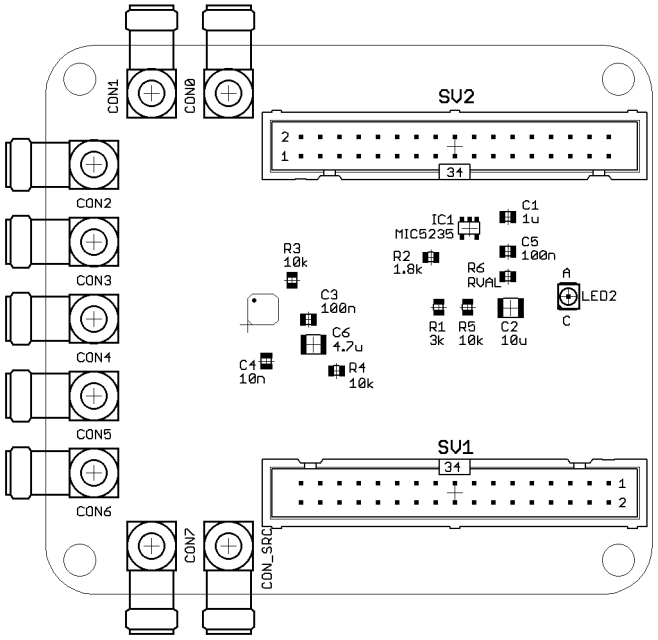

Figure B.9: Assembly diagram: Analog Devices IC AD7143.

B.3.2 Schematic

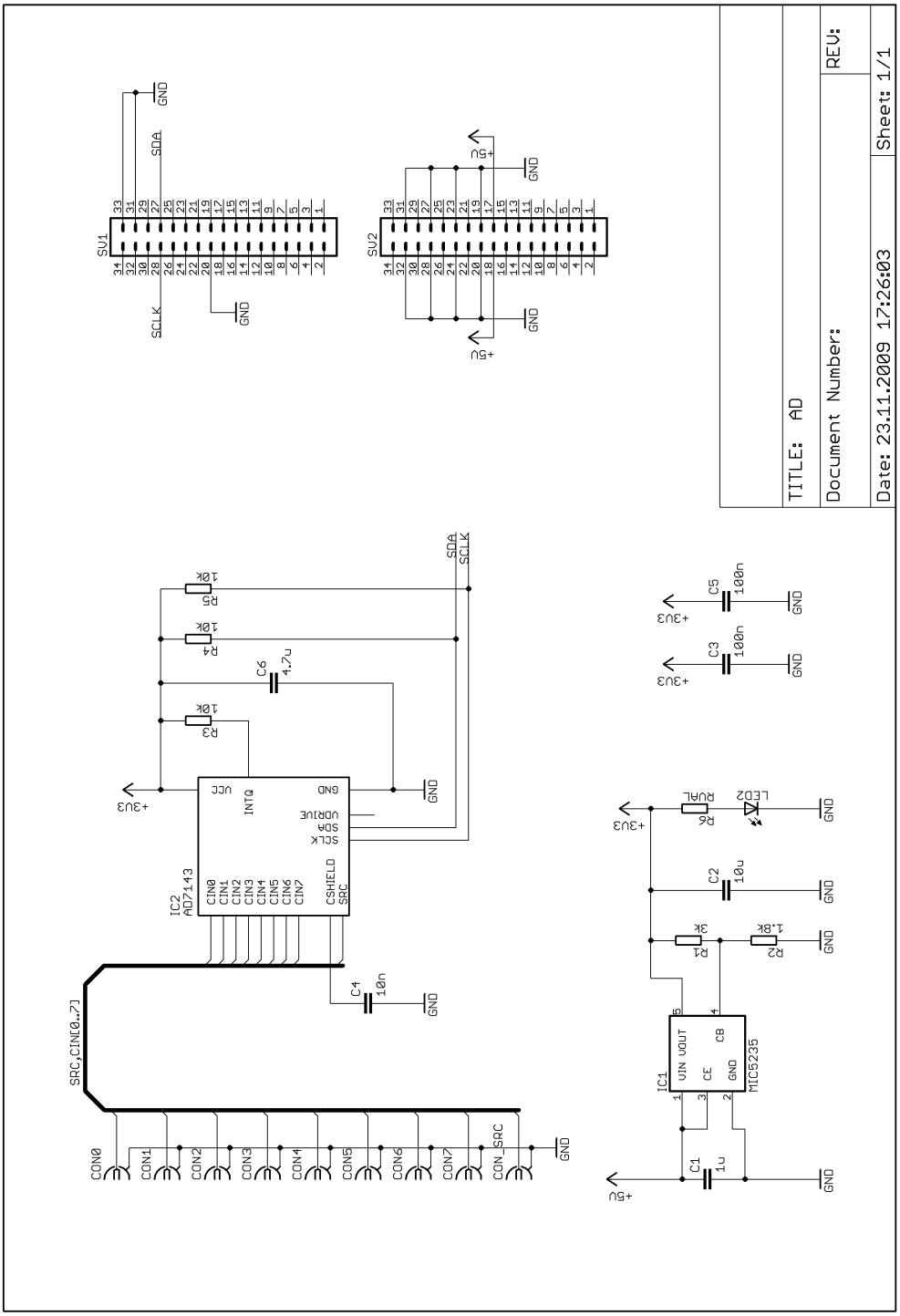

Figure B.10: Schematic: Analog Devices IC AD7143.

Appendix C

Abbreviations

ADC	Analog to Digital Converter
CAD	Computer Aided Design
CapIC	Capacitive Sensor IC
CDC	Capacitive to Digital Converter
CMC	Common Mode Choke
DAC	Digital to Analog Converter
ECU	Electronic Control Unit
EKF	Extended Kalman Filter
EMI	Electro Magnetic Interferences
EMC	Electro Magnetic Compatibility
ESD	Electro Static Discharge
FIR	Far Infrared Radiation
FMCW	Frequency Modulated Continuous Wave
ESD	Electro Static Discharge
FSR	Full Scale Range
IC	Integrated Circuit
I2C Bus	Inter- Integrated Circuit Bus
IR	Infrared Radiation
ISP	In System Programmer
ISR	Interrupt Service Routine
LDO	Low Dropout Regulator
Lidar	Light Detection And Ranging
ML	Maximum Likelihood
NIR	Near Infrared Radiation
PCB	Printed Circuit Board
PDC	Park Distance Control

PGA	Programmable Gain Amplifier
Radar	Radio Detection and Ranging
RPS	Rapid Prototyping System
SNR	Signal to Noise Ratio
SPI	Serial Peripheral Interface
$\Sigma\Delta$ CDC	Sigma Delta Capacitive to Digital Converter
TDMA	Time Division Multiple Access
TWI	Two Wire Interface
US	Ultrasonic
USB	Universal Serial Bus

List of Figures

List of Tables

Bibliography

[Ana07] Analog Devices. *AD7143 - Programmable Controller for Capacitance Touch Sensors*, 2007. 34, 35, 44, 88

[Atm07] Atmel. *AT90CAN128 - 8bit Microcontroller with 32K/64K/128K Bytes of ISP Flash and CAN Controller*, 2007. 25, 26, 41, 42, 45, 85, 86

[Bax97] L.K. Baxter. *Capacitive Sensors, Design and Applications*. IEEE Press, 1997. 1, 14, 15, 16, 66

[Bos07] R. Bosch. *Sensoren im Kraftfahrzeug*. Robert Bosch GmbH, 2007. 9, 10, 12, 13, 81

[BZB09] T. Bretterklieber, H. Zangl, and G. Brasseur. Capacitance mismatch correction for a fluidic inclinometer. In *I2MTC 2009 - International Instrumentation and Measurement*, 2009. 32, 34

[BZH+08] T. Bretterklieber, H. Zangl, G. Holler, D. Hrach, D. Hammerschmidt, and M. Motz. Versatile programmable integrated interface for robust capacitive sensors. *Elektrotechnik & Informationstechnik*, 125(4):132–137, 2008. 2, 16, 27

[BZM+08] T. Bretterklieber, H. Zangl, M. Motz, T. Werth, and D. Hammerschmidt. Versatile sensor front end for low-depth modulation capacitive sensors. *IEEE International Instrumentation and Measurement Technology*, pages 830–835, May 2008. 27, 28, 29

[Dep08] Department of Transportation, National Highway Traffic Safety Administration, U.S. *National Pedestrian Crash Report*, June 2008. 1

[Fle08] W. J. Fleming. New automotive sensors - a review. In *IEEE Sensors Journal*, volume 8, pages 1900–1921. IEEE, November 2008. 2, 4, 6, 7, 13

[Foe06] F. Foelster. *Erfassung ausgedehnter Objekte durch ein Automobil-Radar*. PhD thesis, Hamburg University of Technology (TUHH), Dezember 2006. 2, 4, 6, 106

[GA08] M. S. Grewal and A. P. Andrews. *Kalman Filtering: Theory and Practive Using Matlab*. Wiley-Interscience Publication, September 2008. 70

[GT07] T. Ghandi and M. M. Trivedi. Pedestrian protection systems: Issues, survey, and challenges. *IEEE Transactions on Intelligent Transportation Systems*, 8(3):413–430, September 2007. 1, 2, 5, 6, 7

[GZB08] B. George, H. Zangl, and T. Bretterklieber. A warning system for chainsaw personal safety based on capacitive sensing. In *IEEE Sensors*, pages 419–422, 2008. 1, 18, 19

[Hon99] Honeywell. *Applying Ultrasonic Proximity Sensors*, 1999. 9, 12, 13

[Kay98] S. M. Kay. *Fundamentals of Statistical Signal Processing, Volume 2, Detection Theory*. Prentice Hall PTR, 1998. 74

[Lin01] Linear Technology. *LM134 Series, Constant Current Source and Temperature Sensor*, 2001. 29

[LSW09] R. Lerch, G. Sessler, and D. Wolf. *Technische Akustik, Grundlagen und Anwendungen*. Springer-Verlag Berlin Heidelberg, 2009. 1, 2, 3, 9, 10, 11, 12

[Max05] Maxim. *Max 1651, 5V, High-Efficiency, Low-Dropout, Step-Down DC-DC Controller*, 2005. 26

[Mic05] Micrel. *MIC5235, Ultra-Low Quiescent Current, 150mA uCap LDO Regulator*, 2005. 34

[Nat08] National Instruments. *CAN and LIN Interfaces for Hi-Speed USB*, 2008. 39

[NXP06] NXP. *AN00020 TJA1050 high speed CAN transceiver - Application Note*, November 2006. 26, 27

[Sch05] M. Schneider. Automotive Radar - Status and Trends. In *GeMiC*. Robert Bosch GmbH, 2005. 6

[SMG07] H. Schweitzer, M. Menghin, and J. Grinschgl. Modellauto. Technical report, Graz University of Technology, March 2007. 24, 26

[SS06] M. Spies and H. Spies. Automobile Lidar Sensorik: Stand, Trends und zukünftige Herausforderungen. In *Advances in Radio Science*, pages 99–104, 2006. 2, 5, 6, 106

[SWS04] G. Steiner, D. Watzenig, and B. Schweighofer. Time optimal control of ultrasonic transducers for improved multiple object recognition. In *International Workshop on Robot Sensing*, pages 69–73. IEEE, 2004. 11

[TH08] R. Troppman and A. Höger. An introduction to adaptive cruise control (acc). In *EE Times-India*, 2008. 8

[Zan05] H. Zangl. *Design Paradigms for Robust Capacitive Sensors*. PhD thesis, Graz University of Technology, May 2005. 14, 15, 16, 18

[ZBH08] H. Zangl, T. Bretterklieber, and G. Holler. On the design of a fully differential capacitive sensor front-end interface circuit. *Microelectronic Conference*, page 5, October 2008. 68

[ZBHW08] H. Zangl, T. Bretterklieber, D. Hammerschmidt, and T. Werth. Seat occupancy detection using capacitive sensing technology. *SAE World Congress and Exhibition*, 1:7, 2008. 29